# ABOUT THE PERFORMANCE OF A SINGLE POROUS COOLING FIN

**Master thesis**

**Wessel Schilders** **STUDENT NUMBER: 5176654**

DEPARTMENT OF PROCESS, FLOW AND ENERGY

Supervisor: Emanuele Zanetti
Co-supervisor: Prof.dr. K. (Kamel) Hooman

Delft, February 23, 2025

# Nomenclature

| Symbol | Meaning | Units |
|---|---|---|
| a | fin parameters | - |
| $\mathcal{A}$ | area | $mm^2$ |
| $c_p$ | specific heat capacity | J/kg/K |
| d | (average) pore size | - |
| E | energy | J |
| g | gravitational acceleration | $m/s^2$ |
| h | convective heat transfer coefficient | $W/m^2/K$ |
| k | conductive heat transfer coefficient | W/m/K |
| L | length | mm |
| $\mathcal{P}$ | perimeter | mm |
| $\dot{q}$ | heat flux | $W/m^2$ |
| $\dot{Q}$ | heat flow | W |
| T | temperature | °C |
| $v$ | velocity | m/s |
| | | |
| $\Delta$ | difference in quantity | - |
| $\varepsilon$ | porosity | % |
| $\nu$ | kinematic viscosity | $m^2/s$ |
| $\rho$ | density | $kg/m^3$ |
| $\sigma$ | Stefan-Boltzmann constant | $W/m^2/K$ |

| Sub-/superscript | Meaning |
|---|---|
| avg | average |
| c | cross section/ Convective |
| b | base |
| e | external/ambient |
| max | maximum |
| $\sim$ | dimensionless quantity |

| Abbreviation | Meaning |
|---|---|
| DC | Direct current |
| Gr | Grashof number |
| Nu | Nusselt number |
| PPI | pores per inch |
| Ra | Rayleigh number |
| Re | Reynolds number |
| STD | standard deviation |

# Contents

## Abstract

In this master thesis, an experimental study has been performed to explore if the temperature profile along a porous fin can be predicted by the existing analytical solution for solid cooling fins. The experiments performed during this thesis show that the temperature profile can indeed be represented by the existing solid-fin model. However, a correction for the existing model for the effective conductivity of a porous material is needed. The measurements were taken under a natural convection regime. The literature study revealed that very little experimental research has been done on porous cooling fins. The studies that were published, focus on the total heat removal of an entire heat sink, not just a single fin. These studies ignore the three-dimensional structure of the fin itself, which makes the results often case-specific and difficult to compare with each other. This method does not provide a way of predicting a fin's performance beforehand. The experiments indicate that the effective conductivity of a porous material will stay a material property, as is the case for solid material. The correction that is needed for existing model looks to be a strong function of porosity, but a very weak function of pore size and fin orientation. The porous samples outperformed the solid one in both heat removal and fin base temperature, which is in agreement with existing literature. The result from thesis can be used to design a setup in which the effective heat transfer coefficient and conductivity can be determined in a much simpler way. This enables for collecting more data and create empirical correlations for these two parameters, which predict fin performance.


# 1 Introduction

Cooling fins are often used in devices that require a rapid and efficient heat exchange with the surrounding environment. This includes a very wide range of applications. Examples can be components that create heat such as CPU units, engines and even hydrogen fuel cells (El-Samrah, Tawfic, and Chidiac, 2021). Another example is that of microelectronics. According to Qats, n.d., every reduction of 10°C will approximately double the electronics life span.

A porous fin increases the heat transfer by increasing the effective surface area. The effective area per unit volume can potentially be increased even further by replacing the solid material in cooling fins by a porous material, increasing its performance. When it comes to porous cooling fins, there seems to exist very little experimental work. This fact, and the complexity of porous materials, make it currently very difficult to predict the performance of porous material cooling fins.

This document is a graduation thesis for the Master of engineering at the department of Process, Flow and Energy, Tu Delft. Its purpose is to create more insight into the predictability of porous cooling fins. This will be obtained by means of an experimental setup. The main question is:

**Can the temperature profile along a porous cooling fin be predicted by the existing mathematical model constructed for solid fins?**

This questions will be backed-up by several sub-questions:

- What additional parameters play an important role?
- Where do these parameters show up?
- Does the thermal conductivity $k$ stay solely a material property?

This last point is the case for solid materials. During the literature review, citations were tracked to get a complete overview of the current literature. From this literature less relevant papers were later removed. Examples are paper concerning porous materials used for cooling, but not necessarily related to cooling fins. Examples are the metal foam heat exchanger of Kim, Paek, and Kang, 2000 and the experimental investigation of single- and two-phase flow and heat transfer in aluminium foams, written by H.Y. Li and Leong, 2011. A complete list of the most relevant reviewed literature can be found in appendix A. This list includes experimental, numerical and analytical studies concerning porous cooling fins. The results from the literature review are used to set up the experiment for this thesis.

The next section of the document will go over the derivation for the analytical solution of a simple solid cooling fin. The solution represents the temperature profile along the fin. The section after that, section 3, contains summaries of the encountered relevant experimental literature. Section 4 contains a table that lists the most important findings per article. A summary of the conclusions found in literature is given in section 5. It addresses the general trends, contradictions and gaps in the encountered literature. Section 6 goes into the prediction of performance of a single porous fin, treated as a three-dimensional object. It also tests the available data from literature. A method is proposed to find the effective heat transfer coefficient for a single porous cooling fin. Section 7 explains the quantification of the experimental setup and estimates the errors. Section 8 contains the experimental results. The conclusion is found in section 9 and the recommendations for a follow-up study are found in the last section, section 10.

# 2 Analytical derivation of the temperature profile in a solid fin with adiabatic tip

The analytical derivation of the temperature profile along a simple solid cooling fin is worked out in this section. This solution can be used to find the effective convective heat transfer coefficient for a single porous fin. This is explained in section 6. The derivation below is performed in dimensionless form, which results in an analytical equation that describes the dimensionless temperature in the solid fin as a function of a single dimensionless coordinate $\tilde{x}$, the relative position along the length of the fin. The derivation starts by looking at figure 1, taken from Mills, 2014. It shows a sim-

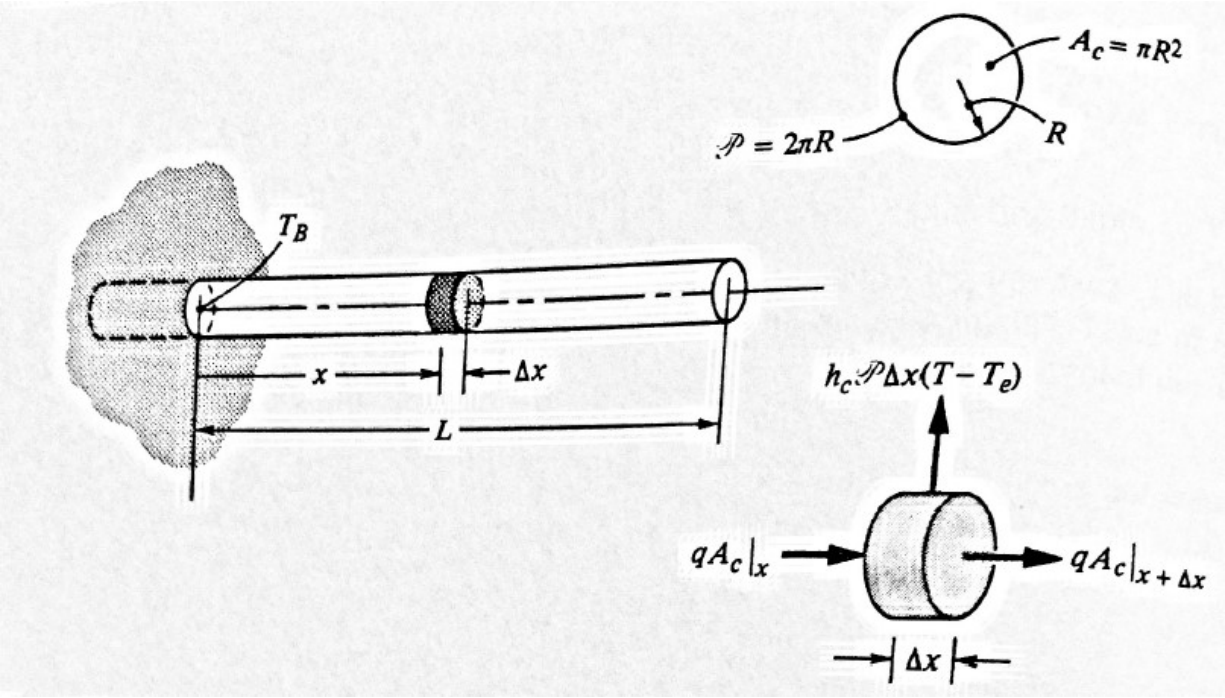


Figure 1: *Image from Mills, 2014. It shows a simple pin fin and the used coordinate system for setting up the differential equation that describes the heat flows inside such a cooling fin.*

ple solid pin fin and the coordinate system that was used for setting up the differential equation. This equation describes the total sum of the heat flows. The base of the fin is on the left side, where the fin base temperature $T_b$ is located. A section of the fin, having width $\Delta x$, can be seen at the bottom right of the figure. Three main types of heat flow occur:

- conductive heat flow into the fin portion at the left side;
- conductive heat flow out of the fin portion at the right side;
- convective heat towards the surroundings at the periphery of the fin section.

At steady state, the sum of these should be zero. By taking the incoming flows as being positive, this results in:

$$\frac{dE}{dt} = \dot{q}\mathcal{A}_c|_x - \dot{q}\mathcal{A}_c|_{x+\Delta x} - h_c\mathcal{P}\Delta x\,(T - T_e) = 0 \tag{1}$$

Here, $\frac{dE}{dt}$ represents the change in energy for an infinitesimally small section of the fin with respect to time, $\dot{q}$ is the heat flow per unit of surface area due to conduction, $\mathcal{A}_c$ describes the cross sectional area of the fin, $h_c$ the convective heat transfer coefficient between the fin and the surrounding fluid, $\mathcal{P}$ the periphery of the cooling fin element and $T_e$ the (ambient) fluid temperature.

Dividing equation 1 by $\Delta x$ and letting $x \rightarrow 0$ yields the following differential equation:

$$-\frac{d}{dx}\left(\dot{q}\mathcal{A}_c\right) - h_c\mathcal{P}\left(T - T_e\right) = 0 \tag{2}$$

For the heat flux per surface area $\dot{q}$, Fourier's

law of conduction can be substituted:

$$\dot{q} = -k\frac{dT}{dx} \tag{3}$$

Which then gives the second order differential equation that describes the temperature in the fin as a function of a single coordinate $x$:

$$k\mathcal{A}_c\frac{d^2T}{dx^2} - h_c\mathcal{P}\left(T - T_e\right) = 0 \tag{4}$$

Some important assumptions simplified this governing equation:

1. The radiative heat transfer from the fin to its surroundings in negligible.
2. The fin's cross section is a constant over the entire length of the fin: $\mathcal{A}_c \neq \mathcal{A}_c(x)$
3. The convective heat transfer coefficient $h_c$ is an average over the entire circumference of the fin.
4. The convective heat transfer coefficient is a constant: $h_c \neq h_c(x)$.
5. The temperature $T$ is an average temperature of a section of the fin: $T = T(x), T \neq T(y)$.

The first assumption is made based on the low emissivity of metal and the relative low temperature at which cooling fins operate ($T_{avg} \approx 150°$C). These two things make radiative heat transfer usually more than an order or magnitude smaller than the convective heat transfer. Since equation 4 is differential equation of second order, it required two additional boundary conditions. The first boundary condition can be taken at a location where the temperature is likely known: at the base of the fin, where $x = 0$.

$$T|_{x=0} = T_b \tag{5}$$

The second boundary is the adiabatic tip condition and is taken at the end of the fin:

$$\left.\frac{dT}{dx}\right|_{x=L} = 0 \tag{6}$$

This states that there is no heat loss through the end face of the fin. In the case of cooling fins this is normally a fair assumption, since the surface area of this face is usually very small compared to the periphery face of the fin. Also, the temperature gradient is lowest at this point between the fin and its surroundings, provided that heat is added to the fin at the base only. Equation 4 can be made dimensionless by setting up the dimensionless variables:

$$\tilde{x} = \frac{x}{L} \qquad \tilde{T} = \frac{T - T_e}{T_b - T_e} \tag{7}$$

$L$ is here the fin length, $T$ the local fin temperature and $T_b$ the fin's base temperature. The derivatives of the x-coordinate and temperature can be expressed as a function of the dimensionless variables:

$$\frac{d\tilde{x}}{dx} = \frac{1}{L} \qquad \text{or} \qquad dx = Ld\tilde{x} \tag{8}$$

So that:

$$\frac{d\tilde{T}}{dT} = \frac{1}{T_b - T_e} \quad \text{or} \quad dT = (T_b - T_e)d\tilde{T} \tag{9}$$

Substitution into equation 4 and rearranging the terms then leads to the following dimensionless second order differential equation:

$$\frac{d^2\tilde{T}}{d\tilde{x}} - \frac{h_c\mathcal{P}L^2}{k\mathcal{A}_c}\tilde{T} = 0, \quad \text{for} \quad (T_0 - T_e) \neq 0 \tag{10}$$

Which has the dimensionless solution:

$$\tilde{T} = B_1\mathsf{sinh}(a\tilde{x}) + B_2\mathsf{cosh}(a\tilde{x}) \tag{11}$$

with dimensionless fin parameter $a$ being:

$$a^2 = \frac{h_c\mathcal{P}L^2}{k\mathcal{A}_c} \tag{12}$$

The constants $B_1$ and $B_2$ can now be found, using the new dimensionless boundary conditions:

$$\tilde{T}\Big|_{\tilde{x}=0} = 1, \qquad \frac{d\tilde{T}}{d\tilde{x}}\bigg|_{\tilde{x}=1} = 0 \tag{13}$$

Applying the boundary conditions to equation 11 results in the following equation describing the dimensionless temperature profile along a simple fin in steady state:

$$\tilde{T} = -\tanh(a)\sinh(a\tilde{x}) + \cosh(a\tilde{x}) \tag{14}$$

For $a \neq 0$, and valid for $0 < \tilde{x} < 1$. Figure 2 Shows the dimensionless temperature profiles as described by this equation for different values of fin parameter $a$.

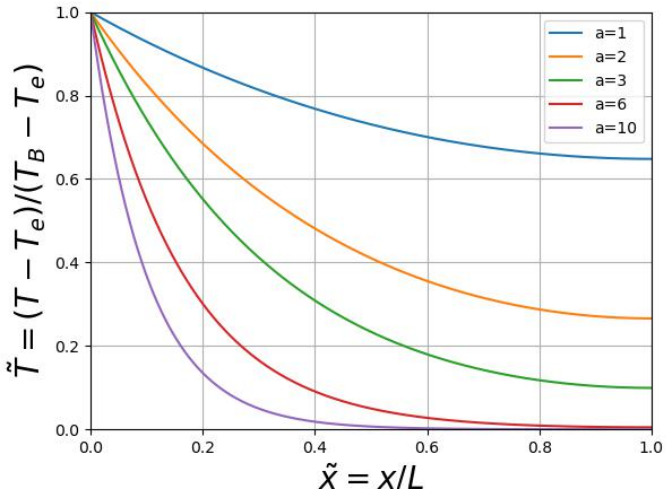


Figure 2: *Dimensionless temperature profiles along a simple pin fin for different values of fin parameter a, under the adiabatic tip assumption.*

# 3 Summaries of the experimental literature

The difficult part about porous fins is predicting their performance and optimizing its parameters. Important parameters that seem to be linked to heat dissipation performance of the fin are listed below. All of these parameters have a direct or indirect influence on the effective thermal conduction and the effective thermal convection of the porous fin. These parameters are:

- convective heat transfer coefficient;
- fin length scale;
- fin/fluid conductivity;
- fin/fluid temperature;
- fin/fluid heat capacity.
- fluid density;
- fluid velocity;
- fluid viscosity;

- gravity;
- porosity;
- pore size;

Almost all the literature regarding performance of porous fins are based on either numerical simulations, analytical derivations or a combination of those two. A common approach in the literature is to extend the simple solid fin energy balance, described by equation 1, with an extra term which accounts for a mass flow of $\rho v c_p \Delta T$ of the surrounding fluid going through the porous medium. It is then assumed that the fluid enters the porous medium at ambient temperature $T_e$ and reaches the local fins temperature before exiting. If radiation effects are taken into account, the extended energy balance becomes as written below. In this equation the coefficient for thermal conduction $k$ in Newton's law of conduction is replaced by an estimate (equation 17) for the effective conduction of the porous medium.

$$\begin{aligned}\frac{dE}{dT} =& \dot{q}\mathcal{A}_c|_x - \dot{q}\mathcal{A}_c|_{x+\Delta x} \\ &- h_c \mathcal{P} \Delta x \left(T - T_e\right) \\ &- \rho v c_p \Delta T \\ &- \mathcal{P} \Delta x \sigma \left(T_1^4 - T_2^4\right)\end{aligned} \tag{15}$$

In case of natural convection, Darcy's model for fluid flow through a porous medium is used to model the Buoyancy-driven flow:

$$v = \frac{g\beta \left(T - T_e\right)}{\nu} \tag{16}$$

in which $g$ is the gravitational constant, $\beta$ is the volumetric coefficient of expansion of the fluid, $T$ is the local fin temperature, $T_e$ is the ambient temperature and $\nu$ the kinematic viscosity of the fluid. This equation can then be solved numerically to predict a fin's performance. Examples of the usage of this model are Kiwan, 2006, Kiwan, 2007, Gorla and Bakier, 2011, Saedodin, Sadeghi, and Sadeghi, 2013, Das and Ooi, 2013, Das, 2014 and Sowmya et al., 2020. Other, more complex approaches, involve simulating the complete set of Navier-Stokes equations and energy equation simultaneously.

There also exist countless other articles that use a (semi-)analytical approach for solving the governing equations. Examples of this are the adomian decomposition method was used by Bhanja et al., 2010, but also Kundu and Bhanja, 2011 used a decomposition method. A differential transformation method was used by Torabi and Yaghoobi, 2013 to obtain a series solution. Türkyılmazoğlu, 2014 converted the governing differential equation into a Bessel differential equation with a non-homogeneous term, to obtain a solution.

These publications are some examples of non-experimental papers. After further evaluation, seem to be very little studies available that performed experiments on porous cooling fins. The next section contains summaries of relevant experimental work that was encountered during the literature study. The summaries appear in chronological order. A complete list that contains all relevant encountered articles (experimental, analytical and numerical) can be found in appendix A. This list gives an idea of the scarcity of experimental studies performed.

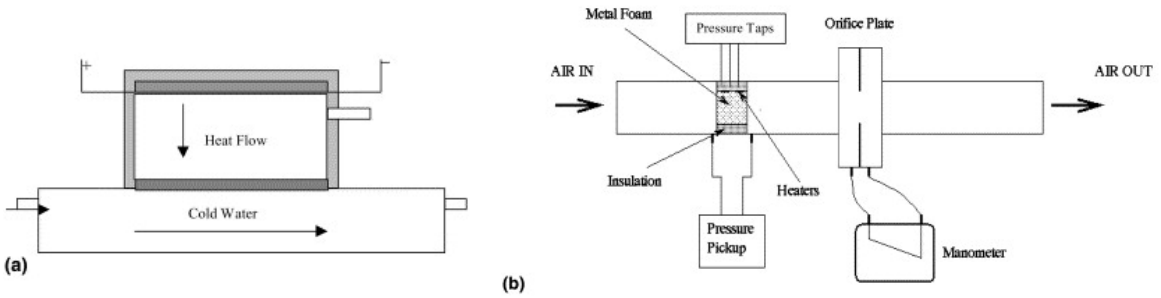


Figure 3: *Schematics of the setups used to determine the thermophysical properties. Image taken from A. Bhattacharya, Calmidi, and R. Mahajan, 2002.*

## 3.1 Thermophysical properties of high porosity metal foams

The oldest experimental article encountered is that of A. Bhattacharya, Calmidi, and R. Mahajan, 2002. The purpose of the paper is to find the thermal conductivity, permeability and inertial coefficient of (high) porosity foams. This is done by providing a comprehensive analytical and experimental investigation. The experiment is not so much about porous fins, but is nonetheless included in the summaries. The reason is that this article provides an empirical correlation (equation 17) as a way of calculating the effective conductivity of a porous metal, which is used extensively in analytical and numerical models encountered.

Two setups were used, which are shown in figure 3. The first setup (a) is used to measure the effective thermal conductivity. The aluminium foam sample is heated from above and cooled with cold water at the bottom side. The steady-state readings were taken from the temperature difference between the hot and the cold plate. Two formulas, including the heat flow and heat loss, were used to calculate the effective thermal conductivity. The second setup is about a porous sample, which is subjected to forced convection (b). The foam sample is positioned in a duct and spans the entire width and height of the duct. This way, an estimate of the pressure drop can be achieved.

The analysis shows that the effective thermal conductivity depends on the conductivity of the fluid $k_f$, the conductivity of the solid medium $k_s$ and its porosity $\varepsilon$. It does not depend on the pore size (or pore density). They proposed an empirical formula that describes the effective thermal conductivity $k_e$ for any random porous medium:

$$k_e = \mathcal{A}\left(\varepsilon k_f + (1-\varepsilon)\, k_s\right) + \frac{1-\mathcal{A}}{\frac{\varepsilon}{k_f} + \frac{1-\varepsilon}{k_s}} \quad (17)$$

The constant $\mathcal{A}$ has a value of 0.35.

## 3.2 Metal foam heat sinks for electronics cooling in Buoyancy-induced convection

The second experiment in this review was performed by Amitabh Bhattacharya and R. L. Mahajan, 2005. Figure 4 shows a schematic of the setup. The right side shows an image of the porous fin that was used. The samples that were tested were

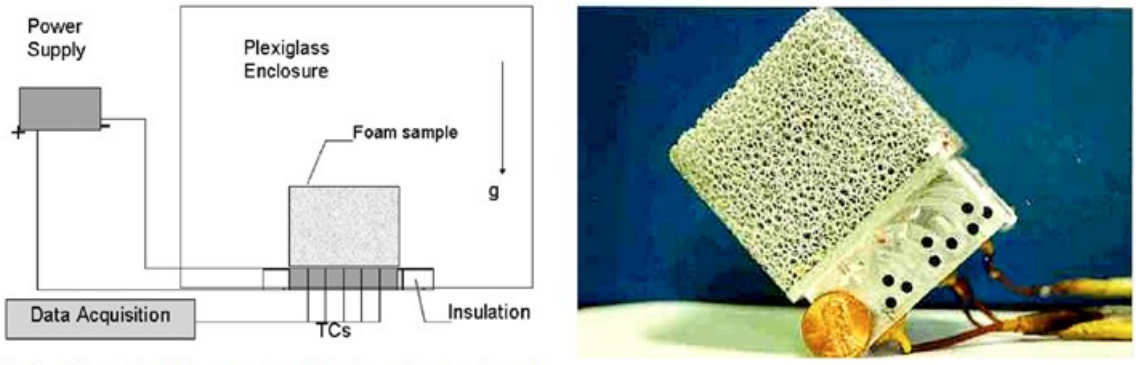


Figure 4: *Schematic of the experimental setup and image of the aluminium porous fin, published by Amitabh Bhattacharya and R. L. Mahajan, 2005.*

made out of aluminium and had a porosity of 0.89 to 0.96 with pore densities of 5, 10, 20, 40 pores per inch (PPI). The paper states that not many experiments have been performed on buoyancy-induced convection through a porous medium. They say that it seems that numerical analysis seem to consistently under-predict the experimental results. From their study, it looks like the porous sink heat transfer seems to be "marginal" compared to commercially available solid heat sinks of similar dimensions.

For the experiment, the test sample from figure 4 is set in a Plexiglas housing (isolated from the ambient). For each pore density corresponding to 5, 10, 20 and 40 PPI. Two different porosities were chosen as shown in table 1. The samples were fixed in vertical position and heated from the side.

Table 1: *Overview of the tested samples by Amitabh Bhattacharya and R. L. Mahajan, 2005. Values taken from the article.*

| Sample no. | PPI | Porosity | Permeability (x$10^7$) ($m^2$) | Inertial coefficient | Effective conductivity ($W/mK$) |
|---|---|---|---|---|---|
| 1* | 5 | 0.899 | 2.28 | 0.075 | 7.32 |
| 2 | 5 | 0.93 | 2.40 | 0.084 | 5.33 |
| 3 | 10 | 0.9085 | 1.62 | 0.078 | 6.71 |
| 4 | 10 | 0.9386 | 1.54 | 0.085 | 4.78 |
| 5 | 20 | 0.92 | 1.11 | 0.081 | 5.97 |
| 6 | 20 | 0.9353 | 1.14 | 0.085 | 4.99 |
| 7 | 40 | 0.9091 | 0.51 | 0.078 | 6.67 |
| 8 | 40 | 0.9586 | 0.54 | 0.086 | 3.48 |

* Could not be tested in vertical orientation.

The overall heat transfer coefficient for the entire heat sink (base plate and fin) was calculated using the total heat flow input $\dot{Q}$, the base plate area $\mathcal{A}_b$ and the difference in temperature between the base plate and ambient $T_b - T_e$, using the equation below:

$$h_c = \frac{\dot{Q}}{\mathcal{A}_b \left(T_b - T_e\right)} \tag{18}$$

**Influence of pore size on heat transfer**
If the porosity is held constant, the heat transfer rate is found to be lower at higher pore densities (smaller pore size). The explanation was given that the smaller pores make it harder for hot air to rise and escape from the fin.

**Influence of porosity on heat transfer**
For a given pore size, the heat transfer rate increases with porosity. This suggests that conduction is the dominant mode of heat transfer. An empirical correlation for the Nusselt number is proposed as:

$$\bar{Nu}_L = 38.94 Ra^{0.25} Da^{0.23} \tag{19}$$

This relation was found using a least squares fit on the data in from the plot for the Nusselt number above.

The next part of the experiment was performed using a horizontal position of the fins. In this part, the fins were heated from the side as opposed to the bottom in the previous part of the experiment. The found trends are similar to the vertical position and the same conclusions are drawn.

## 3.3 Natural convection in metal foam strips with internal heat generation

Hetsroni, Gurevich, and Rozenblit, 2008 set up an experimental study which aimed to investigate the heat transfer by natural convection of a horizontally suspended aluminium foam strip with internal heat generation. Two porosities were investigated: 0.896 and 0.97. An estimate of the non-equilibrium temperature distribution was done by image processing of the thermal maps on both the surface and the inner region of the metal foam specimen. Figure 5 below shows the schematics of the test setup. The thermal field of the outside of the porous strip was measured by a high-speed infrared camera. The specimen were therefore coated in black mat paint. The air temperature was measured by T-type thermocouples. The experiments were carried out under constant heat flux conditions.

The test samples were made from aluminium. The specific surface area ranged from 500 to 10,000 $m^2/m^3$. The pore densities were 20 and 40 PPI and the samples were tested in both horizontal and vertical position. Using an infrared camera, a temperature distribution and its standard deviation were established. The maximum, minimum and average temperature could be determined from this reading. The thermal heat values were recorded for every value of heat flux. An example of this is figure 6, which shows the spatial temperature distribution of the surface of the metal foam, as well as a histogram of the distribution. It shows a slight decrease in temperature along the length of the specimen towards the ends. The mean temperature can be estimated from the histogram plots. The following parameter was introduced:

$$\frac{STD\left(T_w\right)}{\left(T_w - T_a\right)} \tag{20}$$

in which $STD\left(T_w\right)$ is the standard deviation of the temperature and, $T_w - T_a$ is the difference in temperature between the

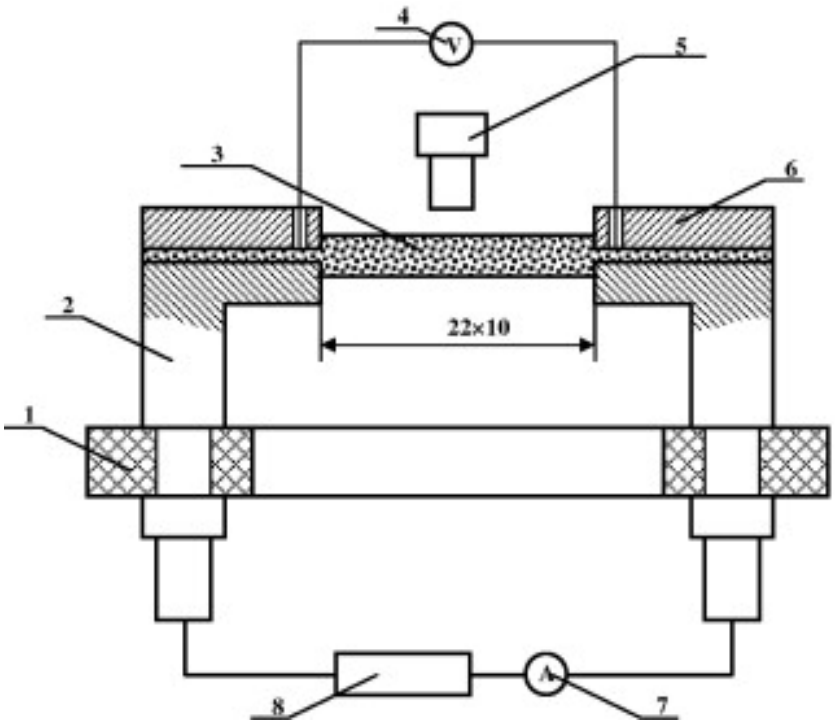


Figure 5: *Experimental apparatus: (1) housing, (2) aluminum contacts, (3) metal foam specimen, (4) voltmeter, (5) IR camera, (6) holder, (7) amperemeter, and (8) power supply. Image taken from Hetsroni, Gurevich, and Rozenblit, 2008.*

average cross section and the air-ambient temperature. They used the empirical correlation to predict the effective conductivity for porous metals (equation 17), as proposed by A. Bhattacharya, Calmidi, and R. Mahajan, 2002.

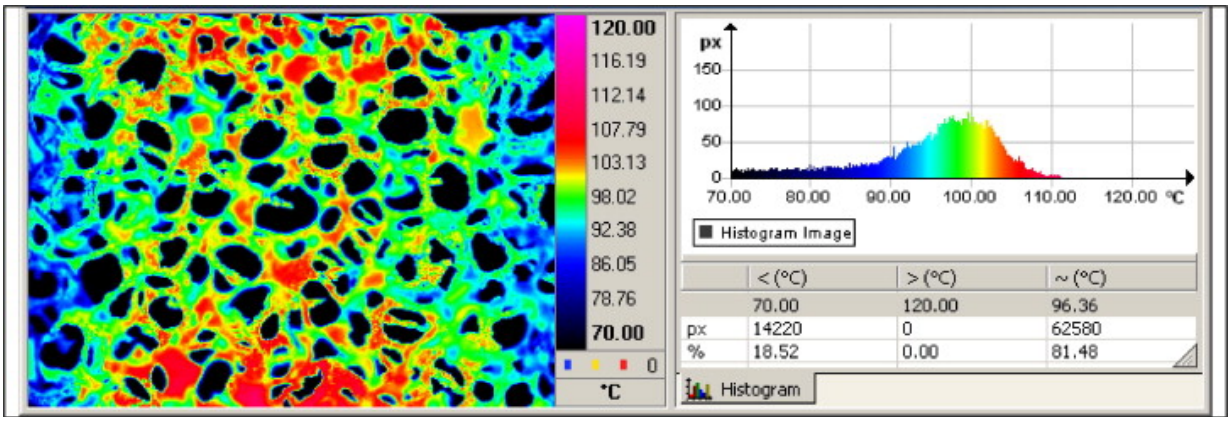


Figure 6: *Spatial temperature distribution of the surface of the metal foam, as well as a histogram of the distribution. Image published in Hetsroni, Gurevich, and Rozenblit, 2008.*

**Heat transfer**
The experimental setup was validated using a stainless steel strip with thickness of 50$\mu$m thickness. The Nusselt number was calculated and compared to literature. The experiment was performed on the metal foam specimen, both in horizontal and vertical positions. The heat transfer is increased dramatically (up to 18 – 20 times) for metal foam of 20 PPI relative to the flat plate of same dimensions.

## 3.4 Air natural convection on metallic foam-sintered plate

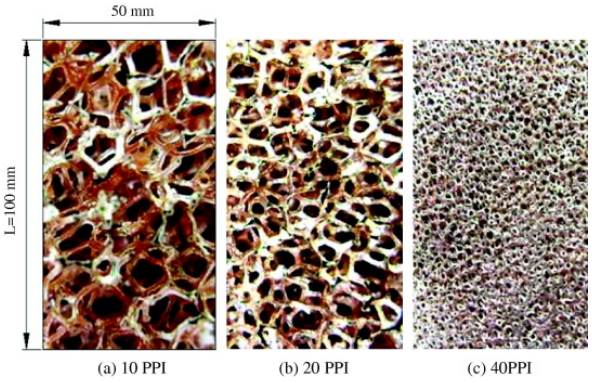


Figure 7: *Close-up of the copper foam-sintered samples used by Qu et al., 2012. The images show different pore densities.*

Copper samples like the ones shown in figure 7 were tested under natural convection regime by Qu et al., 2012. The goal of the study was to come up with an empirical correlation to predict natural convection on a plate sintered with foam at different inclination angles. The test samples are copper foam, as shown in figure 7. The length and width of the fins are both kept constant at 100 millimeters, with the thickness ranging from 10 to 50 millimeters. There were seven samples with two distinct porosities (0.90 and 0.95) and three different pore densities (10, 20 and 40 PPI). Figure 8 below shows the schematics of the experimental setup. The foam sample is attached to a heated bottom plate, which contains thermocouples to measure the temperature. The sample can be set at inclined angles: 0 (vertical orientation), 15, 30, 45, 60, 75 and 90 degrees. Nine T-type thermocouples are located at the substrate. Another two were positioned along the sample length to investigate the local heat transfer coefficient. The heat flux density was adjusted from 300 to 3000 W/m$^2$. All measurements were taken at steady state conditions. The convective heat transfer coefficient was determined using equation 18, for both the local and the overall heat transfer coefficient. The distinction is made by varying the power $\dot{Q}$ and temperature accordingly.

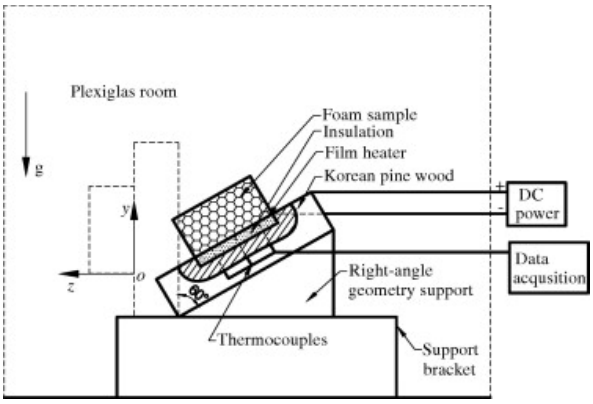


Figure 8: *Schematic of the experimental setup used by Qu et al., 2012.*

**Heat transfer performance**
The aspect ratio is fixed at 0.5 and the heat flux is set to 1000 W/m$^2$. The optimal inclination range seems to be 60 to 75 degrees. An increase in porosity leads to heat transfer enhancement to the air. However, the

dominant process seems to be the heat conduction through the foam, which reduces with increasing porosity. The average Nusselt number decreases with increasing pore density. The average Nusselt number increases with increasing heat flux. Also, the effect of inclination angle on the average Nusselt number is more evident for higher heat fluxes.

**Local heat transfer**
Two samples are used for this part of the experiment. The porosity is kept fixed at a value of 0.9 and the aspect ratio at 0.5. One sample with pore density of 10 PPI and one with 40 PPI. The 10 PPI sample had a higher heat transfer coefficient.

## 3.5 Buoyancy-driven flow in open-cell aluminium foam heat sinks

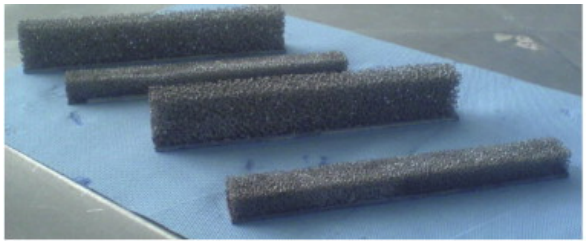

Figure 9: *Image of the aluminium foam sample from De Schampheleire et al., 2013.*

De Schampheleire et al., 2013 study focused on heat removal by the use of buoyancy driven flow through a aluminium foam heat fin. The foams are show in figure 9. The length-to-width ratio of the samples is kept constant at a ratio of 10. The studied samples have pore densities of 10 and 20 PPI, both with a porosity of 0.93. The following parameters are investigated:

- the foam height (varied between 6 and 40 mm for the 10 PPI foam between 6 and 18 millimeters for the 20 PPI foam);
- bonding method to the base plate;
- influence of the Rayleigh number on heat transfer.

The samples are fixed to a copper plate which has six flat K-type thermocouples mounted onto it to ensure a uniform heat flux from below. The entire setup is then place inside an insulating box. The air temperature inside the box is measured by twelve thermocouples which are placed near the walls. The applied heat flux can be set to 100 watts. The bonding of the samples is different for the 10 PPI and the 20 PPI. All measurements were performed at steady state conditions. The validation of the test setup is done by comparing the flat plate conditions (no heat sink) to that of existing literature. The sensitivity to the test setup geometry was also evaluated as a validation. The lumped Nusselt number was reported, as this number is of most relevance in industry according to the authors.

**Influence of pore density**
Lower pore densities seem to increase the heat transfer. The explanation is given that a bigger pore size makes it easier for the buoyancy driven flow to get through the foam. The difference in heat transfer is mostly due to the limitation of heat transfer by conduction through the solid material

**Influence of foam height**
Increasing the foam height leads to an increase in heat transfer. The effect (within the uncertainty) seems to be the same for both pore densities. The article notes that the heat transfer decreases again for heights above a certain point. The expla-

nation provided is that a very long foam fin obstructs the buoyancy-driven flow of hot air away from the fin.

## 3.6 Heat dissipation performance of copper with elongated cylindrical pores

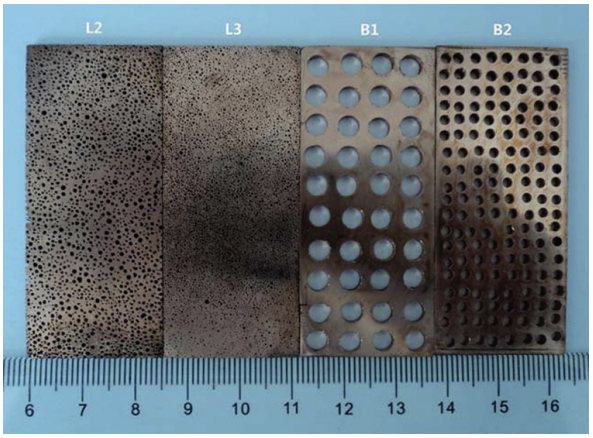


Figure 10: *Image of the samples used by Du et al., 2014. L2 and L3 were formed using a unidirectional solidification method. The holes in samples B1 and B2 were drilled.*

Du et al., 2014 focuses is their paper on the heat dissipation of porous copper fins. Figure 10 shows four samples of the tested fins. Two of the porous samples in this study were fabricated by the unidirectional solidification method. They are labeled L2 and L3 in the figure. The fins labeled with B1 and B2 have bored holes in them. All the samples were cut to the right thickness along the vertical direction of the pore axis. The heat dissipation of the L2 and L3 samples were compared to that of bulk copper, as well as the bored samples. The samples had the following characteristics:

- dimensions: 60 x 26 x 2 $mm^3$;
- porosities: 0.298, 0.345 and 0.510.

They also used equation 18 to determine the heat transfer coefficient. The performance of the samples was tested under transient conditions, forced convection and air as the cooling fluid. The air speed for forced convection was 2 m/s. The samples were heated at the bottom by water at a temperature of 80 °C. The heat dissipation was determined by checking the temperature of the water. The setup validation is done by comparing the performance of the copper plates with that of the heated water and the bottom plate only. Figure 11 shows a schematic of the test setup.

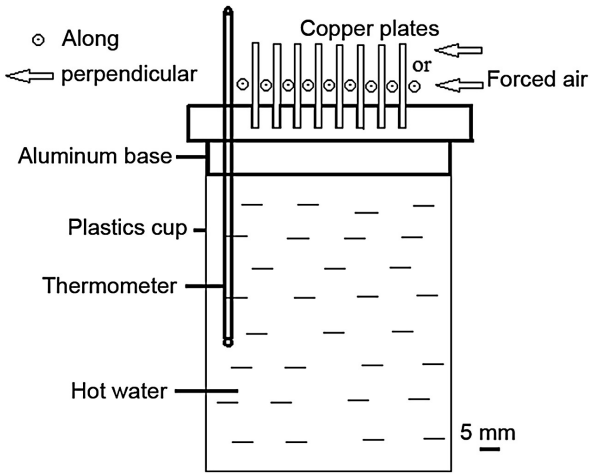


Figure 11: *Schematic of th setup used by Du et al., 2014.*

**The influence of the copper plates on heat dissipation**

The performance of the different copper plates from figure 10 in their heat dissipation capacity were tested against that of the aluminium base plate only. A graph in their article shows that the copper plates do help dissipate the heat faster. However, the difference between the copper plates seems indistinctive.

**Forced convection (and direction) vs natural convection**
Samples with porosities of 0.510 and 0.299 were chosen. The results show that the heat dissipation rate is about five to six times higher for forced convection than it is for natural convection. The influence of forced convection direction was also tested: the heat dissipation rate is higher in the case were the air is forced along the copper plates. The assumption for this is given to be caused by the fact that the performance declines per plate in case the air flows perpendicular to the plates, as the air is having more and more trouble flowing past and through the plates.

**The influence of porosity and pore density**
This part of the experiment was done under forced convection, with the fluid direction parallel to the plates. It seems that the heat dissipation rate increases with increasing porosity, especially at temperatures higher than 50°C. The paper states that a clear relation between porosity and heat dissipation rate does not exist. They mention that the dissipation rate is likely a balance between heat conduction and convection. Conduction will decrease with increasing porosity, but heat convection will increase with increased porosity due to the positive relation between porosity and surface area. The porosity of the four samples were kept within four percent of the same porosity. The heat dissipation rate is higher for the smaller pore sizes. There seems however not a simple linear relation between pore size and heat dissipation.

## 3.7 Performance of open pore metal foam heat sinks

Aly, Arif, et al., 2016 performed an experimental study on aluminium porous fins. They used a reverse engineering technique of CT scanning to make a three dimensional CAD model of their porous fin, after it was physically build. Three fins were fabricated:

- solid;
- metal foam (joined to base plate with a conductive epoxy);
- metal foam (joined to base plate with thermal spray).

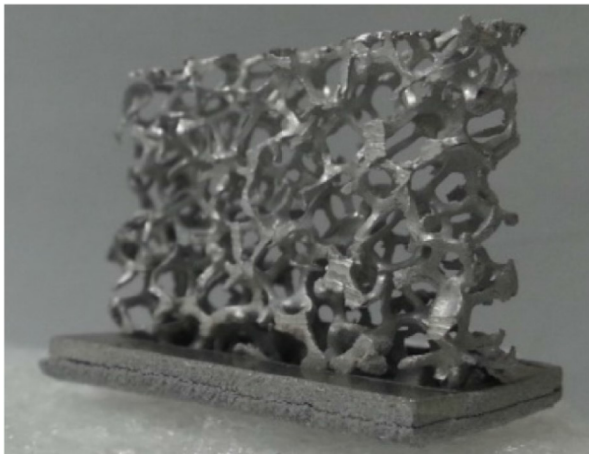

Figure 12: *Image of the physical porous aluminium fin, used in the experiments performed by Aly, Arif, et al., 2016.*

The metal foam fins were made from aluminium 6101 alloy with a 0.93 porosity. The single-fin samples had a pore density of approximately 10 PPI, and the multiple-fin samples of approximately 20 PPI. Figure 12 shows an image of the physical porous aluminium fin as used in their experiments. The aim of the study was to analyze the performance of different heat sinks.

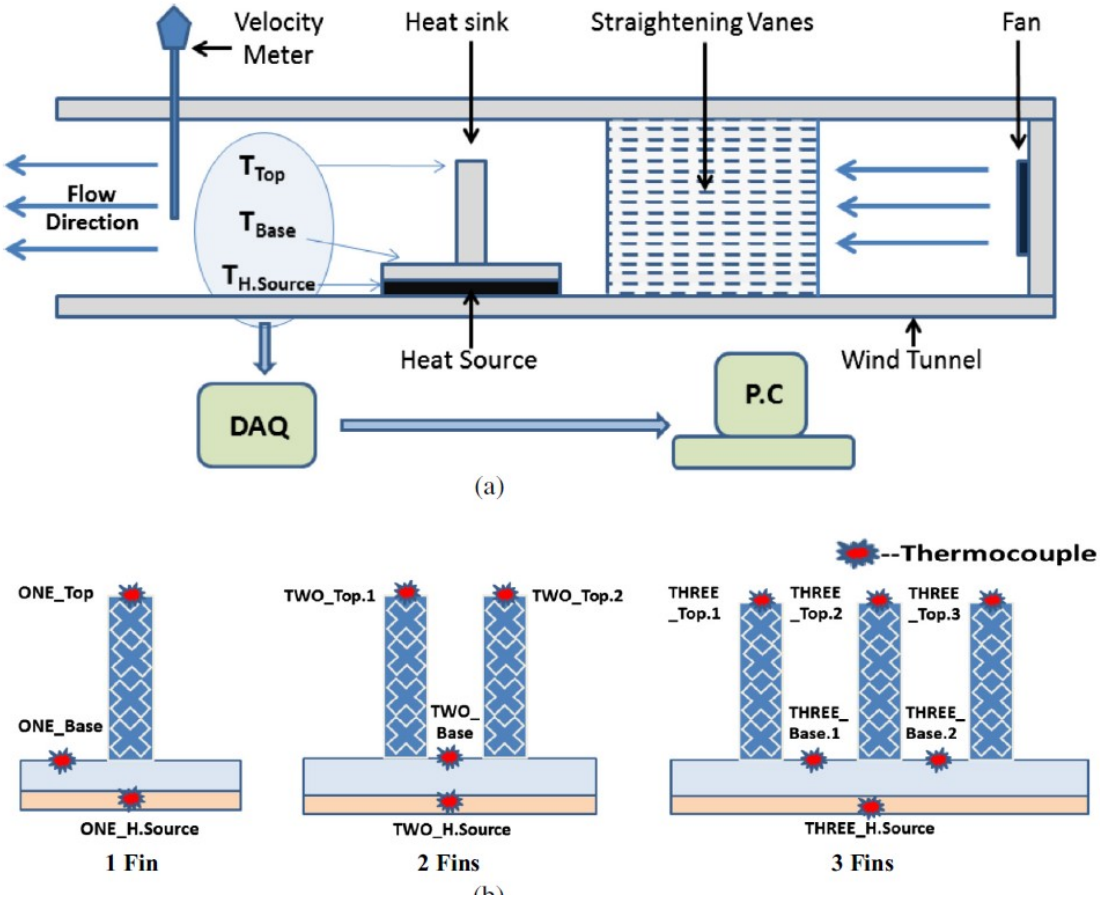


Figure 13: *Schematic of the setup used by Aly, Arif, et al., 2016. A 5 Watt heat source is attached to a base plate which is made from the same material as the fins.*

Figure 13 shows a schematic of the setup. A 5 watt heat source is attached to a base plate which is made from the same material as the fins. Attached to this plate is the fin itself. The sample is placed inside a duct through which air can be blown by a fan at a controlled speed. The orientation shown in the figure is 90 degrees with respect to the air flow. The fan is turned off at be beginning of every experiment while the sample is heated up. When the source reaches a temperature of 60°C, the fan is turned on. The following parameters were tested:

- fin type (solid/porous);
- air speed;
- fin orientation;
- number of fins;
- type of thermal coupling to base plate.

Thermocouples were placed at the source, the base and the fin tip as indicated by figure 13. Based on those readings, the overall performance could be expressed as the convective heat transfer coefficient of the complete setup, using again equation 18.

Using a FEM-method on their CAD model, they managed to "tune" the heat transfer

coefficient for the fin only, so that the simulation matched the readings of the thermocouples. This effective heat transfer coefficient was approximately 132, 210 and 245 for the solid fin, porous fin (conductive epoxy) and porous fin (thermal spray) respectively.

The conductivity was found in literature to be 218 W/m/K for the solid material, and the effective conductivity for the porous samples was found to be 5.8 W/m/K, using the results published by A. Bhattacharya, Calmidi, and R. Mahajan, 2002.

**Influence of fin type on performance**
The results show that for the solid fin, the base and tip temperature are practically the same under the natural convection (fan-off) conditions. In forced convection, the temperature gradient along the fin is still small. The temperature gradient is much larger for the porous fins under forced convection. The effective heat transfer coefficient for both porous fins are comparable and are both higher than for the solid fin.

**Influence of air speed on performance**
The influence of air speed on heat dissipation by the fin was only tested for the porous fin that was attached to the base with thermal spray. The experiment revealed that the effective heat transfer coefficient increases almost linearly with increasing air speed.

**Influence of fin orientation on performance**
The experiment shows that, under forced convection, the orientation to get the higher effective convective heat transfer coefficient is when the fin is oriented perpendicular to the direction of the fluid flow. In this orientation, the steady state is reached the quickest and the base temperature reaches its lowest value at steady state.

**Influence of number of fins on performance**
The experiment shows that an array of multiple fins has a relative lower overall convective heat transfer coefficient than a single fin only. An orientation of 45 degrees, with respect to the fluid flow direction, seems to result in the highest overall convective heat transfer coefficient by reducing hinder of the air flow through the metal matrix.

## 3.8 The effect of aluminium porous fins on heat transfer

Figure 14: *Impression of the porous aluminum fins configuration on the test section. Image taken from Bilen et al., 2017.*

Figure 14 shows an impression of the array of aluminium porous fins that were used in an experimental study performed by Bilen et al., 2017. They investigated the array under forced convection conditions. They state that porous fins, in comparison to solid fins, could decrease the pressure drop over the fins while also enhancing heat transfer to the fluid. A setup was built in which the gap-to-fin height inside a duct could be varied. This open gap above the array of fins plays an important role in the total pressure drop and heat transfer. The specification of the fins tested are listed in table 2. The specifications of the channel geometry and fin arrangement are listed in table 3.

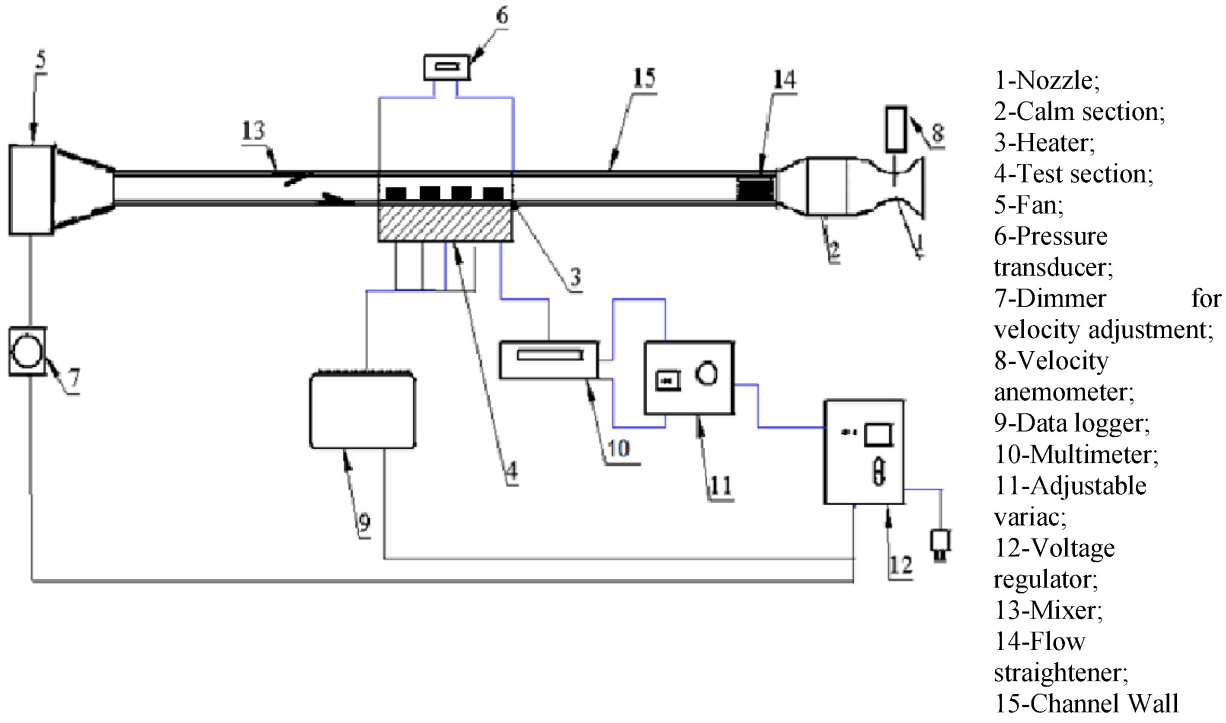


Figure 15: *Image of the setup schematic as published by Bilen et al., 2017.*

Figure 15 shows the schematics of the setup. Air is forced through a closed duct by a fan. In the middle of the duct is the array of fins located. An open gap can be seen above the fins. Three longitudinal pitches were tested for Reynolds numbers varying from 5,000 to 35,000. Number 3 indicates the heater. Nine T-type thermocouples were installed to measure the temperature at the base of the fins. A total of sixteen fins were places in an array. The longitudinal pitch in the fluid flow direction was varied as follows: 116, 126 and 136 millimeters. The transversal pitch was kept constant at 40 millimeters. The gap height was varied by varying the top height of the duct. The gap heights were studied: 50, 75 and 100 millimeters. The tempera-

Table 2: *Physical properties of foam materials. Here, $k_{eff}$ [W/m/K] is effective thermal conductivity, $\varepsilon$ is porosity, $\alpha$ (1/m) is surface area to volume ratio, K ($m^2$) is permeability, F is inertia coefficient. Data taken from Bilen et al., 2017.*

| Material | $k_{eff}$ | $\varepsilon$ | PPI | $\alpha(1/m)$ | $K(m^2)$ | F | Ref. |
|---|---|---|---|---|---|---|---|
| Aluminium | 4.1 | 0.91 | 10 | 820 | $4.21\text{x}10^{-8}$ | 0.0076 | Leong and Jin, 2006 |
| Aluminium | 5.1 | 0.9 | 20 | 1700 | $3.12\text{x}10^{-8}$ | 0.0105 | Leong and Jin, 2006 |
| Aluminium | 5.9 | 0.9 | 40 | 2800 | $2.86\text{x}10^{-8}$ | 0.0155 | Leong and Jin, 2006 |
| Ceramic | 3.38 | 0.875 | 20 | | $2.2\text{x}10^{-7}$ | 0.162 | Jeng and Tzeng, 2006 |
| Bronze | 10.29 | 0.38 | | | $1\text{x}10^{-9}$ | 0.118 | Jeng and Tzeng, 2006 |
| Graphite | 130 | 0.728 | | | $7.924\text{x}10^{-10}$ | 0.071 | Leong, Hongyu Li, et al., 2010 |

ture of the fluid was measured both at the entrance and the outlet of the duct. A total convective heat transfer coefficient $h_c$ was calculated using equation 18. The net heat flow is calculated as below:

$$Q = Q_{\text{vol}} - (Q_{\text{con}} + Q_{\text{rad}} + Q_{\text{axi}}) \qquad (21)$$

In which $Q_{\text{vol}}$ is the applied heat and the other three terms are the heat losses (conduction, radiation and the axial heat loss along the channel wall). The following parameters were varied:

- material (table 2);
- porosity (table 2);
- pore density (table 2);
- channel height (table 3);
- hydraulic diameter (table 3);
- fin-to-gap height ratio C/H (table 3);
- longitudinal pitch (table 3);
- Reynolds number.

**The influence of geometric parameters on performance**
It was observed that the ratio gap to fin height (C/H) played an important role on the heat transfer enhancement in the channel. The case C/H=0 provided the highest heat transfer rate, because air is now forced through the porous fins. The results were also plotted against different types of (solid) fins, such as Incropera, 2006. Staggered ribs from the literature provided better heat transfer than the foam fins for C/H=1. However, the heat transfer of porous fins is always higher than that of solid longitudinal fins for the Reynold numbers studied. To see the influence of the longitudinal pitch, C/H was kept fixed at 0.5 and 1. Nusselt numbers become close to each other with increasing Reynolds numbers. The change in Nusselt number was much higher for 0.0 < C/H < 0.5 than for 0.5 < C/H < 1.0. It was found that the friction factor is very dependent on C/H. It appeared that the friction factor was not influenced much by changing the longitudinal pitch.

**The heat transfer enhancement ratio**
The heat transfer enhancement ratio ($Nu^*$) is determined as follows:

$$Nu^* = Nu/Nu_0 \qquad (22)$$

In which $Nu_0$ is the case without any fins (empty duct). The longitudinal pitch is varied: 116, 126, 136 millimeters. For a fixed pitch, the heat transfer enhancement ratio decreases with increase in gap height. The results of this part of the study were compared with two different results from literature: ribs and one block of porous material as published by Jeng and Tzeng, 2006.

Table 3: *Geometrical variation of the test setup for the cases studied by Bilen et al., 2017.*

| | **Case 1** | **Case 2** | **Case 3** |
|---|---|---|---|
| Channel height (mm) | 50 | 75 | 10 |
| Hydraulic diameter (m) | 0.080 | 0.109 | 0.133 |
| Fin-to-gap-height ratio C/H | 0 | 0.5 | 1 |
| Longitudinal pitch | 116 | 126 | 136 |

## 3.9 Natural Convection in open slots Metal Foam Heat Sinks

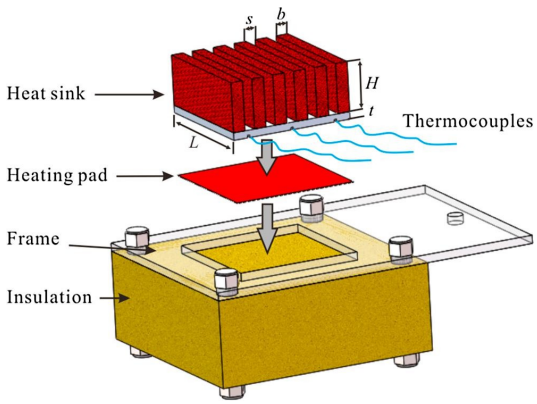


Figure 16: *Schematic of the setup used by Feng et al., 2018.*

Feng et al., 2018 published an article about natural convection in open-foam heat sinks. Figure 17 shows an impression of the different fins that were tested. The samples were made out of copper foam with a porosity of 0.91 and a pore density of 5 PPI. The fin geometry (b x L) was 10 x 100 millimeters. Table 4 gives an overview of the 29 heat sink samples that were tested. The following parameters were varied:

- fin separation distance;
- fin height (10, 20, 40 and 80 mm);
- heat sink orientation.

Figure 16 shows the schematic of the used setup. The copper porous fins are connected to a aluminium base plate. Contact resistance is assumed to be negligible. The base plate has grooves cut into its bottom in which 36 T-type bead thermocouples are embedded. The applied power input ranged from 0.8 to 24 watts. The performance of the setup was evaluated by calculating the overall convective heat transfer coefficient using equation 18.

**Open slot distance and performance**

This effect is tested in horizontal position (fins pointing up). The base plate has fixed dimensions. They found in this test that the ideal number of fins varies somewhat with fin height. The heat sinks with zero open slot distance (ten fins), or foam block, performed the worst for all the tested fin lengths. The highest overall convective heat transfer coefficient was reached for five, six or seven fins, depending on their lengths. This result is consistent for a difference in temperature between $T_b$ and $T_e$ ranging from 5°C to 75°C.

The article also reports findings about the optimum open slot distance. When fixing the difference in temperature between $T_b$ and $T_e$ at 50°C, it seems that the optimum distance is 5 to 8 millimeters for both horizontal and vertical orientation.

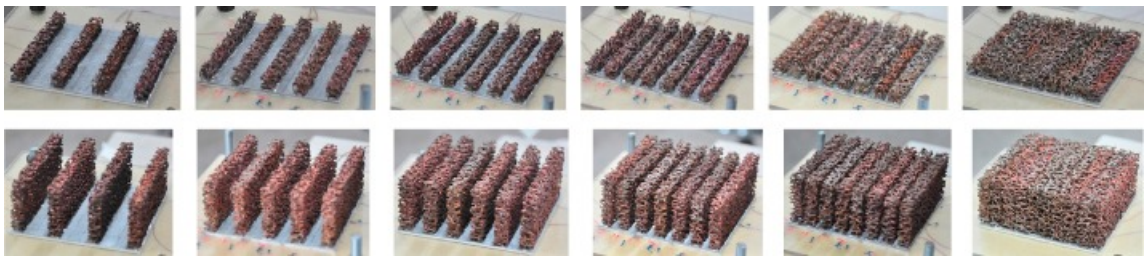

Figure 17: *The copper fins attached to an aluminium base plate. Image from Feng et al., 2018.*

Table 4: *Total overview of heat sink samples. The values were copied from Feng et al., 2018.*

| No. | Height (mm) | Slot width (mm) | Number of fins | No. | Height (mm) | Slot width (mm) | Number of fins |
|---|---|---|---|---|---|---|---|
| 1 | 10 | 0 | 10 | 16 | 40 | 8 | 6 |
| 2 | 10 | 2.86 | 8 | 17 | 40 | 12.5 | 5 |
| 3 | 10 | 5 | 7 | 18 | 40 | 20 | 4 |
| 4 | 10 | 8 | 6 | | | | |
| 5 | 10 | 12.5 | 5 | 19 | 60 | 2.86 | 8 |
| 6 | 10 | 20 | 4 | 20 | 60 | 5 | 7 |
| 7 | 20 | 0 | 10 | 21 | 60 | 8 | 6 |
| 8 | 20 | 2.86 | 8 | 22 | 60 | 12.5 | 5 |
| 9 | 20 | 5 | 7 | 23 | 60 | 20 | 4 |
| 10 | 20 | 8 | 6 | 24 | 80 | 0 | 10 |
| 11 | 20 | 12.5 | 5 | 25 | 80 | 2.86 | 8 |
| 12 | 20 | 20 | 4 | 26 | 80 | 5 | 7 |
| 13 | 40 | 0 | 10 | 27 | 80 | 8 | 6 |
| 14 | 40 | 2.86 | 8 | 28 | 80 | 12.5 | 5 |
| 15 | 40 | 5 | 7 | 29 | 80 | 20 | 4 |

**Foam height and performance**
Tests were performed in both horizontal and vertical orientation. The overall performance of the heat sink increased with increased fin length for the tested heights, although it seems to be flattening off.

**Orientation and performance**
The difference in performance was evaluated between horizontal and vertical orientation. The fin length was varied (10, 20, 40 and 80 mm). Two runs were performed for each fin length. The number of fins per heat sink was fixed at six and ten. The overall heat transfer coefficient turned out be be higher for the horizontal position for all tested fin lengths. The only exception was the vertical orientation that performed better for 80 millimeter fins, with six fins per heat sink.

**Fluid temperature profile above the fin**
A sample with six porous fins of fin height 40 millimeters was positioned horizontally. The distribution of air was measured at various points above the fins. figure 18 shows the obtained temperature profiles. The temperature profile demonstrates that the air is passing through the porous filters, enhancing heat transfer away from the heat source.

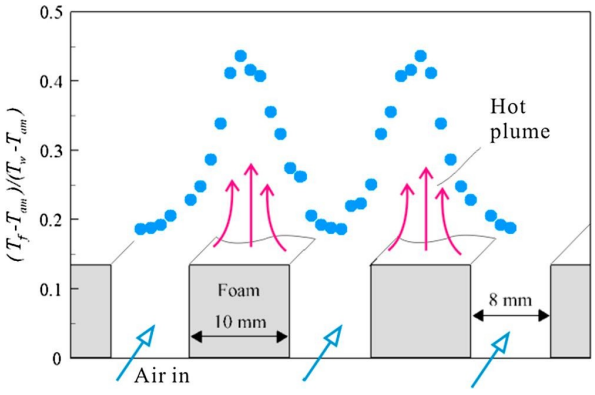


Figure 18: *Schematic image of the Gaussian-like temperature distribution as measured above the fin. Image from Feng et al., 2018.*

## 3.10 3D Metal printed heat sinks

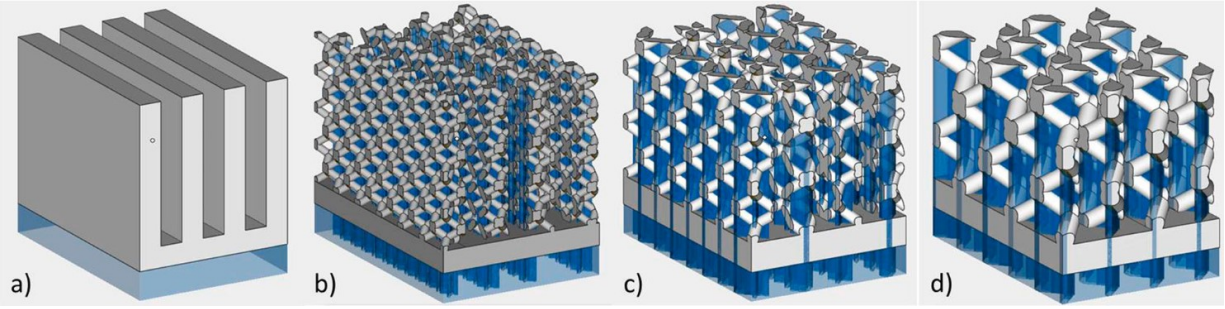


Figure 19: *(a) Solid, (b) Lattice 1, (c) Lattice 2, (d) Lattice 3. Image from Shamvedi et al., 2018.*

Figure 19 shows an image of the CAD models of the heat sinks that were tested by Shamvedi et al., 2018. The left heat sink (a) is made out of solid material and is claimed by the authors to be comparable to commercially available heat sinks. The other three were obtained using 3D printing. The heat sinks are made out of maraging steel and the samples differ only in their lattice sizes. The authors of the article state that the big advantage of 3D printing is that the printed structures (Direct Metal Laser Sintering in this case) have predictable, repeatable patterns. This is not the case for metal foams, as its structure is random, which complicates production of heat sinks and prediction of their behavior.

**The effect of lattice structure on heat dissipation**

The experiment was performed for the natural convection regime. The results of the printed porous fins are compared to longitudinal fin solid heat sink (LFSHS). A constant heat flux of 11 watts was supplied. A surprising result was that the solid fins outperformed all the porous structured ones. The explanation was given that the heated air can advect less freely due to the lattice structure than it will in the case of solid fins.

## 3.11 heat transfer from a vertical cylinder using porous fins

Kiwan, Alwan, and Abdelal, 2020 performed an experimental study on annular porous heat fins around a suspended heated cylinder. Figure 20 shows a picture of some of the setups. The fins were made using anvil expanded mesh cladding, which creates a mesh-like structure in the metal. Two types of porosities were created: one with higher porosity/lower permeability and vice versa. The experiment was conducted for steady state, natural convection heat transfer. A constant heat flux was applied. The effect of varying the following parameters was studied:

- Type of fins
- Number of fins
- Fin thickness
- Cylinder diameter

Figure 21 shows the schematic of the setup. Seven k-type thermocouples measured the temperature along the cylinders length. When steady state was reached (when the change in temperature in the cylinder becomes less than +/- 0.5 kelvin over 45 minutes), the analysis was made.

Figure 20: *Some examples of the annular porous fins attached to a suspended heated cylinder that were tested by Kiwan, Alwan, and Abdelal, 2020.*

The permeability of each fin was tested experimentally by placing it in a wind tunnel and measuring the pressure drop for a range of fluid velocities. The experimental setup was verified by comparing the experimental results for the Nusselt number of a vertically suspended heated cylinder with data from literature. The diameters studied were: 50, 60 and 80 millimeters. Two types of porosities were studied: 0.969 (A) and 0.979 (B). The three setups were as follows:

- One and three of porous ring fins (type A and B), fin thickness of 10 millimeters, attached to all cylinders.
- One, three and five of porous ring fins (type A and B), fin thickness 20 millimeters, attached to all cylinders.
- Fin thickness 50 millimeters, attached to the 50 millimeter cylinder.

**Varying number of fins and porosity**

The Nusselt number appears to be a strong function of the permeability of the fins. Higher permeability enhances the fluid flow through the fins. There is a direct proportionality between the number of fins and the heat transfer rate. The difference in temperature between the cylinder and surrounding fluid increases with increasing applied power. The other test samples (60 and 80 millimeters cylinders) show the same trends.

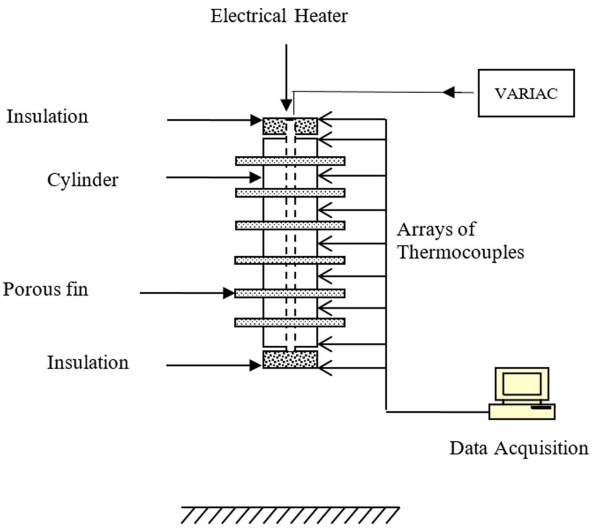


Figure 21: *Schematic of the suspended heated cylinder setup used by Kiwan, Alwan, and Abdelal, 2020*

**The effect of fin thickness**

The Nusselt number appears to strongly de-

pend on the fin thickness. An increase in fin thickness results in an increase in Nusselt number.

## 3.12 open-pore metal foam and foam-fin heat sinks

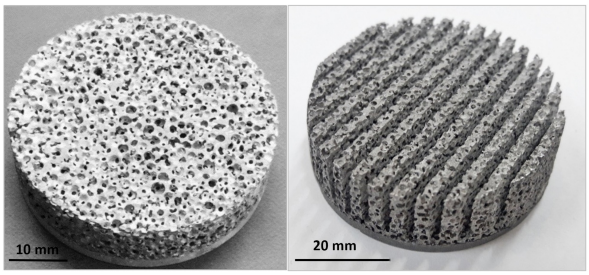


Figure 22: *Image of the porous heat sinks tested by Samudre and Kailas, 2022. Two of the samples are shown: no fins (left) and thirteen fins (right).*

This experiment was performed by Samudre and Kailas, 2022 and tests the performance of porous fins, without having to deal with the coupling of the fins to a base plate. Instead, the fins are directly made out of one piece of foamy material. The foam and the substrate are then thermally fused bonded. Aluminium foam with a porosity of 0.65 is used. The sample on the right consists of thirteen fins. The next parameters are investigated:

- geometrical configuration;
- pore density;
- fin height;
- number of fins.

Table 5 Shows an overview of the tested fin samples. Tests were performed both in natural and forced convection. During testing of the natural convection, heat is applied through the circular copper plate at the bottom of the heat sink. The bottom side is insulated. Three thermocouples register the temperature at the bottom of the heat sink. A funnel-like casing separates the experiment from its surroundings.

For the forced convection tests, an imitation of the cooling procedure for a typical CPU was set up. Cold air is forced by 12 volt CPU fans onto the heat sink from above. The air can flow away through the sides at the bottom. The air velocities range from 1 to 6 m/s. The temperature is measured at the heating element ($T_b$) and the surroundings ($T_e$). From this, the overall heat transfer coefficient for the entire heat sink is calculated using equation 18. This means that the heat sink performance is inversely proportional to the base plate temperature.

**Varying pore density and fin height under natural convection**
The finned heat sink is tested in both horizontal and vertical orientation. The foam heat sink with fins cut into it in vertical orientation shows the lowest bottom temperature.

The results show that the porous samples (both with and without fins) consistently outperform the solid ones. To look into the effect of pore density, the pore diameters that were tested were varied: 0.3, 1.1, 1.9 and 3.1 millimeters. The fin heights were varied from 2 to 25 millimeters. The result shows that the overall heat transfer coefficient varies linearly with fin height for the all-foam samples. Also, the heat transfer coefficient increases with decreasing pore diameter.

**Varying pore density and fin height under forced convection**
The same parameters were tested under forced convection.

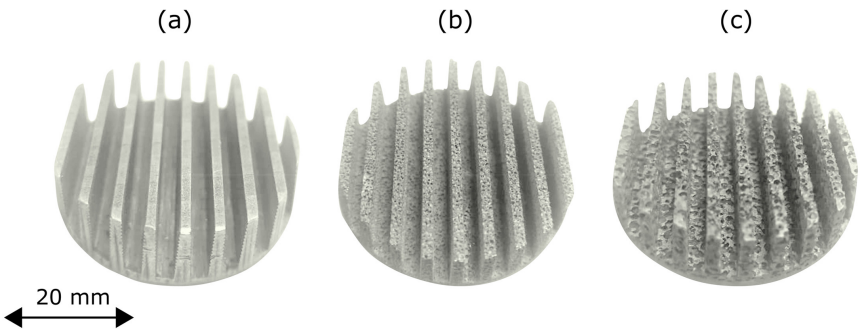


Figure 23: *Overview of the heat sinks that were compared by Samudre and Kailas, 2022. solid CF-1 (a), Porous (b) and (c). All samples were given the same dimensions as the commercially available CF-1.*

The air velocity is kept fixed at 2 m/s, while the influence of foam height (no fins) for different pore diameters was evaluated. Also in this case, the heat transfer coefficient increases with an increase in foam height. Heat transfer also increases by reducing the pore diameters.

**Comparison with commercially available solid heat sink**

Figure 23 shows the heat sinks that were compared. The comparison happened under forced convection. The most left sample is the solid CF-1, which is commercially available. The results show that the foamy fins always perform better in transferring the heat away from the heat source. Also, the sample with the smallest pore diameter performs the best.

Table 5: *Overview of fin samples tested by Samudre and Kailas, 2022*

| Type<br>- | Height<br>(mm) | Number of fins<br>- | S / V approx.<br>(1/m) | Weight<br>(gm) | Diameter<br>(mm) |
|---|---|---|---|---|---|
| CF-1 | 10 | 09 | 670 | 16.61 | 45.5 |
| CF-2 | 17 | 09 | 670 | 22.12 | 45.5 |
| Foam | 10 | - | 3141 | 16.32 | 45.5 |
| Foam-fin | 10 | 09 | - | 11.56 | 45.5 |

# 4 Listed overview of the findings per article

The table below contains an overview of the most important findings drawn from the encountered experimental research papers. The articles are placed in chronological order. To make a distinction between natural convection and forced convection, the findings of forced convection are displayed in a blue font.

| Article | Findings |
|---|---|
| A. Bhattacharya, Calmidi, and R. Mahajan, 2002 | • The effective thermal conductivity of porous metal foam depends strongly on the porosity and the ratio of cross-sections of the fiber and the intersection.<br>• An analytical model is proposed to predict the friction factor.<br>• An empirical formula is proposed to predict the effective conductivity of metal foams:<br>$$k_e = \mathcal{A}\left(\varepsilon k_f + (1-\varepsilon)\, k_s\right) + \frac{1-\mathcal{A}}{\frac{\varepsilon}{k_f} + \frac{1-\varepsilon}{k_s}} \quad (23)$$ |
| Amitabh Bhattacharya and R. L. Mahajan, 2005 | **Aluminium foam strip (one fin).**<br>• Numerical analysis seems to systematically underpredict experimental results.<br>• The heat transfer increase for porous strips seems to be marginal compared to commercially available ones.<br>• The heat transfer is found to be lower at higher pore densities.<br>• The heat transfer rate increases with porosity.<br>• Same conclusions for vertical orientation. |
| Hetsroni, Gurevich, and Rozenblit, 2008 | **Suspended aluminium foam strip with internal heat generation.**<br>• The porous strip increases the heat transfer 18 to 20 times, compared to a solid strip of the same dimensions. |
| Qu et al., 2012 | **Copper foam sintered plate.**<br>• The optimal inclination seems to be around 60 to 75 degrees.<br>• An increase in porosity leads to an increase in heat transfer.<br>• The dominant process seems to be conduction through the metal.<br>• The average Nusselt number decreases with increasing pore density. |
| De Schampheleire et al., 2013 | **Aluminium foam strips (one fin).**<br>• Lower pore density seems to increase the heat transfer.<br>• Conduction of heat through the solid seems to be the limiting factor.<br>• Increased foam height leads to an increase in heat transfer.<br>• Too much of a length increase of the fin decreases heat transfer again. |

| Article | Findings |
|---|---|
| Du et al., 2014 | **Comparison between bored and porous copper plates**<br>• Forced convection dissipates heat five to six times faster compared to natural convection in the same setup.<br>• Heat dissipation in forced convection is higher when the air is forced in the direction along the plates.<br>• The heat dissipation increases somewhat with increased porosity.<br>• This effect becomes bigger for temperatures above 50 degrees Celsius.<br>• The exact relation between heat dissipation and porosity is unclear, according to the article.<br>• Heat dissipation is likely a balance between conduction and convection.<br>• The heat dissipation is higher for higher pore density. |
| Aly, Arif, et al., 2016 | **Fabricated aluminium porous fins on rectangular plate, backed up with FEM analysis in different study. Fan switched on when steady state was reached.**<br>• Lower conductivity for porous fins due to decrease in solid material.<br>• Higher convection for porous fins due to increased surface area.<br>• Induced turbulence by the fins pores, enhancing heat convection.<br>• Fin base and tip temperature decrease almost linearly with increased air velocity.<br>• Steady state conditions were reached quickest for the 90 degrees orientation.<br>• Both the base and tip reached the lowest temperature in this orientation.<br>• Increasing the number of fins seems to increase the heat transfer, but every additional fin seems to contribute less and less.<br>• Orientation can have a positive influence, because the air flow is less obstructed for the trailing fins. |
| Bilen et al., 2017 | **Array of aluminium porous fins mounted to a rectangular plate, subjected to forced convection in a tunnel.**<br>• Enhanced heat transfer due to increased surface area of the fins.<br>• An increased fin-to-gap-height ratio increases heat transfer.<br>• The friction factor is very dependent on fin-to-gap-height ratio.<br>• The friction factor does not seem to be influenced by parallel pitch.<br>• The efficiency $\eta = Nu^*/(f/f_0)^{1/3}$ decreases slightly with increasing air flow. |

| Article | Findings |
|---|---|
| Feng et al., 2018 | **Copper foam heat fins on rectangular plate.**<br>• Increasing the number of fins has a positive effect on heat transfer, but every additional fin seems to contribute less and less.<br>• For the same temperature difference between base and tip, longer fins will have a higher heat transfer coefficient.<br>• For the same temperature difference between base and tip, increasing the number of fins will increase the heat transfer coefficient quicker for shorter fins.<br>• For the same temperature difference between base and tip, increasing the number of fins will increase the heat transfer coefficient quicker for shorter fins.<br>• A spacing gap between the fins of five to eight millimeters seems optimum, independent of fin length, both for horizontal and vertical position.<br>• The heat transfer coefficient increases more around the optimum spacing gap for longer fins than for shorter fins.<br>• Analysis of the fluid flow shows that fluid indeed flows through the pores, creating a sort of Gaussian temperature profile above each fin. |
| Shamvedi et al., 2018 | **3D printed maraging steel rectangular metal heat sinks, compared to solid commercially available heat sink. Main dimensions are equal, only the lattice sizes vary.**<br>• It was found that the solid fins outperformed all the porous ones, in terms of keeping the base temperature low. An explanation could be that the heated air can advect less freely due to the lattice structure. |
| Kiwan, Alwan, and Abdelal, 2020 | **Porous annular fins, mounted to a vertically suspended heated cylinder.**<br>• Two materials: one with higher porosity/lower permeability and vice versa.<br>• The Nusselt number seems to be a strong function of fin permeability.<br>• An increase in permeability increases heat transfer.<br>• There is a direct proportionality between the number of fins and the heat transfer rate.<br>• An increase in fin thickness leads to an increased Nusselt number.<br>• The heat transfers for both pore densities are comparable. |

| Article | Findings |
|---|---|
| Samudre and Kailas, 2022 | **Aluminium foam heat sink (circular bottom) in a vertical duct.**<br>• Heat transfer coefficient increases with increasing fin length.<br>• Heat transfer coefficient decreases somewhat with increase in pore size.<br>• Heat transfer coefficient increases with increasing fin length.<br>• Heat transfer coefficient decreases somewhat with increase in pore size. |

# 5 Patterns, contradictions and gaps from studied articles

The conclusions in this section are derived from the findings listed in section 4. It contains the findings per article for the experimental studies found in the literature study. A lot of the conclusions seem to be for the specific case that was investigated only. besides this, many of the encountered studies varied more than one parameter (or dimensionless group) per experiment. The ones that were varied were also different per article. This makes it difficult to analyze the effect of such groups or parameters in the general sense.

What adds to this is that not all the materials and manufacturing methods of the fins were even similar in the reviewed papers. The materials from which the fins were manufactured are copper, aluminium and maraging steel. The methods used to produce the samples varied from using a sintering method to unidirectional solidification, 3D-printing, gas-bubble moulding, anvil expanded mesh cladding or simply drilling holes. Some basic relations that seem to be holding throughout all the studies reviewed came forward. The sections that follow will answer the questions below.

1. What is the main pattern that can be seen in existing literature?
2. What are the characteristic parameters and can they used as a comparison?
3. What are the biggest contradictions?
4. Are there any gaps in the existing literature?

## 5.1 The main patterns that were observed in existing literature

**Porous fins almost always perform better than solid ones**

For both the forced convection and natural convection case, all of the porous fins outperformed the (comparable) solid fins. Outperforming means that a greater heat transfer from the heated base to the environment was observed. The only exception on this are the 3D printed lattice structured fins, investigated by Shamvedi et al., 2018. A possible explanation could be the lower heat conduction of the material (maraging steel) or the fact the the structure of the 3D

printed material is fundamentally different, possibly resulting in a lower heat conduction. The authors themselves suspect that the lattice structure obstructs the heat flow away from the fins. Among the other articles, this effect has only been observed in relatively long fins.

**The heat transfer increases with increasing porosity**

A higher porosity leads to a higher heat transfer in all reviewed articles. It was observed by Amitabh Bhattacharya and R. L. Mahajan, 2005, Qu et al., 2012 and Kiwan, Alwan, and Abdelal, 2020. Aly, Arif, et al., 2016 also found that the heat transfer coefficient increased by increasing porosity. However, they observed a weaker influence. It is likely that there exists a maximum value for the porosity after which the heat transfer decreases again upon further increase. Such a optimum has not been found in the literature and is most probably a complex function of other parameters.

**Pore size: bigger pores seems to translate into greater heat transfer**

Amitabh Bhattacharya and R. L. Mahajan, 2005 and De Schampheleire et al., 2013 found that under natural convection, increasing the pore size will lead to an increase in heat transfer coefficient. Only Du et al., 2014 found that under forced convection, their samples with a smaller pore size had a higher heat transfer. It should be mentioned that the manufacturing process for the smaller holes (unidirectional solidification) was different than that for the larger holes (drilling). Samudre and Kailas, 2022 found that the heat transfer coefficient somewhat increased for increased pore size for both natural and forced convection. For the samples made by anvil expanded mesh cladding, used by Kiwan, Alwan, and Abdelal, 2020, a higher permeability lead to a higher heat transfer.

**An increase in fluid speed increases performance**

Another finding is that a higher fluid speed in forced convection results in a higher heat dissipation. An almost linear relation was observed by Aly, Arif, et al., 2016. According to Bilen et al., 2017 however, the overall efficiency of the cooling setup will be less for higher fluid speeds.

**Fin length: longer fins will enhance heat convection, but obstruct fluid flow**

An increase in heat transfer with increasing fin length was observed by Samudre and Kailas, 2022 under forced convection. It was found by Feng et al., 2018 and De Schampheleire et al., 2013 that under natural convection, an increasing fin height will also increase the heat transfer, just like in the forced regime. However, after a certain height is reached, performance starts to decline again. Their explanation is that an "excess" part of fin lengthwise will not contribute much to the performance, but will negatively affect advection of the hot fluid.

**An increase in number of fins will increase overall heat transfer**

In forced convection, adding extra fins will increase the total heat transfer according to Aly, Arif, et al., 2016. However, every additional fin will contribute less and less as the leading fins obstruct the flow for the trailing fins. Kiwan, Alwan, and Abdelal, 2020 found that there is a direct proportionality between heat transfer and number of fins for the natural convection regime.

**Fin orientation can enhance heat transfer**

Feng et al., 2018 found that a horizontal orientation of set of porous fins will perform better than a vertical orientation. This

holds for all the lengths they tested under natural convection. Du et al., 2014 found an increase in heat transfer for forced convection when the fluid was forced along the fins, instead of perpendicular.

**Case-specific conclusions**
Placing the fins in a duct will increase the airflow through and around the fins, according to Bilen et al., 2017. This increases the rate of heat transfer. Increasing the ratio fin-to-gap-height will increase the heat transfer even more. Adding a duct will also increase the power consumption. Power consumption increases further by increasing the fin-to-gap-height ratio.

Some other parameters were tested like the spacing between the fins. It was found by Feng et al., 2018 that a gap of 5 to 8 millimeters is optimum for all fin lengths. However, these numbers seem specific for the case investigated. What might be interesting is that it seems that finding the optimum fin spacing has a much bigger effect on heat transfer for longer links, compared to shorter ones.

**To summarize, the main patterns observed are the following:**

- Porous materials seem to outperform solid materials in heat dissipation.
- The total heat transfer of a fin will increase with increasing porosity up to a certain point. Conduction through the fin should not become too poor due to high porosity. It is not clear when this occurs.
- The total heat transfer of a fin will increase with increasing pore size, likely because bigger pores allow for both better conduction and convection. It is not clear when the pore size becomes too large.
- The total heat transfer of a fin will increase with fin length, up to a certain point. After this point, performance decreases again as air flow gets obstructed. It is not clear when this occurs.
- The total heat dissipation capacity for a fin seems to be a balance between thermal conductivity through the solid material and thermal convection to the surrounding fluid.

## 5.2 Important parameters: porosity and pore size

Along important cooling fin parameters such as: geometry, fluid properties and regime, temperature and the fins heat capacity, at least two important parameters need to be added in the case of porous fins: porosity and pore size (or pore density). Besides this, the heat conduction through the fin is replaced by the effective thermal conductivity through the porous material and the convective heat transfer coefficient is replaced by the effective convective heat transfer, which is based on the effective fin dimensions as if it were a solid. A complete list of parameters that are considered important can be found in table 8.

## 5.3 Not many contradictions in the existing literature

Not many contradictions have been found in the experimental research encountered. Some small contradictions about performance seem to be easily explainable by the variation of certain important parameters when comparing two results. This makes their results probably less comparable than

how they were presented. An example of this is the comparison of the performance of bigger drilled holes with smaller-size unidirectional solidification created holes, investigated by Du et al., 2014. Another example is the comparison of performance of a solid fin heat sink with a 3D printed porous structure, as done by Shamvedi et al., 2018.

## 5.4 Gaps in the existing literature: only one study looked at the individual fin

The biggest gap in the current literature seems to be the fact that it is currently not clear how to optimize the important parameters or to even predict the performance of porous fins. By looking at the studied articles, it becomes obvious that not a lot of experimental work has been performed on porous fins in general. If experiments have been done, they focus on the total heat dissipation for a certain setup. Such a setup usually consists of multiple fins, mounted to a base plate to create a heat sink. The overall performance of the entire heat sink is then evaluated. This is done by either measuring the temperature of the base plate, or by calculating the total convective heat transfer coefficient, using the base plate area $\mathcal{A}_b$, the total heat flow $\dot{Q}$ and the base and ambient difference in temperature $T_b - T_e$:

$$h_c = \frac{\dot{Q}}{\mathcal{A}_b \left(T_b - T_e\right)} \tag{24}$$

This coefficient tells something about the total heat transfer of the heat sink (base plate and fins) for that specific situation. As mentioned before: it ignores the 3D structure of the heat sink.

The only experimental paper attempting to determine the convective heat transfer coefficient for the fin only was published by Aly, Al-Athel, et al., 2015. In their experiment they performed a finite-element simulation to match the temperature boundary conditions (base and tip temperature of the fin) obtained from an experiment by Aly, Arif, et al., 2016. They then "fine tuned" the effective convective heat transfer coefficient for the fin only ($h_e$) until the boundary conditions were met. In the finite-element simulation, they used the conductive properties of the solid material.

## 5.5 Two relevant models taken from literature

Two important models came forward from the experimental studies. These models have been used extensively in (semi-)analytical solutions and numerical simulations. One empirical relation was proposed by A. Bhattacharya, Calmidi, and R. Mahajan, 2002. It predicts the effective thermal conductivity of porous materials, based on the porosity, the conductivity of the solid and the conductivity of the fluid:

$$k_e = \mathcal{A}\left(\varepsilon k_f + (1-\varepsilon)\, k_s\right) + \frac{1-\mathcal{A}}{\frac{\varepsilon}{k_f} + \frac{1-\varepsilon}{k_s}} \tag{25}$$

Together with Darcy's law of natural convection of a fluid through a porous material, a simple energy balance can be set up as described at the beginning of section 3.

$$v = \frac{g\beta\left(T - T_e\right)}{\nu} \tag{26}$$

This relation predicts the fluid velocity through a porous medium by using the gravitational constant $g$, the volumetric expansion ratio $\beta$, the difference in temperature between the local temperature in the

porous medium ($T$) and the external temperature ($T$) and the kinematic viscosity of the fluid $\nu$.

# 6 Predicting the performance of a single porous cooling fin

From the literature review, performed in section 3 and the conclusions drawn in section 5, it becomes clear that performance of an entire porous material heat sink varies drastically with orientation, porosity, fluid flow regime, geometry, material, number of fins and many other parameters. The performances are often very difficult to compare with each other. If the behavior of a single porous fin were predictable, it could function as a simpler building block for designing more complex porous heat sinks. Two concepts would be helpful in prediction of the performance of a single porous fin:

- The effective convective heat transfer coefficient $h_c$ for a single fin.
- A mathematical prediction of the temperature profile along a single fin.

## 6.1 Convective heat transfer coefficient for a single porous fin

Right now, it is not easy to directly measure the effective convective heat transfer coefficient for a single porous cooling fin only. To obtain this value, either the fin efficiency $\eta_f$ or the average temperature $T_{avg}$ of the entire fin have to be known, as well as the exact heat flux through the bottom of the fin. This is often a difficult job. Equation 27 shows how these values would be used to calculate the convective heat transfer coefficient $h_c$ for a single fin. The measurements would require a single fin to be isolated from its heat sink and getting the average fin temperature would require many measurements along the entire fins length.

$$h_c = \frac{\dot{Q}}{\eta_f \mathcal{A}\left(Tb - Te\right)} = \frac{\dot{Q}}{\mathcal{A}\left(T_{avg} - T_e\right)} \tag{27}$$

From the literature encountered, Aly, Arif, et al., 2016 were the only ones to attempt getting a value $h_c$ for a single fin only. Their method combined numerical simulations with experimental data and was addressed in the previous sections. It would be useful if an easier method could be applied to determine the effective heat transfer coefficient for the fin only, as the finite-element method performed by Aly, Arif, et al., 2016 is quite calculation intensive.

As can be read in Mills, 2014, many empirical correlations have been established that can be used to calculate the convective heat transfer coefficient for geometries made out of solid materials. The chapter shows that these relations often depend on many parameters and only work between certain ranges. Parameters are grouped into meaningful dimensionless numbers. The relations, as well as the ranges for which they hold, are expressed in these dimensionless numbers.

One example of such empirical correlation for a solid material, taken from Mills, 2014,

is the equation below. It describes the average Nusselt number ($Nu$) as a function of the Rayleigh number ($Ra$) and a Prandtl ($\Psi$) number function for a single sharp plate. This relation seems to hold for Rayleigh numbers smaller than $10^9$ and can be adjusted for inclined plates. The total heat transfer for a flat plat under natural convection can be predicted, at different orientations using the equation below.

$$\bar{Nu}_L = 0.68 + 0.67\left(Ra_L\Psi\right)^{1/4}, Ra_L \lesssim 10^9$$

Analogous relations could be constructed for porous materials.

## 6.2 Predicting the temperature profile along a porous fin

Knowing the analytical solution for the temperature profile along the fin would help optimizing its efficiency, effectiveness and geometry. In section 2, an analytical solution for the temperature profile along a single solid fin was derived. It is not clear whether this mathematical solution holds for porous fins. The solution is repeated below and looks in dimensionless form as follows:

$$\tilde{T} = -\tanh(a)\sinh(a\tilde{x}) + \cosh(a\tilde{x}) \quad (28)$$

with:

$$a^2 = \frac{h_c\mathcal{P}L^2}{k\mathcal{A}_c}, \quad \tilde{x} = \frac{x}{L}, \quad \tilde{T} = \frac{T - T_e}{T_b - T_e} \quad (29)$$

In which $h_c$ is the convective heat transfer coefficient at the fins outer surface, $\mathcal{P}$ is the fin perimeter, $L$ is the length of the fin, $k$ is the conductive heat transfer coefficient and $\mathcal{A}_c$ is the cross sectional area of the fin. $T_b$ is the base temperature of the fin, $T$ is the local fin temperature and $T_e$ is the ambient fluid temperature. This equation was obtained by imposing the following boundary conditions on the governing equation 10:

$$\tilde{T}\Big|_{\tilde{x}=0} = 1, \qquad \frac{d\tilde{T}}{d\tilde{x}}\Big|_{\tilde{x}=1} = 0 \quad (30)$$

In the case of porous material, $h_c$ and $k$ will represent effective values. An empirical model was proposed by A. Bhattacharya, Calmidi, and R. Mahajan, 2002 to calculate the effective value of $k$ for porous materials, using the porosity, fluid conductivity and material conductivity (equation 17). But as was stated above, obtaining the value for the effective convective heat transfer coefficient for porous materials is much more difficult.

## 6.3 Using the temperature profile model to find $h_c$

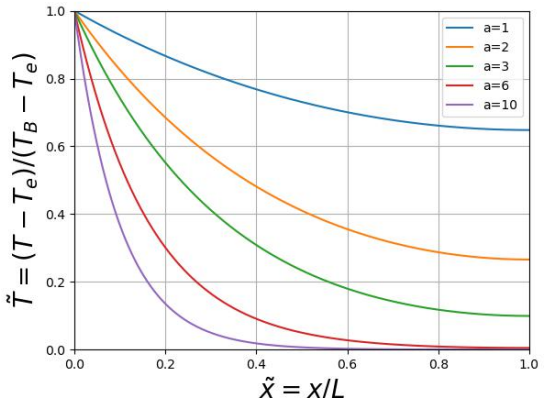


Figure 24: *Dimensionless temperature profiles along a single fin for different values of a (adiabatic tip assumption).*

Some modifications might be required before equation 28 for solid fins can be applied to a porous fin in an analogous way.

But if possible, it can be used to quickly and easily find the convective heat transfer coefficient for a single porous fin. This is because the first boundary condition in 30 fixes the temperature at the fins base ($T_b$) at $\tilde{x} = 0$. The second boundary condition only imposes the line of the temperature profile to be horizontal at the fins tip ($\tilde{x} = 1$). It does not impose a value for the temperature itself at this point. Figure 24 illustrates how the tip temperature is a function of the heat transfer coefficient, when keeping the other variables in the fin parameter $a$ fixed. This means that $h_c$ can be found by measuring the tip and base fin only. It is important to realize that the adiabatic tip condition is assumed to get to the solution of equation 28. Section 6.5 explains how the mathematical solution still can be used if the adiabatic tip assumption is not valid.

## 6.4 Testing the available data

Aly, Arif, et al., 2016 were the only ones encountered who directly measured the temperature at both the base and the tip of the fin. They were also the only ones that investigated a single fin only. Table 6 shows an overview of the data obtained. The effective thermal conductivity ($k_e$) was calculated using equation 17, published by A. Bhattacharya, Calmidi, and R. Mahajan, 2002, to be 5.8 $W/m/K$. The column under $h_e$ contains the effective convective heat transfer coefficient, determined using the numerical simulation in combination with experimental data. The last column contains the analytically predicted tip temperature by equation 28. The column before that contains the tip temperatures as measured by Aly, Arif, et al., 2016. Figure 25 shows a visual representation of these results. The dots represent the measured values, the lines represent the analytical temperature profile predicted by equation 28.

It can be seen that the temperatures, predicted by the analytical solution, are somewhat higher than the measured temperatures. A possible reason for this can be the fact that the fins studied by Aly, Arif, et al., 2016 are relatively short, compared to their cross-sectional area, making the solution for the adiabatic tip assumption inaccurate. Another reason could be that the model does any correction for porosity of the material into account. By setting up an experiment with a relative smaller heat flux through the tip of the fin, equation 28 can potentially still be used to obtain a value for the effective heat transfer coefficient of porous fins.

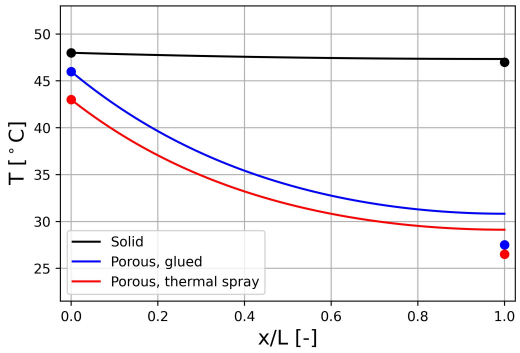


Figure 25: *Temperature profiles as predicted by equation 28 for three type of fins tested by Aly, Arif, et al., 2016. The dots represent the measured base and tip temperatures*

## 6.5 The fixed tip temperature method

In case the adiabatic tip solution turns out to be inaccurate, another method to determine the value of this coefficient could be used. This is the analytical solution for the

fixed-tip-temperature boundary condition. In this case, the prescribed boundary conditions are the temperatures at the base and the tip of the fin ($T_b$) and ($T_t$) respectively. This translates into the following dimensionless boundary conditions for the governing equation 10:

$$\tilde{T}\Big|_{\tilde{x}=0} = 1, \qquad \tilde{T}\Big|_{\tilde{x}=1} = \frac{T_t - T_e}{T_b - T_e} \tag{31}$$

Which results in the following analytical solution:

$$\tilde{T} = \mathrm{B} \cdot \sinh(a\tilde{x}) + \cosh(a\tilde{x}) \tag{32}$$

In which:

$$B = \frac{(T_t - T_e) \,/\, (T_b - T_e) - \cosh(a)}{\sinh(a)} \tag{33}$$

$$a^2 = \frac{h_c \mathcal{P} L^2}{k \mathcal{A}_c} \tag{34}$$

Figure 26 shows what the temperature profiles look like under the fixed-tip-temperature boundary condition for different values of $a$, which is a function of the convective heat transfer coefficient $h_c$.

The advantage of using equation 28 would be that the heat transfer coefficient could be determined by only measuring the fins base temperature $T_b$ and tip temperature $T_t$, as the tip temperature is a function of the convective heat transfer coefficient. However, more information than the temperature at just these two locations is needed if equation 32 is used, because the tip temperature has now become independent of the convective heat transfer coefficient. Measuring the temperature in a third location, somewhere along the fins length, would yield the convective heat transfer coefficient as the shape of the function is now a function of it. Determining the base and tip temperatures only would be easier. However, neglecting the heat flux through the tip of the fin should be justified.

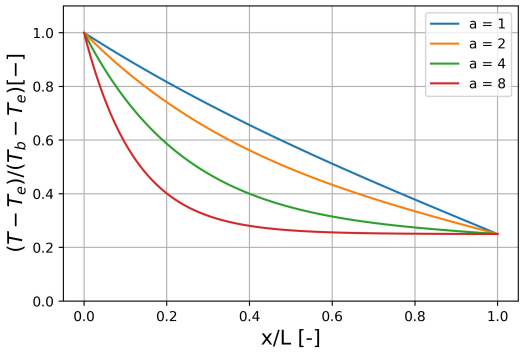


Figure 26: *Dimensionless temperature profiles along a simple pin fin for different values of fin parameter a, using a fixed tip temperature as the second boundary condition.*

Table 6: *Data obtained from Aly, Arif, et al., 2016. It contains the fins measured base ($T_b$) and tip temperature ($T_t$) and effective convective ($h_e$) and conductive ($k_e$) heat transfer coefficients. The last column contains the values as predicted by equation 28.*

| Fin type | $T_b$ | $h_e$ | $k_e$ | $T_t$ | $T_t$(predicted) |
|---|---|---|---|---|---|
| Solid | 48 | 218 | 132 | 47 | 47.3 |
| Porous, glued to base plate | 46 | 5.8 | 210 (estimated) | 27.5 | 30.8 |
| Porous, thermal spray | 43 | 5.8 | 245 | 26.5 | 29.1 |

# 7 Experimental setup for measuring the temperature profile

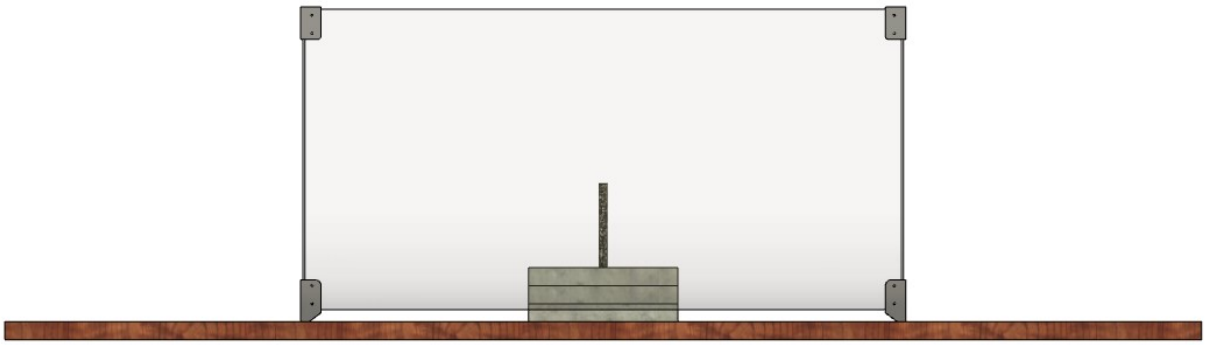

Figure 27: *Side view of the CAD model of the experimental setup. A cylindrical cooling fin is placed in the center of the setup with its bottom placed inside three layers of insulation. The entire setup is shielded, so natural convection is ensured.*

Figure 27 shows a side view of the CAD model of the entire experimental setup. The heated part of the setup is shielded by a square construction made out of Plexiglass to block any forced convection. A small slit is left all around the bottom of the shielding to enable natural convection. The setup will measure the temperature profile along several open-foam porous fins. This will be done by placing several thermalcouples along the fins length as explained in more detail in section 7.2. These measurements provide the average temperature of the fin $T_{avg}$, which can then be used to calculate the effective convective heat transfer coefficient $h_c$, using equation 27. The same measurements will be performed on a solid fin as a baseline, for which the mathematical solution of equation 28 is known to hold.

A closeup view of the bottom side of one of the cooling fins is shown in figure 28. The insulation has been made transparent to illustrate the position of the cooling fin inside of it. This particular example shows a porous fin, but the solid fin is positioned in the same manner. It can be seen that the fin reaches two layers deep in the three-layer insulation stack. This way, heat loss through the bottom of the fin is limited. The insulation material used is calcium silicate. The fin is heated from the bottom. The heating pad can be seen in red, inside the insulation. The self-sticking rectangular-shaped heating foil is wrapped around the circumference of the bottom of the cooling fin.

Figure 27 shows a fin in vertical orientation, but experiment will take measurements of the fins temperature profile in both horizontal as vertical orientation. All the measurements will taken at steady state. This is defined to be reached when the base temperature of the fin varies less than 0.3 degrees Celsius over a time span of fifteen minutes.

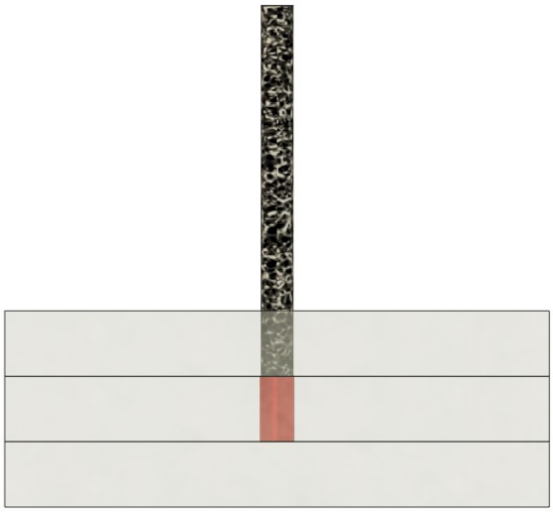

Figure 28: *Closeup side view of the bottom of the cooling fin with the rectangular-shaped heating foil (red) wrapped around it.*

## 7.1 Quantification of the setup

An overview of the important physical characteristics of the different parts used for the setup are listed below. The calculations for determining the fin dimensions follows after the list. The image in figure 29 shows what the porous fins look like.

- **Solid fin**
  *Macking Green Herbal Store* 2024
  Material: 99.99% nickel
  Thermal conductivity: 86 W/m/K
  *SubsTech, High purity nickel* 2023
  Dimensions: 15mm x 200mm
- **Porous fins**
  *Zopin Group - Metal Foam Manufacturer* n.d.
  Material: $\geq 95\%$ nickel
  Porosity 95%, pore size 0.5mm
  Porosity 95%, pore size 0.8mm
  Porosity 98%, pore size 0.5mm
  Dimensions: 15mm x 200mm
- **Heating pads**
  *Home Huxuan store - AliExpress 15* n.d.
  dimensions: 25mm x 50mm
  Max. voltage: 12 volts (7 watts)
- **Insulation**
  *Elektrobode - CALCIUMSILICATE* n.d.
  Material: calcium silicate
  dimensions: 250mmx250mmx30mm
  thermal conductivity: 0.065 W/m/K
  (Engineeringtoolbox, 2023)
- **Shielding**
  *Kunststof platenshop* 2024
  Dimensions: 500mm x 1000mm (4x)
  Material: Plexiglass, casted
- **T-type thermocouples**

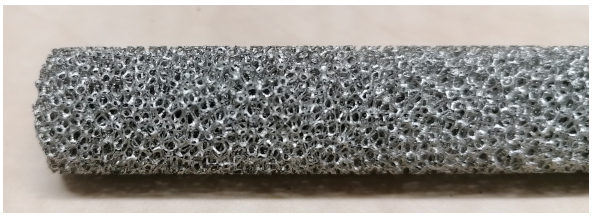

Figure 29: *Closeup image of the open foam porous material.*

To make an estimation for the fins exposed length, equation 27 can be rewritten as below. Here, the area $A$ is replaced by the fin perimeter, multiplied by the fin's exposed length: $\mathcal{P}L$.

$$L = \frac{\dot{Q}_{\text{fin}}}{\mathcal{P}h_c\left(T_{\text{avg}} - T_e\right)} \tag{35}$$

The average temperature can be determined by integrating the dimensionless solution. Since this analysis is only a rough calculation to get insight in the behavior of the experimental setup, the adiabatic tip solution is integrated:

$$\tilde{T}_{\text{avg}} = \int_0^1 \left[-\tanh(a)\sinh(a\tilde{x}) + \cosh(a\tilde{x})\right] d\tilde{x} \tag{36}$$

and using the fact that the following transformation was used:

$$\tilde{T} = \frac{T - T_e}{T_b - T_e} \tag{37}$$

After integration can be rewritten as:

$$T_b = \frac{a\,(T_{\text{avg}} - T_e)}{\tanh(a)(1 - \cosh(a)) + \sinh(a)} + T_e \tag{38}$$

With $a$ being the fin parameter as described by equation 34 In other words: both the fin base temperature, as well as the required fin length, depend on the average temperature. So, an iterative method for determining the fins dimensions was used:

1. Fix applied power to the porous fin.
2. Fix the average temperature to determine the required fin length and to calculate the base temperature that will be reached for the porous fin.
3. use equation 28 to predict the temperature profile for the porous fin.
4. rewrite equation 35 with $T_{\text{avg}}$ on the left side and substitute the length required for the porous fin into equation 35 to obtain the average temperature that will be reached by the solid fin. [1]
5. Use equation 38 to predict the base temperature that will be reached in case of the solid fin.
6. Use equation 28 to predict the temperature profile for the solid fin.

In order to make the estimate for the fin dimensions, the applied heat flux is set to be 4.5 watts. $h_c$ is taken from the natural convection case investigated by Aly, Arif, et al., 2016 to be approximately 12 $W/m^2/K$. The ambient temperature $T_e$ is taken to be 20 degrees Celsius and the conductive heat transfer coefficient $k$ is calculated using equation 17, in which the fluid conductivity $k_f$ is estimated to be 0.040 $W/m/K$ (at 500 K) as calculated by E. Engineeringtoolbox, 2024. The conductivity for the (solid) nickel is taken to be 86 $W/m/K$, as proposed by E. Engineeringtoolbox, 2024.

The initial idea was to fabricate the cylindrical fins, using a water jet cutter. It is beneficial to have longer fins, as this increases the temperature difference between the thermocouples along the fins length. This makes it easier to apply the thermocouples to the fins, but also generates a difference in temperature of approximately 1 degree Celsius between base and tip temperature, in case of the solid fin. Companies such as Watersnijden, 2024 consider 200 millimeters as maximum thickness for water jet cutting, so this was used as a guideline. However, *Zopin Group - Metal Foam Manufacturer* n.d. turned out to be able to deliver customized cylindrically shaped fins in porosities and pore sizes as mentioned in the list above. Fixing the average temperature in equation 38 to be at 37 degrees Celsius, with a prescribed heat flux of 4.5 watts results in the results as shown in figure 30.

From this prediction, it is interesting to note that a too high value for porosity results in a cooling fin that is actually performing worse in terms of predicted base temperature, compared to the solid fin. But these plots are only rough estimates and the convective heat transfer coefficient is kept fixed when varying the porosity. Also,

[1] The convective heat transfer coefficient is iteratively estimated using the equation 1.23a for natural convection along a vertical solid wall from Mills, 2014, once the base temperature is known. It is approximately 7.2 $W/m/K$.

it is not clear at this point if the model can be used to predict porous-fins temperature profiles. The base temperature is somewhat high for the porous fins, but since the convective heat transfer coefficient will be directly measured in the setup, the input power could be varied during the experiment if needed.

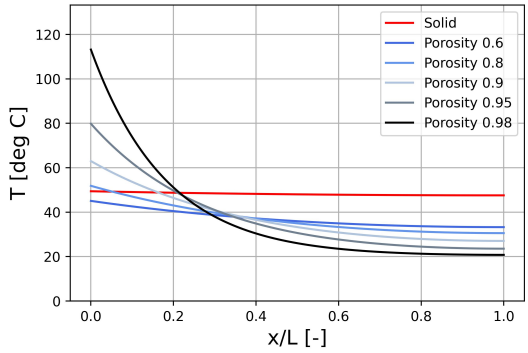


Figure 30: *Temperature profiles for a solid fin (red) and fins of different porosities.*

## 7.2 Measuring the average fin temperature

The use of an infrared camera for determining the temperature profile (and average fin temperature) is difficult. The low emissivity of metal, in combination with the porous medium, makes it almost impossible to get accurate measurements of the surface area temperature. A possible solution could be to coat the material to higher the emissivity, like the way Aly, Al-Athel, et al., 2015 did, but the influence of the coating on the total convection would be unclear in the case of a porous medium.

For this reason, a temperature profile will be constructed by the use of T-type thermocouples at equidistant locations on the fin's outer surface. The temperature profile is not known beforehand, so the average temperature will be calculated, using linear interpolation of the measured temperature readings. The left image in figure 31 illustrates this in the case when only four thermocouples are used. The dots represent the measured temperatures. The average temperature can then be calculated using:

$$T_{avg} = (x[i+1] - x[i])\, T[i+1] + \frac{1}{2}(x[i+1] - x[i])\,(T[i] - T[i+1]) \tag{39}$$

The graphs show that an error is made when determining the average temperature, compared to the exact profile of equation 32. This error is calculated and plotted at the right side of the figure for an effective Nusselt number, ranging from zero to a little over 3. Nusselt numbers higher than this will not be reached in the experiment as parts of the fin will have reached lower temperatures than the tip, which is not physically possible. The plots shows an almost linear dependence of the average temperature in this range. It also shows that the slope of the error varies somewhat with the difference in temperature between the base and the tip of the fin ($\Delta T$). The error lays somewhere around 0.75 degrees Celsius maximum, but this error will decrease tenfold (to 0.07 degrees Celsius) in the case where ten thermocouple are used. This knowledge, together with the uncertainty in the thermocouples, can be used to estimate the maximum error in the resulting average temperature.

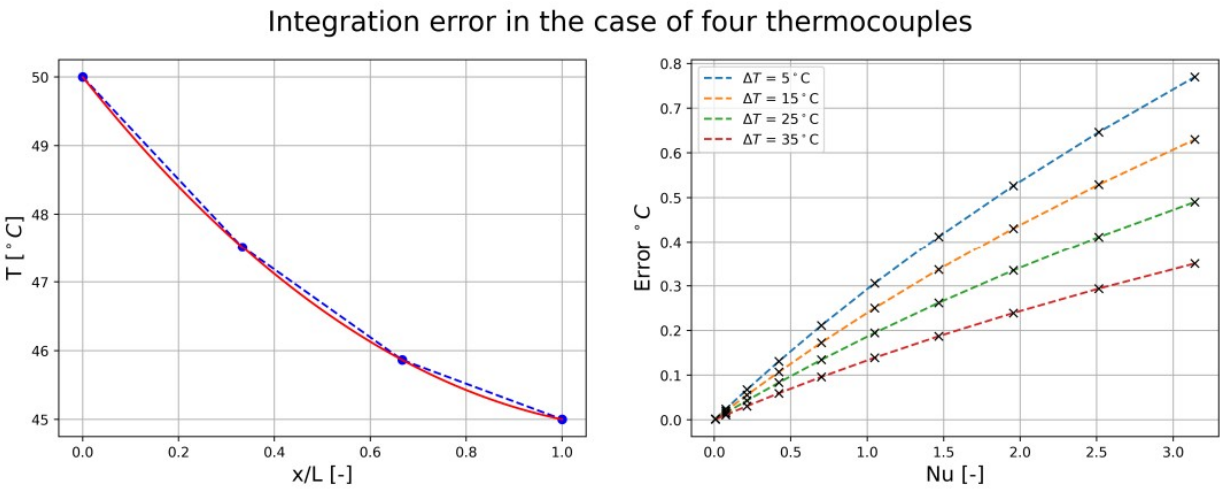


Figure 31: *Left: The real temperature profile plotted according to the fixed-tip boundary condition (equation 32, the blue dots represent the locations at which the temperature was measured (four in this example). The dotted lines is the interpolated temperature profile. Right: calculations for the error between the analytical average and the interpolated temperature profile average.*

## 7.3 Estimating the heat losses

To estimate $\dot{Q}_{\text{fin}}$ it is important that the heat losses to all sides, other than the fin, can be estimated. A simple numerical finite-volume scheme is set up to estimate the heat losses. The scheme can be found in appendix C.3 and uses a cubic grid of the size of the calcium silicate (WxWxH = 250 x 250 x 90 $mm^3$). The grid used in x, y and z directions is 100, 100 and 61 respectively. The z-direction points in the direction of the cooling fin. A prescribed temperature is set at the location where the heating pad is located, inside the calcium silicate. The value for this temperature is set to the measured base temperature of the fin $T_b$. The outside walls will each be prescribed a different temperature, which will be measured by thermocouples placed at this location. From this scheme, the total heat loss will be estimated, which will be subtracted from the total applied heat flux. This results in the total heat flux through the cooling fin only:

$$\dot{Q}_{\text{fin}} = \dot{Q}_{\text{applied}} - \dot{Q}_{\text{losses}} \tag{40}$$

The theoretical heat losses were estimated to be of the order of $1.6 \cdot 10^{-6}$ Watt, so they are ignored in further calculations.

## 7.4 Setting up the thermocouples

As mentioned above, the thermocouples used were type T. The constantan and copper wires were spot welded together, using a *CD-A1000A CD Welder | AMADA WELD TECH* 2021. The thermocouples were then calibrated and a linear error function was created between 0 degrees Celsius and 100 degrees Celsius. Once calibrated, the thermocouples were glued onto the fin at equidistance locations along the length of the fin. *Thermal Glue – Jaden Technologies GmbH* 2024 was used for this. Figure 32 shows the solid fin with its thermocouples attached, as an example.

As mentioned, a linear error function was constructed for every thermocouple, between 0 and 100 degrees Celsius. The error in reading for each thermocouple ($e$) becomes a function of the temperature reading of the thermocouple:

$$e = aT_{read} + b \tag{41}$$

a and b are coefficients. Each thermocouple got its own values calculated for a and b. These coefficients were calculated using:

$$a = \frac{e_{100} - e_0}{T_{100} - T_0}, \qquad b = e_0 \tag{42}$$

In which:

$e_{100} = T_{read,100} - T_{100}$
$e_0 = T_{read,0} - T_0$

Here, $e_{100}$ and $e_0$ are the errors made at 100 and 0 deg C, respectively. $T_{read,100}$ and $T_{read,0}$ are the thermocouple readings at 100 and 0 deg C. $T_{100}$ and $T_0$ are the temperatures of the boiling water and ice water.

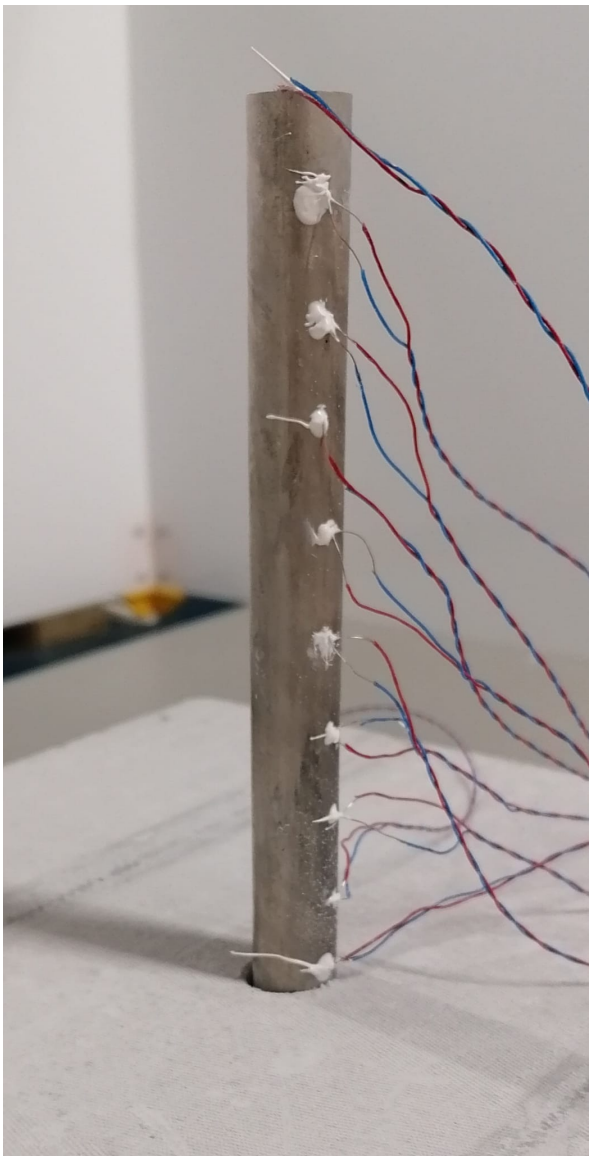

Figure 32: *Closeup image of the solid fin with its thermocouples attached, after these were calibrated.*

## 7.5 Error propagation

The total error in the temperature readings is composed of:

- uncertainty in calibration;
- uncertainty in thermocouple reading.

Taking the variance of the error function, expressed in equation 41, results in equation 43 below, which expresses the **uncertainty in calibration**.

$$\text{var}(e) = T_{read}^2 \cdot \text{var}(a) + \text{var}(b) = \left(\frac{T_{read}}{T_{100} - T_0}\right)^2 \cdot [\text{var}(T_{read,100}) + \text{var}(T_{read,0})] + \text{var}(T_{read,0}) \tag{43}$$

This variance of the error will be approximately be 0.003 degrees Celsius.

The other uncertainty is the **uncertainty in thermocouple reading**. From the obtained data, a typical variance of the reading is observed to be: var$(T_{read}) = 0.01$ degrees Celsius. The raw experimental data can be found in appendix D.

The total uncertainty on a temperature reading is constructed as follows:

$$\mathsf{U}_T = \sqrt{\mathsf{var}(e) + \mathsf{var}(T_{read})} \tag{44}$$

In which U is the uncertainty. This results in:

$$\mathsf{U}_T \approx \pm 0.224^{\circ}C \tag{45}$$

**Uncertainty in heat transfer coefficient**
The equation below is used to make an estimate for the uncertainty of the heat transfer coefficient $hc$. Equation 27 is used and the exposed surface area $\mathcal{A}$ and power input $Q$ are assumed to be known quite accurately. Substituting the numbers results in the uncertainties shown in table 7.

$$U_{hc} = \sqrt{\frac{\partial h_c}{\partial T}\mathsf{var(T)} + \frac{\partial h_c}{\partial T_e}\mathsf{var}(T_e)} = \sqrt{(\mathsf{var}(T) + \mathsf{var}(T_{avg}))\,\frac{Q^2}{\mathcal{A}^2(T - T_e)^4}} \tag{46}$$

# 8 The experimental results

All Fins were tested in horizontal and vertical orientation, both shown in figure 33. The fin in the image is one of the porous ones. The images were taken inside the Plexiglass shielding.

Figure 34 shows eight plots. They represent the results of the measurements taken along the fins. These measurements are displayed in black dots. The best fitting line of the form of equation 28 is added (black dotted line). From these measurements, the average temperature is determined as explained in subsection 7.2. This average temperature is then used in equation 27 to get to the overall effective convective heat transfer coefficient for the fin ($h_c$). This heat transfer coefficient is then plugged into equation 28 to get a prediction for the analytical solution. The green line represents this analytical solution. It uses the base temperature as its starting point. The calculated effective convective heat transfer coefficients ($h_c$) for each situation are listed in table 7

Table 7: *Experimental results for all fins and orientations tested*

| Type - | $Q_{in}$ $[W]$ | $T_b$ $[°C]$ | $T_{avg}$ $[°C]$ | $T_e$ $[°C]$ | $h_c$ $[W/m^2/K]$ |
|---|---|---|---|---|---|
| SolidV | 4.6 | 52.7 | 44.2 | 18.6 | 27.2± 0.1 |
| SolidH | 4.6 | 50.9 | 45.6 | 18.3 | 25.5± 0.1 |
| 9505V | 4.6 | 47.2 | 21.4 | 17.1 | 156.4 ± 2.0 |
| 9505H | 4.6 | 42.0 | 20.1 | 18.1 | 348.4 ± 9.9 |
| 9508V | 4.6 | 47.1 | 21.0 | 17.1 | 170.0 ± 2.4 |
| 9508H | 4.7 | 42.6 | 21.0 | 19.3 | 372.3 ± 11.2 |
| 9805V | 4.7 | 47.7 | 23.2 | 19.2 | 159.4 ± 2.1 |
| 9805H | 4.7 | 39.7 | 20.9 | 18.8 | 338.8 ± 9.6 |

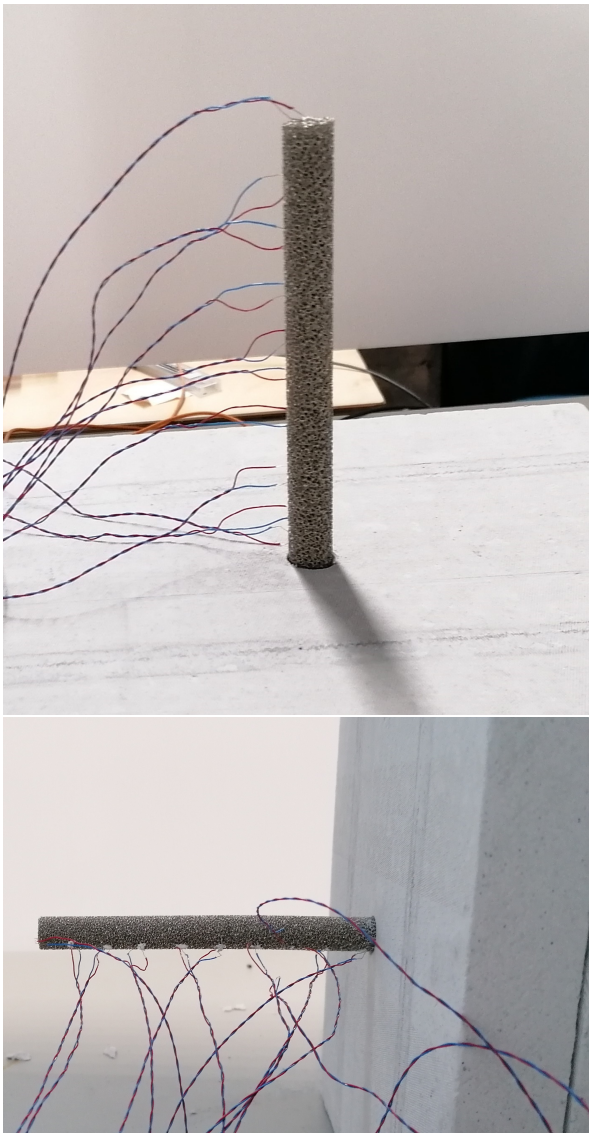

Figure 33: *Image taken from the actual experimental setup. The image shows one of the porous fins as an example. The top image shows the vertical orientation. The bottom image shows the horizontal orientation.*

The following tags were used to identify each fin: [Type][orientation]. The type of fin can either be solid or porous. The solid fin

is simply called "Solid". The porous fins are expressed in their porosity first (two numbers), followed by the pore size (two numbers). The orientation can either be vertical (V) or horizontal (H). A 95% porosity fin with pore size 0.8 mm, vertical orientation would be called: 9508V.

From the plots in figure 34, it can be seen that the measurements for the solid fins have a lot more uncertainty. The reason is that the attachment of the thermocouple is a lot harder for the solid fins, than it is for the porous ones. The tip of a thermocouple can be stuck inside one of its pores. It will sort of stay in this position by itself. The thermocouple can then be "covered" by the thermal glue, which keeps the thermocouple embedded in the fin's surface. In contrast, for the attachment of the thermocouples to the solid fin, getting them onto the surface is a much more delicate task: the tip of the thermocouple has to be in contact with the metal in order to get a correct reading. If a little bit of glue comes in between the thermocouple tip and the fin surface, the reading will be too low. It is easy to imagine how this can happen during drying of the glue, as each fin needs ten thermocouples, which tend to bend in all directions.

## 8.1 Heat transfer coefficient

From table 7, it can be seen that all porous fins performed better in heat dissipation to the surroundings: the heat transfer coefficient (last column) is higher for all porous fins, compared to the solid fin measurements. Also, comparing the third column, each porous fin performed better in terms of lowering the base temperature at steady state ($T_b$). The next paragraphs will evaluate influence of orientation, porosity and pore sizes on performance.

**Performance and orientation**
Comparing the different orientations of the same fin in the table, a clear difference in performance is observed. For porous fins, the heat transfer to the surroundings is substantially higher for the horizontal orientations. The difference in performance due to its orientation is a lot smaller for the solid fin. Given the difference in experimental conditions and the uncertainty in measurements, this difference is insignificant.

**Performance and porosity and pore size**
Looking at the influence of porosity on performance, an evaluation between fin 9505 and 9805 can be made, keeping the orientations the same. Looking at the graphs, it does not immediately become obvious which fin performs better. By looking at the value for the heat transfer coefficient in table again, it seems that the performances of both porosities are comparable.

For evaluating the influence of pore size on performance, an evaluation between fin 9505 and 9508 can be made, keeping the orientation again the same. From the table it can be seen that the bigger pore size fin performed better in both orientations: 9505V: 156.4, 9508V: 170.0 and 9505H: 348.4, 9508H: 372.3.

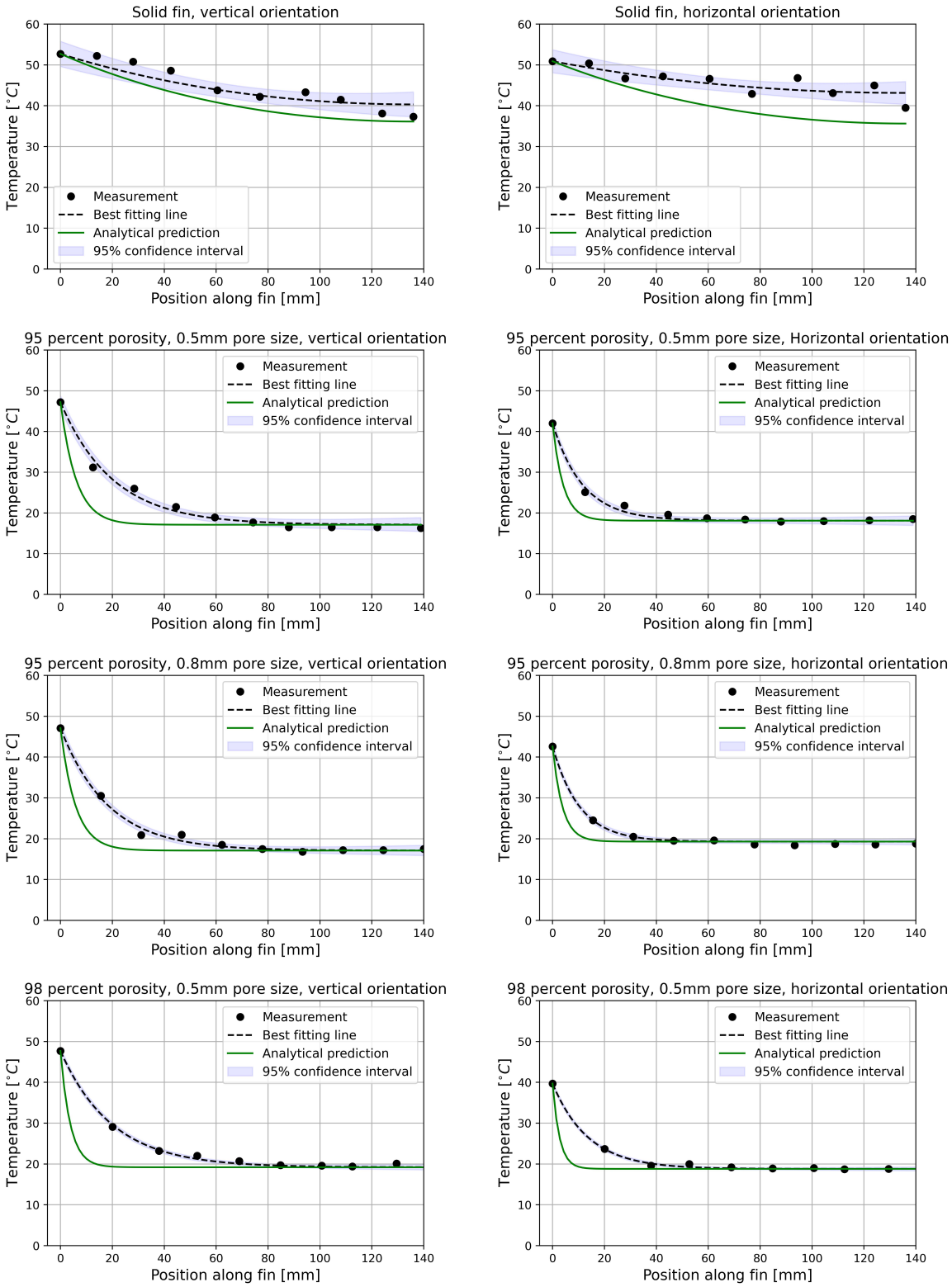


Figure 34: *Plots of the results for all fins and orientations: measurements (dots), the best fitting line (dotted line), and the analytical solution (solid green line).*

## 8.2 Temperature profile

Looking at figure 34, the graphs on the left represent the vertical orientation of the fins, and the graphs on the right the horizontal orientation. The first row holds the results for the solid fin, which functions as a validation for the setup. It can be seen that the temperature profile holds a lot better for the solid fin than it does for the porous fins. The analytical prediction for all porous fins decreases too quickly, regardless of orientation, porosity or pore size.

The dimensionless adiabatic tip solution, derived in section 2, is repeated here for clarity:

$$\tilde{T} = -\tanh(a)\sinh(a\tilde{x}) + \cosh(a\tilde{x}) \quad (47)$$

with:

$$a^2 = \frac{h_c \mathcal{P} L^2}{k \mathcal{A}_c}, \;\; \tilde{x} = \frac{x}{L}, \;\; \tilde{T} = \frac{T - T_e}{T_b - T_e} \quad (48)$$

In equation 47, the shape of the temperature profile can only be effected by the fin parameter $a$. This was illustrated in figure 2. The fin parameter $a$ (equation 48) consists of the convective heat transfer coefficient $h_c$, the fin perimeter $\mathcal{P}$, the exposed fin length $L$, the (effective) conductivity $k$, and the cross-sectional are of the fin $\mathcal{A}_c$.

The heat transfer coefficient was measured during the experiment. Its perimeter, exposed length and cross-sectional area are constant for a particular fin. This leaves the effective conductivity "$k$" to be adjusted to see if the analytical solution can be corrected to match the measured shape of the analytical temperature profile. This will be explored in the next subsection.

## 8.3 Correction for the effective conductivity model

The previous section contained plots of the experimental results. These plots revealed that the analytical solution for a solid fin, cannot immediately be used for porous fins. The temperature in steady state drops significantly slower along the fins length when measured, compared to the mathematical prediction. A possible explanation is that the effective conductivity of a porous fin is in reality higher than the model proposed by A. Bhattacharya, Calmidi, and R. Mahajan, 2002 predicts. The model is repeated here for clarity:

$$k_e = \mathcal{A}\left(\varepsilon k_f + (1-\varepsilon)\, k_s\right) + \frac{1-\mathcal{A}}{\frac{\varepsilon}{k_f} + \frac{1-\varepsilon}{k_s}} \quad (49)$$

In which the effective conductivity of a porous material $k_e$ depends on a constant $\mathcal{A}$, the porosity $\varepsilon$, the fluid conductivity $k_f$ and the solid conductivity $k_s$. The model was proposed, using a setup that consists a static fluid in a closed container. It does not take into account any fluid flow through the porous medium.

Figure 35 shows the analytical prediction after the effective conductivity was corrected (as red dots). Looking at the graphs, it seems that the predicted analytical solution for the corrected conductivity actually coincides with the measured temperature profile. It seems that the correction is mainly a function of the porosity value. The top four plots are all about 0.95 porosity fins, but differ in pore sizes and orientation. However, they all start coinciding for the same correction: $k = 10k_e$. A different single correction is needed for the 0.98 porosity regardless of orientation: $k = 25k_e$. This indicates a quite strong dependence on porosity.

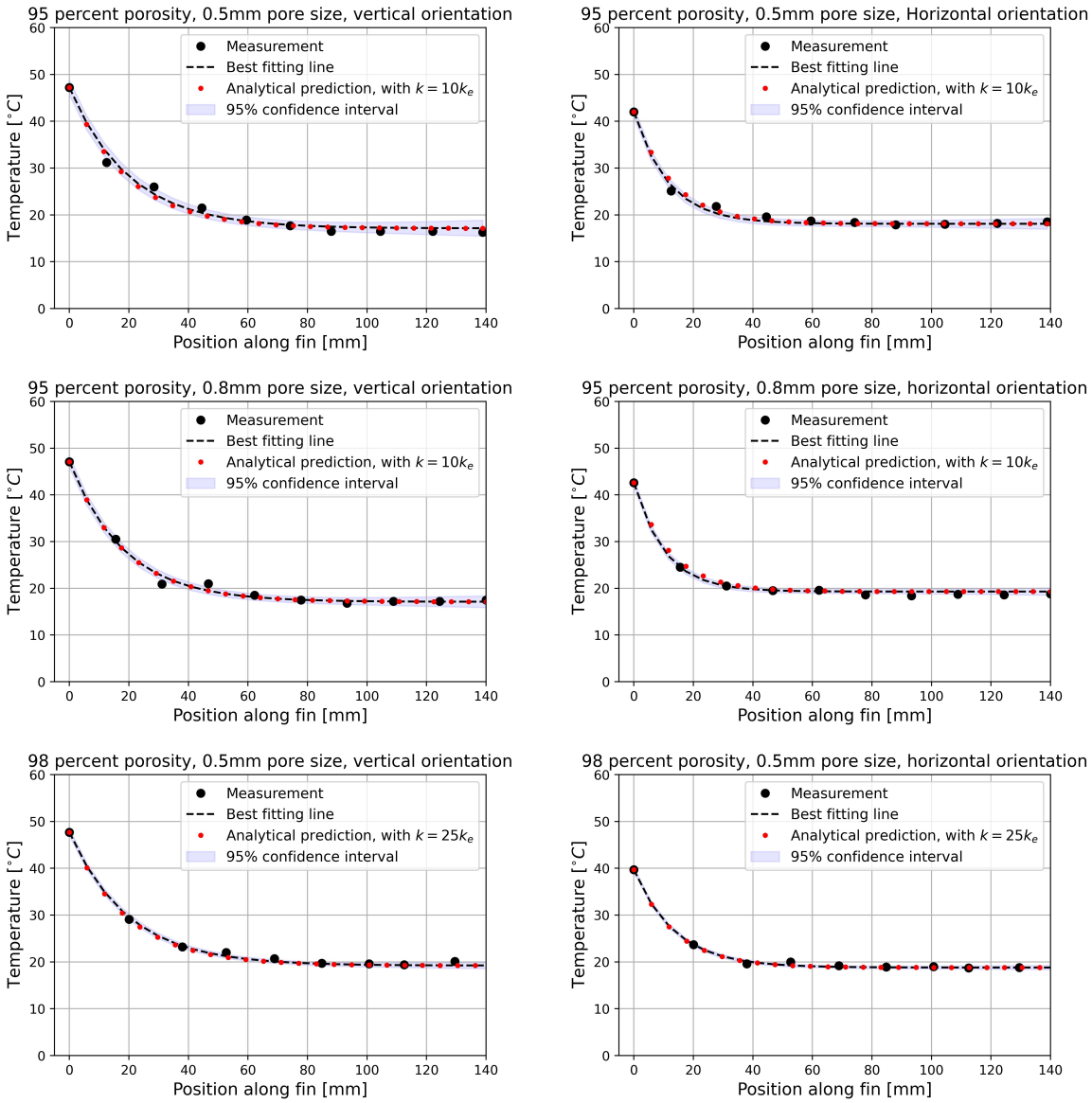


Figure 35: *The analytical solution (red dots) vs best fitting line (black dashes), after a correction for conductivity $k$ has been applied.*

# 9 Conclusion

This document has captured the experimental investigation of the temperature profile for a single porous cooling fin under the natural convection regime. The main question was whether the analytical model for a single simple solid fin can be applied on a porous cooling fin. The experimental measurements, as part of this thesis,

revealed that this is indeed the case. However, the current model for calculating the effective conductivity for a porous material (equation 17, that was proposed by A. Bhattacharya, Calmidi, and R. Mahajan, 2002, does need a correction or extension: in reality, the heat propagates further into the fin than predicted by the model. This is likely because the model assumes a static fluid. After a correction for this effective conductivity for a porous material, the solid-fin model will be applicable. This model can then be used as a convenient method to reveal the temperature profile, and to quickly find the convective heat transfer coefficient for a single fin. This method was proposed in section 6. It seems that the needed conductivity correction is a strong function of the fin porosity, but not of pore size or fin orientation. In this thesis, it has not been investigated how other parameters or dimensionless numbers influence the needed correction for the effective thermal conductivity.

Some other, more case-dependent conclusions can be made and are listed below.

- All porous fins tested, showed a higher effective convective heat transfer coefficient, and a lower base temperature than the solid one. This is despite their orientation, pore size or porosity. This is in agreement with almost all encountered experimental literature.
- A vertically oriented fin clearly shows a higher heat transfer, and lower base temperature than a horizontally oriented one.
- The effect of pore size on performance is insignificant. However, only two pore sizes have been tested (0.5mm and 0.8mm).
- Orientation has a greater influence on the porous fins, than it has on the solid one.

# 10 Recommendations

The experiments performed for this thesis were set up to measure the entire temperature profile along the different fins. This was needed, because it was not yet clear if the temperature profile inside a porous fin could be represented by equation 11. Ten thermocouples were used for each fin to create the complete temperature profile. All these thermocouples have to be spot welded, calibrated and applied to the surface of each fin. This is quite laborious and makes it unfeasible to test many fins and thereby measuring the influence of every important parameter. For follow-up research, fewer thermocouples can be used, as it has been demonstrated in this thesis that the temperature profile in porous fins can be represented by equation 11. Using this result, the entire temperature profile can be constructed by measuring the temperature at locations only: the base, the tip and somewhere in the middle. A solution of the form of equation 11 can be fitted through those three points, by optimizing the value for the fin parameter a. This solution can then be integrated to find

the average temperature, after which equation 27 can be used to calculate the average heat transfer coefficient for the fin. Using the optimized value for $a$, a value for effective conductivity $k$ can quickly be calculated from equation 34.

As a result of this, the fins can be smaller in size and therefore cheaper. More fins with different parameter values can be tested and different materials can be selected. In addition to this, the thermocouple might be able to be spot welded directly onto the fins to eliminate a bias in temperature readings.

## 10.1 Correction factor for k

For follow-up research, it would be interesting to look into how the mathematical model for calculating the effective conductivity of a porous material, as proposed by A. Bhattacharya, Calmidi, and R. Mahajan, 2002 (equation 17) can be extended or adjusted. This thesis showed that equation 11, which is derived for a solid fin, can accurately predict the temperature profile along a porous fin after a correction is applied. This thesis also showed that orientation of the fin and pore size likely barely influence the value of the needed correction.

## 10.2 Dimensional analysis

The Buckingham Pi theorem can be applied on the parameters listed in table 8. The first column lists the parameter name, the second column their corresponding symbols used, and the third lists the base units for these parameters: mass ($M$), time ($T$), length ($L$) and temperature ($\Theta$). Since four independent base units are present, ten independent pi-groups can be expected. Using air density ($\rho$), fluid velocity ($V$), fin length scale ($L$) and Temperature ($T$) as the four general parameters, the following dimensionless pi-groups are constructed:

Table 8: *Important parameters for the creation of relevant dimensionless groups.*

| Parameter | Symbol | Base units |
|---|---|---|
| Conv. heat tr. coef. | $h_c$ | $MT^{-3}\Theta^{-1}$ |
| Fin length scale | $L$ | $L$ |
| Fin conductivity | $k_{fi}$ | $MLT^{-3}\Theta^{-1}$ |
| Fluid conductivity | $k_{fl}$ | $MLT^{-3}\Theta^{-1}$ |
| Fin temperature | $T_{fi}$ | $\Theta$ |
| Fluid temperature | $T_{fl}$ | $\Theta$ |
| Fin heat capacity | $C_{fi}$ | $L^2T^{-2}\Theta^{-1}$ |
| Fluid heat capacity | $C_{fl}$ | $L^2T^{-2}\Theta^{-1}$ |
| Fluid density | $\rho$ | $ML^{-3}$ |
| Fluid velocity | $V$ | $LT^{-1}$ |
| Fluid viscosity | $\mu$ | $ML^{-1}T^{-1}$ |
| Gravity | $g$ | $LT^{-2}$ |
| Porosity | $\varepsilon$ | - |
| Pore size | $d$ | $L$ |

$$\Pi_1 = \varepsilon \qquad \Pi_2 = \frac{d}{L}$$

$$\Pi_3 = \frac{Tk}{\rho V^3 L} \qquad \Pi_4 = \frac{Th_c}{\rho V^3}$$

$$\Pi_5 = \frac{Lg}{V^2} \qquad \Pi_6 = \frac{\rho V L}{\mu}$$

$$\Pi_7 = \frac{CT}{V^2} \qquad \Pi_8 = \frac{k_{fi}}{k_{fl}}$$

$$\Pi_9 = \frac{\Theta_{fi}}{\Theta_{fl}} \qquad \Pi_{10} = \frac{C_{fi}}{C_{fl}}$$

$\Pi_6$ by itself can be recognized as being the Reynolds number ($Re$).

$$Re = \Pi_6 = \frac{\rho V L}{\mu} \tag{50}$$

Combining pi-groups 3 and 4 as below, creates either the Nusselt number ($Nu$) in case

of fluid conductivity $k_{fl}$, or as the Biot number ($Bi$) in case of fin (solid) conductivity ($k_{fi}$):

$$\frac{\Pi_4}{\Pi_3} = \frac{h_c L}{k} \tag{51}$$

Combining groups 3, 6 and 7 as below results in something that can be recognized as the Prandtl number ($Pr$):

$$Pr = \frac{\Pi_7}{\Pi_3 \cdot \Pi_6} \tag{52}$$

And groups 5 and 6 create the Grashof number ($Gr$):

$$Gr = \Pi_5 \cdot (\Pi_6)^2 \tag{53}$$

From this, the following relation can be constructed:

$$Ra = Gr \cdot Pr = \frac{\Pi_5 \cdot \Pi_6 \cdot \Pi_7}{\Pi_3} \tag{54}$$

In which $Ra$ is the Rayleigh number.

The influence of these dimensionless groups can be experimentally investigated to come up with empirical correlations that help predict performance of a single porous cooling fin.

# References


Aly, Shahzada Pamir, Abul Fazal M. Arif, Khaled S. Al-Athel, Javad Mostaghimi, and Syed M. Zubair (July 2016). "Performance of open pore metal foam heat sinks fabricated with thermally sprayed interface". In: *Applied thermal engineering* 105, pp. 411–424. DOI: 10.1016/j.applthermaleng.2016.03.012. URL: https://www.sciencedirect.com/science/article/pii/S1359431116303039.

Aly, Shahzada Pamir, Khaled Al-Athel, Abul Fazal Arif, and Javad Mostaghimi (May 2015). "Computational modeling and calibration of a 3d metal foam heat sink". In: *CANCAM*, https://www.researchgate.net/publication/327624037$_{COMP}$ DOI: 10.13140/RG.2.2.27473.58721. URL: https://www.researchgate.net/publication/327624037_COMPUTATIONAL_MODELING_AND_CALIBRATION_OF_A_3D_METAL_FOAM_HEAT_SINK.

Bhanja, Dipankar, Balaram Kundu, Swapan Paruya, Samarjit Kar, and Suchismita Roy (Jan. 2010). "Heat Transfer and Fin Performance Comparison between Constructal T-shaped Porous and Solid Fin". In: *AIP Conference Proceedings*. DOI: 10.1063/1.3516287. URL: https://doi.org/10.1063/1.3516287.

Bhattacharya, A., V.V. Calmidi, and R.L. Mahajan (Feb. 2002). "Thermophysical properties of high porosity metal foams". In: *International Journal of Heat and Mass Transfer/International journal of heat and mass transfer* 45.5, pp. 1017–1031. DOI: 10.1016/s0017-9310(01)00220-4. URL: https://doi.org/10.1016/s0017-9310(01)00220-4.

Bhattacharya, Amitabh and Roop L. Mahajan (Sept. 2005). "Metal Foam and Finned Metal Foam Heat Sinks for Electronics Cooling in Buoyancy-Induced Convection". In: *Journal of electronic packaging* 128.3, pp. 259–266. DOI: 10.1115/1.2229225. URL: https://doi.org/10.1115/1.2229225.

Bilen, Kadir, Soner Gök, Ali Bahadır Olcay, and İsmail Solmuş (Nov. 2017). "Investigation of the effect of aluminum porous fins on heat transfer". In: *Energy* 138, pp. 1187–1198. DOI: 10.1016/j.energy.2017.08.015. URL: https://doi.org/10.1016/j.energy.2017.08.015.

*CD-A1000A CD Welder | AMADA WELD TECH* (Jan. 2021). URL: https://amadaweldtech.com/news-room/new-cd-a1000a-capacitive-discharge-welder/.

Das, Ranjan (Nov. 2014). "Forward and inverse solutions of a conductive, convective and radiative cylindrical porous fin". In: *Energy conversion and management* 87, pp. 96–106. DOI: 10.1016/j.enconman.2014.06.096. URL: https://doi.org/10.1016/j.enconman.2014.06.096.

Das, Ranjan and Kim Tiow Ooi (Feb. 2013). "Predicting multiple combination of parameters for designing a porous fin subjected to a given temperature requirement". In: *Energy Conversion and Management* 66, pp. 211–219. DOI: 10.1016/j.enconman.2012.10.019. URL: https://doi.org/10.1016/j.enconman.2012.10.019.

De Schampheleire, Sven, Peter De Jaeger, Robin Reynders, Kathleen De Kerpel, Bernd Ameel, Christophe T'Joen, Henk Huisseune, Steven Lecompte, and Michel De Paepe (Sept. 2013). "Experimental study of buoyancy-driven flow in open-cell aluminium foam heat sinks". In: *Applied thermal engineering* 59.1-2, pp. 30–40. DOI: 10.1016/j.applthermaleng.2013.05.010. URL: https://doi.org/10.1016/j.applthermaleng.2013.05.010.

Du, Hao, Dongzhu Lu, Jianjun Qi, Yunli Shen, Limeng Yin, Yuan Wang, Zhongguang Zheng, and Tao Xiong (Sept. 2014). "Heat Dissipation Performance of Porous Copper with Elongated Cylindrical Pores". In: *Journal of Materials Science and Technology/Journal of materials science technology* 30.9, pp. 934–938. DOI: 10.1016/j.jmst.2014.03.014. URL: https://doi.org/10.1016/j.jmst.2014.03.014.

*Elektrobode - CALCIUMSILICATE* (n.d.). URL: https://www.elektrobode.nl/products/obo-calciumsilicaatplaat-voor-toepassing-brandbeveil-500x250x30mm-grijsw-7202904?gad_source=1&gclid=Cj0KCQjwpNuyBhCuARIsANJqL9MeWSdjObTW4651jlupJsxxXHfpUAretjKXQXwmAPP7DHEYkDE86N8aAcwcB.

Engineeringtoolbox (Sept. 2023). *Calcium silicate insulation*. URL: https://www.engineeringtoolbox.com/calcium-silicate-insulation-k-values-d_1171.html.

Engineeringtoolbox, Editor (Apr. 2024). *Air - Thermal Conductivity vs. Temperature and Pressure*. URL: https://www.engineeringtoolbox.com/air-properties-viscosity-conductivity-heat-capacity-d_1509.html.

Feng, Shangsheng, Fei-Chen Li, Fenghui Zhang, and Tian Jian Lu (Feb. 2018). "Natural convection in metal foam heat sinks with open slots". In: *Experimental thermal and fluid science* 91, pp. 354–362. DOI: 10.1016/j.expthermflusci.2017.07.010. URL: https://doi.org/10.1016/j.expthermflusci.2017.07.010.

Gorla, Rama Subba Reddy and A. Y. Bakier (May 2011). "Thermal analysis of natural convection and radiation in porous fins". In: *International communications in heat and mass transfer* 38.5, pp. 638–645. DOI: 10.1016/j.icheatmasstransfer.2010.12.024. URL: https://doi.org/10.1016/j.icheatmasstransfer.2010.12.024.

Hetsroni, G., Maxim Gurevich, and R. Rozenblit (Sept. 2008). "Natural convection in metal foam strips with internal heat generation". In: *Experimental thermal and fluid science* 32.8, pp. 1740–1747. DOI: 10.1016/j.expthermflusci.2008.06.011. URL: https://doi.org/10.1016/j.expthermflusci.2008.06.011.

*Home Huxuan store - AliExpress 15* (n.d.). URL: https://nl.aliexpress.com/item/1005005240171880.html?src=google&src=google&albch=shopping&acnt=494-037-6276&isdl=y&slnk=&plac=&mtctp=&albbt=Google_7_shopping&aff_platform=google&aff_short_key=UneMJZVf&gclsrc=aw.ds&&albagn=888888&&ds_e_adid=&ds_e_matchtype=&ds_e_device=c&ds_e_network=x&ds_e_product_group_id=&ds_e_product_id=nl1005005240171880&ds_e_product_merchant_id=660423726&ds_e_product_country=NL&ds_e_product_language=nl&ds_e_product_channel=online&ds_e_product_store_id=&ds_url_v=2&albcp=19215243779&albag=&isSmbAutoCall=false&needSmbHouyi=false&gad_source=1&gclid=Cj0KCQjwrKu2BhDkARIsAD7GBotALTPO08dZrwaXzRZ_8UIELVZi9TQLZAHJF7cv0rlFvPSMaKZ3BZsaAls-EALw_wcB.

Incropera, F. P. (Sept. 2006). *Fundamentals of Heat and Mass Transfer*. 6th ed.

Jeng, Tzer-Ming and Sheng-Chung Tzeng (June 2006). "An analytical study of local thermal equilibrium in porous heat sinks using fin theory". In: *International Journal of Heat and Mass Transfer/International journal of heat and mass transfer* 49.11-12, pp. 1907–1914. DOI: 10.1016/j.ijheatmasstransfer.2005.11.012. URL: https://doi.org/10.1016/j.ijheatmasstransfer.2005.11.012.

Kim, S. Y., J. W. Paek, and B. H. Kang (Mar. 2000). "Flow and Heat Transfer Correlations for Porous Fin in a Plate-Fin Heat Exchanger". In: *Journal of heat transfer* 122.3, pp. 572–578. DOI: 10.1115/1.1287170. URL: https://doi.org/10.1115/1.1287170.

Kiwan, Suhil (Oct. 2006). "Thermal Analysis of Natural Convection Porous Fins". In: *Transport in Porous Media* 67.1, pp. 17–29. DOI: 10.1007/s11242-006-0010-3. URL: https://doi.org/10.1007/s11242-006-0010-3.

— (Oct. 2007). "Effect of radiative losses on the heat transfer from porous fins". In: *International journal of thermal sciences (Print)* 46.10, pp. 1046–1055. DOI: 10.1016/j.ijthermalsci.2006.11.013. URL: https://doi.org/10.1016/j.ijthermalsci.2006.11.013.

Kiwan, Suhil, Hamzeh Alwan, and Nisrin Abdelal (Oct. 2020). "An experimental investigation of the natural convection heat transfer from a vertical cylinder using porous fins". In: *Applied Thermal Engineering* 179, p. 115673. DOI: 10.1016/j.applthermaleng.2020.115673. URL: https://doi.org/10.1016/j.applthermaleng.2020.115673.

Kundu, Balaram and Dipankar Bhanja (Jan. 2011). "An analytical prediction for performance and optimum design analysis of porous fins". In: *International journal of refrigeration* 34.1, pp. 337–352. DOI: 10.1016/j.ijrefrig.2010.06.011. URL: https://doi.org/10.1016/j.ijrefrig.2010.06.011.

*Kunststof platenshop* (May 2024). URL: https://kunststofplatenshop.nl/product/plexiglas-helder-3-mm/?_gl=1*1dzu1tc*_up*MQ..&gclid=CjwKCAjwhvi0BhA4EiwAX25uj3ABRmiNe8jeqPUniY0trBwE.

Leong, K.C. and Liwen Jin (Feb. 2006). "Effect of oscillatory frequency on heat transfer in metal foam heat sinks of various pore densities". In: *International Journal of Heat and Mass Transfer/International journal of heat and mass transfer* 49.3-4, pp. 671–681. DOI: 10.1016/j.ijheatmasstransfer.2005.08.015. URL: https://doi.org/10.1016/j.ijheatmasstransfer.2005.08.015.

Leong, K.C., Hongyu Li, Liwen Jin, and John C. Chai (Apr. 2010). "Numerical and experimental study of forced convection in graphite foams of different configurations". In: *Applied thermal engineering* 30.5, pp. 520–532. DOI: 10.1016/j.applthermaleng.2009.10.014. URL: https://doi.org/10.1016/j.applthermaleng.2009.10.014.

Li, H.Y. and K.C. Leong (Nov. 2011). "Experimental and numerical study of single and two-phase flow and heat transfer in aluminum foams". In: *International Journal of Heat and Mass Transfer/International journal of heat and mass transfer* 54.23-24, pp. 4904–4912. DOI: 10.1016/j.ijheatmasstransfer.2011.07.002. URL: https://www.sciencedirect.com/science/article/pii/S0017931011003784.

*Macking Green Herbal Store* (2024). URL: https://nl.aliexpress.com/item/1005005708031285.html?src=google&pdp_npi=4%40dis%21EUR%212.61%212.61%21%21%21%21%210.92%40%211200003407691937 9%21ppc%21%21%21&src=google&albch=shopping&acnt=494-037-6276&isdl=y&slnk=&plac=&mtctp=&albbt=Google_7_shopping&aff_platform=google&aff_short_key=UneMJZVf&gclsrc=aw.ds&&albagn=888888&&ds_e_adid=&ds_e_matchtype=&ds_e_device=c&ds_e_network=x&ds_e_product_group_id=&ds_e_product_id=nl1005005708031285&ds_e_product_merchant_id=105391415&ds_e_product_country=NL&ds_e_product_language=nl&ds_e_product_channel=online&ds_e_product_store_id=&ds_url_v=2&albcp=19215243779&albag=&isSmbAutoCall=false&needSmbHouyi=false&gad_source=4&gclid=Cj0KCQjwrKu2BhDkARIsAD7GBoszBEh1m02zQAF6DDclcm26D8wgaApznEALw_wcB.

Mills, A. F. (Dec. 2014). *Basic heat and mass transfer*. URL: https://www.google.nl/books/edition/Basic_Heat_and_Mass_Transfer/GogNngEACAAJ?hl=nl.

Qats (n.d.). *Qats advanced thermal solutions*. URL: https://www.qats.com/Download/Qpedia_Nov10_HS_manuf_technologies5.ashx.

Qu, Zhiguo, Tiansong Wang, Wen-Quan Tao, and Tianjian Lu (Dec. 2012). "Experimental study of air natural convection on metallic foam-sintered plate". In: *International journal of heat and fluid flow* 38, pp. 126–132. DOI: 10.1016/j.ijheatfluidflow.2012.08.005. URL: https://doi.org/10.1016/j.ijheatfluidflow.2012.08.005.

Saedodin, Seyfolah, Siamak Sadeghi, and Siamak Sadeghi (2013). *Temperature distribution in long porous fins in natural convection condition*. Tech. rep. 6, pp. 812–817. URL: https://www.idosi.org/mejsr/mejsr13(6)13/17.pdf.

El-Samrah, Moamen G., A.F. Tawfic, and Samir E. Chidiac (Sept. 2021). "Spent nuclear fuel interim dry storage; Design requirements, most common methods, and evolution: A review". In: *Annals of nuclear energy* 160, p. 108408. DOI: 10.1016/j.anucene.2021.108408. URL: https://www.sciencedirect.com/topics/earth-and-planetary-sciences/cooling-fin.

Samudre, Prabha and Satish V. Kailas (Mar. 2022). "Thermal performance enhancement in open-pore metal foam and foam-fin heat sinks for electronics cooling". In: *Applied thermal engineering* 205, p. 117885. DOI: 10.1016/j.applthermaleng.2021.117885. URL: https://www.sciencedirect.com/science/article/pii/S1359431121013090#fig1.

Shamvedi, Deepak, Oliver J. McCarthy, Eoghan O'Donoghue, Cyril Danilenkoff, Phil O'leary, and Ramesh Raghavendra (May 2018). "3D Metal printed heat sinks with longitudinally varying lattice structure sizes using direct metal laser sintering". In: *Virtual and physical prototyping* 13.4, pp. 301–310. DOI: 10.1080/17452759.2018.1479528. URL: https://doi.org/10.1080/17452759.2018.1479528.

Sowmya, G., B. J. Gireesha, M. Ijaz Khan, Shaher Momani, and Tasawar Hayat (Apr. 2020). "Thermal investigation of fully wet longitudinal porous fin of functionally graded material". In: *International journal of numerical methods for heat and fluid flow* 30.12, pp. 5087–5101. DOI: 10.1108/hff-12-2019-0908. URL: https://doi.org/10.1108/hff-12-2019-0908.

*SubsTech, High purity nickel* (Dec. 2023). URL: https://www.substech.com/dokuwiki/doku.php?id=commercially_pure_nickel_270_high_purity_nickel#google_vignette.

*Thermal Glue – Jaden Technologies GmbH* (2024). URL: https://www.jadentechnologies.com/thermal-glue/.

## References


Torabi, Mohsen and Hessameddin Yaghoobi (Jan. 2013). "SERIES SOLUTION FOR CONVECTIVE-RADIATIVE POROUS FIN USING DIFFERENTIAL TRANSFORMATION METHOD". In: *Journal of porous media* 16.4, pp. 341–349. DOI: 10.1615/jpormedia.v16.i4.60. URL: https://doi.org/10.1615/jpormedia.v16.i4.60.

Türkyılmazoğlu, Mustafa (Oct. 2014). "Efficiency of heat and mass transfer in fully wet porous fins: Exponential fins versus straight fins". In: *International journal of refrigeration* 46, pp. 158–164. DOI: 10.1016/j.ijrefrig.2014.04.011. URL: https://www.sciencedirect.com/science/article/pii/S0140700714000875?via%3Dihub.

Watersnijden, 247 (May 2024). *247 Watersnijden: De specialist van Nederland in watersnijden!* URL: https://247watersnijden.nl/?gad_source=1&gclid=Cj0KCQjw0_WyBhDMARIsAL1Vz8uQonNQkWfljB7jqGUcKr_XlJbZ7hoof7byPzmxkN9LJUI55NpchJsaAjEoEALw_wcB.

*Zopin Group - Metal Foam Manufacturer* (n.d.). URL: https://www.foam-material.com/cylindrical-nickel-foam-inco-battery-manufacturers-for-sale_p1577.html.

# A The complete list of reviewed literature

Table 9: *Encountered literature in chronological order. The table contains information such as fin shape, fin orientation and the convection condition. The references contain hyperlinks.*

| Authors | Fin shape | Orientation | Conditions | Research type |
|---|---|---|---|---|
| 1. Kiwan, Al-Nmir (2000) | Rectangular | Vertical | Natural | Num[2] |
| 2. Bhattacharya, Calmidi (2001) | Rectangular | Vertical | Forced | Exp |
| 3. Kiwan, Al-Nmir (2001) | Rectangular | Vertical | Natural | Num |
| 4. Phanikumar, Mahajan (2002) | Rectangular | Horizontal | Natural | Exp & Num |
| 5. Bassam, Hijleh (2003) | Rectangular | Annular [3] | Forced | Num |
| 6. Bassam, Hijleh (2003) | Rectangular | Inclinations | Natural | Num |
| 7. Naidu, Rao (2004) | Cylindical | Vertical | Natural | Num |
| 8. Dukhan, Ramos (2005) | Rectangular | Horizontal | Forced | Exp & Ana |
| 9. Bhattacharya, Mahajan (2006) | Metal foam [4] | Vertical | Natural | Exp |
| 10. Kiwan (2006) | Rectangular | Horizontal | Natural | Num |
| 11. Kiwan (2007) | Rectangular | Horizontal | Natural | Num |
| 12. Hetsroni, Gurevich (2008) | Rectangular | Horizontal | Natural | Exp |
| 13. Kiwan, Zeitoun (2008) | Rectangular | Inclinations | Natural | Num |
| 14. Bhanja, Kundu (2010) | T-shaped | Vertical | Natural | Ana |
| 15. Bhanja, Kundu (2010) | Rectangular | Horizontal | Natural | Ana |
| 16. Icoz, Arik (2010) | Rectangular | Vertical | Natural | Exp & Ana |
| 17. Khaled (2010) | Rectangular | Horizontal | Forced | Num |
| 18. Bhanja, Kundu (2011) | T-shaped | Vertical | Natural | Ana |
| 19. Gorla, Baker (2011) | Rectangular | Horizontal | Natural | Num |
| 20. Darvishi, Gorla (2012) | Rectangular | Horizontal | Natural | Ana |
| 21. Kundu (2012) | Rectangular [5] | Horizontal | Natural | Ana |
| 22. Darvishi, Gorla (2012) | Annular | Horizontal | Natural | Ana |
| 23. Petroudi, Ganji (2012) | Rectangular | horizontal | Natural | Ana & Num |
| 24. Qu, Wang (2012) | Rectangular | Inclined | Natural | Exp |
| 25. Torabi, Yaghoobi (2013) | Rectangular | Horizontal | Natural | Ana |
| 26. Bhanja, Kundu (2013) | Cylindrical | Horizontal | Natural | Ana |
| 27 Hatami, Hasanpour (2013) | Rectangular | Horizontal | Natural | Ana |
| 28. Hatami, Ganji (2013) | Annular [6] | Horizontal | Natural | Ana |
| 29. Moradi, Hayat (2013) | Triangular | Horizontal | Natural | Ana |
| 30. Hatami, Ganji (2013) | Annular [7] | Horizontal | Natural | Ana |

[2] Num (Numerical), Exp (Experimental), Ana (Analytical).
[3] Attached to horizontal cylinder.
[4] Placed between solid fins.
[5] Also: convex, parabolic and exponential.
[6] Rectangular, convex, triangular and exponential fins
[7] Convex, rectangular and triangular fins

## A The complete list of reviewed literature

| Authors | Fin type | Orientation | Conditions | Research type |
|---|---|---|---|---|
| 31. Hatami, Ganji (2013) | Rectangular [8] | Horizontal | Natural | Ana |
| 32. Saedodin, Shahbabaei (2013) | Rectangular | Horizontal | Natural | Ana & Num |
| 33. Moradi, Fallah (2013) | Rectangular | Horizontal | Forced | Ana & Num |
| 34. Schampheleire, Jaeger (2013) | Rectangular | Horizontal | Natural | Exp |
| 35. Du, Lu (2013) | Rectangular | Vertical | Forced | Exp |
| 36. Saedodin, Sadeghi (2013) | Cylinderical | Horizontal | Natural | Num |
| 37. Das, Ooi (2013) | Rectangular | Horizotal | Natural | Num |
| 38. Turkyilmazoglu (2014) | Exponential | Horizontal | ?? | Ana |
| 39. Kundu, Lee (2014) | Variable [9] | Horizontal | Natural | Ana |
| 40. Majid, Domiri (2014) | Variable | Horizontal | Natural | Ana & Num |
| 41. Liu, Chen (2014) | Rectangular | Vertical | Forced | Exp & Num |
| 42. Das (2014) | Annular | Horizontal | NAtural | Num |
| 43. Darvishi, Gorla (2014) | Rectangular | Horizontal | Natural | Num |
| 44. Vahabzadeh, Ganji (2015) | Cylindrical [10] | Horizontal | Natural | Ana |
| 45. Patel, Meher (2015) | Rectangular | Horizontal | Natural | Ana |
| 46. Kundu, Lee (2015) | Annular | Horizontal | Forced | Ana |
| 47. Darvishi, Gorla (2015) | Annular[11] | Horizontal | Natural | Ana |
| 48. Cuce, Cuce (2015) | Rectangular | Horizontal | Natural | Ana & Num |
| 49. Wei-Mon (2015) | Rectangular | Vertical | Forced | Num |
| 50. Ma, Sun (2015) | Rectangular | Horizontal | Natural | Num |
| 51. Singh, Das (2016) | Rectangular | Horizontal | Natural | Ana & Num |
| 52. Aly, Arif (2016) | Rectangular | Vertical | Forced | Exp |
| 53. Khani, Darvishi (2016) | Annular [12] | Horizontal | Natural | Num |
| 54. Darvishi, Gorla (2016) | Rectangular | Horizontal | Natural | Num |
| 55. Asadian, Zaretabar (2016) | Rectangular | Horizontal | Natural | Num |
| 56. Deshamukhya, Bhanja (2017) | Rectangular | Horizontal | Natural | Ana |
| 57. Hoshyar, Rahimi (2017) | Rectangular | Horizontal | Natural | Ana & Num |
| 58. Feng, Li (2017) | Rectangular | Both [13] | Natural | Exp |
| 59. Bilen, Gok (2017) | Rectangular | Vertical | Forced | Exp |
| 60. Stark, Prasad (2017) | Annular | Horizontal | Forced | Exp & Num |
| 61. Hazarika, Deshamukhya (2017) | Rectangular [14] | Vertical | Forced | num |
| 62. Wei-mon (2017) | Rectangular | Vertical | Forced | Num |
| 63. Ma, Sun (2017) | Trapezoidal[15] | Horizontal | Forced | num |
| 64. Sobamowo, Kamiyo (2017) | Rectangular | Horizontal | Natural | Num |

[8] Also: triangular, convex and exponential.
[9] General mathematical expression for arbitrary fin shape
[10] Also: convex parabolic, concave parabolic and triangular
[11] With rectangular cross section.
[12] With rectangular cross section.
[13] Both horizontal and vertical orientations were tested.
[14] Follows a wave along its length.
[15] Also: Convex parabolic and concave parabolic.

## A The complete list of reviewed literature

| Authors | Fin type | Orientation | Conditions | Research type |
|---|---|---|---|---|
| 65 Shateri, Salashour (2017) | Rectangular [16] | ?? | Natural | Num |
| 66. Abbasbandy, Shivanian (2018) | Rectangular | Horizontal | Natural | Ana |
| 67. Shamvedi, MaCarthy (2018) | Rectangular | Vertical | Natural | Exp |
| 68. Kiwan (2018) | Rectangular | Inlinations | Natural | Num |
| 69. Hoseinzadeh, Moafi (2018) | Rectangular | Horizontal | Natural | Num |
| 70. Oguntala, Sobamovo (2018) | Rectangular | Vertical | Forced | Num |
| 71. Sobamowo, Kam (2019) | Trapezoidal [17] | Horizontal | Natural | Ana |
| 72. Zargar, Mollaghaee (2019) | Annular [18] | Horizontal | Natural | Ana & Num |
| 73. Hoseinzadeh, Heyns (2019) | Rectangular | Horizontal | Natural | Ana & Num |
| 74. Gireesha, Sowmya (2019) | Annular | Vertical | Forced | Num |
| 75. Shafiei, Talaghat (2019) | Annular [19] | Horizontal | Natural | Num |
| 76. Sowmya, Gereesha (2019) | Rectangular | Horizontal | Natural | Num |
| 77. Waseem, Sulaiman (2019) | Rectangular | Horizontal | Natural | Num |
| 78. Gireesha, Sowmya (2020) | Rectangular | Inclined | Natural | Ana |
| 79. Deshamukhya, Banja (2020) | Arbitrary | Horizontal | Natural | Ana |
| 80. Gupta, Guatam (2020) | Rectangular | Horizontal | Natural | Ana & Num |
| 81. Kiwan, Alwan (2020) | Rectangular | Horizontal | natural | Exp |
| 82. Deshamukhya, Bhanja (2020) | T-shaped | Vertical | Natural | Num |
| 83. Ndlovu, Moitsheki (2020) | Rectangular | Horizontal | Forced | Num |
| 84. Sowmya, Gireesha (2020) | Rectangular | Horizontal | Natural | Num |
| 85. Buonomo, Cascetta (2021) | Rectangular | Horizontal | Natural | Ana |
| 86. Deshamukhya, Bhanja (2021) | Rectangular | Vertical | Natural | Num |
| 87. Oguntala, Sobamovo (2022) | Rectangular | Horizontal | Natural | Ana & Num |
| 88. Samudre, Kailas (2022) | Cyclinderical [20] | Both [21] | Forced | Exp |
| 89. Alhakami, Khan (2022) | Rectangular | Horizontal | Natural | Num |
| 90. Das, Barik (2023) | Elliptical | Forced | Natural | Num |
| 91. Fathi (2023) | Rectangular | Vertical | Forced | Num |
| 92. Liu, Feng (2023) | Rectangular | Vertical | Forced | Num |
| 93. Goud, Srilatha (2023) | Trapezoidal | Horizontal | Natural | Num |
| 94. Jalili (2024) | Rectangular | Horizontal | Natural | Ana & Num |

[16] Also: Trapezoidal and concave
[17] Also: Convex parabolic and concave parabolic
[18] With rectangular cross section
[19] With convex, rectangular and triangular cross section
[20] Also: rectangular
[21] Both horizontal and vertical orientation were tested

# B References corresponding to the complete list of reviewed literature

Order corresponding to the previous section.


1. Kiwan, S., & Al-Nimr, M. A. (2000). Using Porous Fins for Heat Transfer Enhancement. Journal Of Heat Transfer, 123(4), 790–795. https://doi.org/10.1115/1.1371922
2. Saedodin, S., & Shahbabaei, M. (2013). Thermal Analysis of Natural Convection in Porous Fins with Homotopy Perturbation Method (HPM). Arabian Journal For Science And Engineering. Section B, Engineering, 38(8), 2227–2231. https://doi.org/10.1007/s13369-013-0581-6
3. Kiwan, S., & Al-Nimr, M. A. (2000b). Using Porous Fins for Heat Transfer Enhancement. Journal Of Heat Transfer, 123(4), 790–795. https://doi.org/10.1115/1.1371922
4. Phanikumar, & Mahajan, R. (2002). Non-Darcy natural convection in high porosity metal foams. International Journal Of Heat And Mass Transfer/International Journal Of Heat And Mass Transfer, 45(18), 3781–3793. https://doi.org/10.1016/s0017-9310(02)00089-3
5. Abu-Hijleh, B. A. (2003). Enhanced Forced Convection Heat Transfer From a Cylinder Using Permeable Fins. Journal Of Heat Transfer, 125(5), 804–811. https://doi.org/10.1115/1.1599371
6. Abu-Hijleh, B. A. (2003a). Natural Convection Heat Transfer From a Cylinder With High Conductivity Permeable Fins. Journal Of Heat Transfer, 125(2), 282–288. https://doi.org/10.1115/1.1532013
7. 
8. Dukhan, N., Quiñones-Ramos, P. D., Cruz-Ruiz, E., Vélez-Reyes, M., & Scott, E. P. (2005). One-dimensional heat transfer analysis in open-cell 10-ppi metal foam. International Journal Of Heat And Mass Transfer/International Journal Of Heat And Mass Transfer, 48(25–26), 5112–5120. https://doi.org/10.1016/j.ijheatmasstransfer.2005.07.012
9. Bhattacharya, A., & Mahajan, R. L. (2005c). Metal Foam and Finned Metal Foam Heat Sinks for Electronics Cooling in Buoyancy-Induced Convection. Journal Of Electronic Packaging, 128(3), 259–266. https://doi.org/10.1115/1.2229225
10. Kiwan, S. (2006b). Thermal Analysis of Natural Convection Porous Fins. Transport in Porous Media, 67(1), 17–29. https://doi.org/10.1007/s11242-006-0010-3
11. Kiwan, S. (2007b). Effect of radiative losses on the heat transfer from porous fins. International Journal Of Thermal Sciences, 46(10), 1046–1055. https://doi.org/10.1016/j.ijthermalsci.2006.11.013
12. Hetsroni, G., Gurevich, M., & Rozenblit, R. (2008b). Natural convection in metal foam strips with internal heat generation. Experimental Thermal And Fluid Science, 32(8), 1740–1747. https://doi.org/10.1016/j.expthermflusci.2008.06.011
13. Kiwan, S., & Zeitoun, O. (2008). Natural convection in a horizontal cylindrical annulus using porous fins. International Journal Of Numerical Methods For Heat & Fluid Flow, 18(5), 618–634. https://doi.org/10.1108/09615530810879747
14. Bhanja, D., Kundu, B., Paruya, S., Kar, S., & Roy, S. (2010b). Heat Transfer and Fin Performance Comparison between Constructal T-shaped Porous and Solid Fin. AIP Conference Proceedings. https://doi.org/10.1063/1.3516287
15. Kundu, B., & Bhanja, D. (2011b). An analytical prediction for performance and optimum design analysis of porous fins. International Journal Of Refrigeration, 34(1), 337–352. https://doi.org/10.1016/j.ijrefrig.2010.06.011
16. Light Weight High Performance Thermal Management With Advanced Heat Sinks and Extended Surfaces. (2010, 1 maart). IEEE Journals & Magazine | IEEE Xplore. https://ieeexplore.ieee.org/document/5286846
17. Khaled, A. A. (2009). Investigation of Heat Transfer Enhancement Through Permeable Fins. Journal Of Heat Transfer, 132(3). https://doi.org/10.1115/1.4000056
18. Bhanja, D., & Kundu, B. (2011). Thermal analysis of a constructal T-shaped porous fin with radiation effects. International Journal Of Refrigeration, 34(6), 1483–1496. https://doi.org/10.1016/j.ijrefrig.2011.04.003
19. Gorla, R. S. R., & Bakier, A. (2011a). Thermal analysis of natural convection and radiation in porous fins. International Communications in Heat And Mass Transfer, 38(5), 638–645. https://doi.org/10.1016/j.icheatmasstransfer.2010.12.024
20. Darvishi, M., Gorla, R., & Khani, F. (2013). Natural convection and radiation in porous fins. International Journal Of Numerical Methods For Heat & Fluid Flow, 23(8), 1406–1420. https://doi.org/10.1108/hff-12-2011-0264
21. Kundu, B., Bhanja, D., & Lee, K. (2012). A model on the basis of analytics for computing maximum heat transfer in porous fins. International Journal Of Heat And Mass Transfer/International Journal Of Heat And Mass Transfer, 55(25–26), 7611–7622. https://doi.org/10.1016/j.ijheatmasstransfer.2012.07.069
22. Darvishi, M., Gorla, R. S. R., Khani, F., & Aziz, A. (2015). Thermal performance of a porus radial fin with natural convection and radiative heat losses. Thermal Science/Thermal Science, 19(2), 669–678. https://doi.org/10.2298/tsci120619149d
23. Petroudi, I. R., Ganji, D. D., Shotorban, A. B., Nejad, M. K., Rahimi, E., Rohollahtabar, R., & Taherinia, F. (2012a). Semi-analytical method for solving non-linear equation arising of natural convection porous fin. Thermal Science/Thermal Science, 16(5), 1303–1308. https://doi.org/10.2298/tsci1205303p
24. Qu, Z., Wang, T., Tao, W., & Lu, T. (2012b). Experimental study of air natural convection on metallic foam-sintered plate. International Journal Of Heat And Fluid Flow, 38, 126–132. https://doi.org/10.1016/j.ijheatfluidflow.2012.08.005
25. Torabi, M., & Yaghoobi, H. (2013b). SERIES SOLUTION FOR CONVECTIVE-RADIATIVE POROUS FIN USING DIFFERENTIAL TRANSFORMATION METHOD. Journal Of Porous Media, 16(4), 341–349. https://doi.org/10.1615/jpormedia.v16.i4.60

# B References corresponding to the complete list of reviewed literature


26. Bhanja, D., Kundu, B., & Mandal, P. K. (2013). Thermal Analysis of Porous Pin Fin used for Electronic Cooling. Procedia Engineering, 64, 956–965. https://doi.org/10.1016/j.proeng.2013.09.172
27. Hatami, M., Hasanpour, A., & Ganji, D. (2013). Heat transfer study through porous fins (Si3N4 and AL) with temperature-dependent heat generation. Energy Conversion And Management, 74, 9–16. https://doi.org/10.1016/j.enconman.2013.04.034
28. Hatami, M., & Ganji, D. (2013). Thermal performance of circular convective–radiative porous fins with different section shapes and materials. Energy Conversion And Management, 76, 185–193. https://doi.org/10.1016/j.enconman.2013.07.040
29. Moradi, A., Hayat, T., & Alsaedi, A. (2014). Convection-radiation thermal analysis of triangular porous fins with temperature-dependent thermal conductivity by DTM. Energy Conversion And Management, 77, 70–77. https://doi.org/10.1016/j.enconman.2013.09.016
30. Hatami, M., & Ganji, D. (2014). Investigation of refrigeration efficiency for fully wet circular porous fins with variable sections by combined heat and mass transfer analysis. International Journal Of Refrigeration, 40, 140–151. https://doi.org/10.1016/j.ijrefrig.2013.11.002
31. Hatami, M., & Ganji, D. (2014b). Thermal behavior of longitudinal convective–radiative porous fins with different section shapes and ceramic materials (SiC and Si3N4). Ceramics International, 40(5), 6765–6775. https://doi.org/10.1016/j.ceramint.2013.11.140
32. Saedodin, S., & Shahbabaei, M. (2013b). Thermal Analysis of Natural Convection in Porous Fins with Homotopy Perturbation Method (HPM). Arabian Journal For Science And Engineering. Section B, Engineering, 38(8), 2227–2231. https://doi.org/10.1007/s13369-013-0581-6
33. Moradi, A., Fallah, A. P. M., Hayat, T., & Aldossary, O. M. (2013). On Solution of Natural Convection and Radiation Heat Transfer Problem in a Moving Porous Fin. Arabian Journal For Science And Engineering. Section B, Engineering, 39(2), 1303–1312. https://doi.org/10.1007/s13369-013-0708-9
34. De Schampheleire, S., De Jaeger, P., Reynders, R., De Kerpel, K., Ameel, B., T'Joen, C., Huisseune, H., Lecompte, S., & De Paepe, M. (2013b). Experimental study of buoyancy-driven flow in open-cell aluminium foam heat sinks. Applied Thermal Engineering, 59(1–2), 30–40. https://doi.org/10.1016/j.applthermaleng.2013.05.010
35. Du, H., Lu, D., Qi, J., Shen, Y., Yin, L., Wang, Y., Zheng, Z., & Xiong, T. (2014b). Heat Dissipation Performance of Porous Copper with Elongated Cylindrical Pores. Journal Of Materials Science And Technology/Journal Of Materials Science & Technology, 30(9), 934–938. https://doi.org/10.1016/j.jmst.2014.03.014
36. Saedodin, S., Sadeghi, S., & Sadeghi, S. (2013b). Temperature distribution in long porous fins in natural convection condition. In IDOSI Publications, Middle-East Journal Of Scientific Research (Vol. 13, Nummer 6, pp. 812–817) [Journal-article]. https://www.idosi.org/mejsr/mejsr13(6)13/17.pdf
37. Das, R., & Ooi, K. (2013a). Predicting multiple combination of parameters for designing a porous fin subjected to a given temperature requirement. Energy Conversion And Management, 66, 211–219. https://doi.org/10.1016/j.enconman.2012.10.019
38. Turkyilmazoglu, M. (2014). Efficiency of heat and mass transfer in fully wet porous fins: Exponential fins versus straight fins. International Journal Of Refrigeration, 46, 158–164. https://doi.org/10.1016/j.ijrefrig.2014.04.011
39. Kundu, B., & Lee, K. (2015). Exact analysis for minimum shape of porous fins under convection and radiation heat exchange with surrounding. International Journal Of Heat And Mass Transfer/International Journal Of Heat And Mass Transfer, 81, 439–448. https://doi.org/10.1016/j.ijheatmasstransfer.2014.10.044
40. Shahbabaei, M., Ganji, D. D., & Rahimipetroudi, I. (2014). Prediction of a Semi-Exact Analytic Solution of a Convective Porous Fin with Variable Cross Section by Different Methods. Walailak Journal Of Science And Technology (WJST), 12(10), 909–921. https://doi.org/10.2004/wjst.v11i12.960
41. Liu, Y., Chen, H., Zhang, H., & Li, Y. (2015). Heat transfer performance of lotus-type porous copper heat sink with liquid GaInSn coolant. International Journal Of Heat And Mass Transfer/International Journal Of Heat And Mass Transfer, 80, 605–613. https://doi.org/10.1016/j.ijheatmasstransfer.2014.09.058
42. Das, R. (2014b). Forward and inverse solutions of a conductive, convective and radiative cylindrical porous fin. Energy Conversion And Management, 87, 96–106. https://doi.org/10.1016/j.enconman.2014.06.096
43. 
44. Vahabzadeh, A., Ganji, D., & Abbasi, M. (2015). Analytical investigation of porous pin fins with variable section in fully-wet conditions. Case Studies in Thermal Engineering, 5, 1–12. https://doi.org/10.1016/j.csite.2014.11.002
45. Patel, T., & Meher, R. (2015). A Study on Temperature Distribution, Efficiency and Effectiveness of Longitudinal Porous Fins by Using Adomian Decomposition Sumudu Transform Method. Procedia Engineering, 127, 751–758. https://doi.org/10.1016/j.proeng.2015.11.409
46. Kundu, B., & Lee, K. (2016). A proper analytical analysis of annular step porous fins for determining maximum heat transfer. Energy Conversion And Management, 110, 469–480. https://doi.org/10.1016/j.enconman.2015.09.037
47. Darvishi, M., Gorla, R. S. R., Khani, F., & Aziz, A. (2015b). Thermal performance of a porus radial fin with natural convection and radiative heat losses. Thermal Science/Thermal Science, 19(2), 669–678. https://doi.org/10.2298/tsci120619149d
48. Cuce, E., & Cuce, P. M. (2015). A successful application of homotopy perturbation method for efficiency and effectiveness assessment of longitudinal porous fins. Energy Conversion And Management, 93, 92–99. https://doi.org/10.1016/j.enconman.2015.01.003
49. Chuan, L., Wang, X., Wang, T., & Yan, W. (2015). Fluid flow and heat transfer in microchannel heat sink based on porous fin design concept. International Communications in Heat And Mass Transfer, 65, 52–57. https://doi.org/10.1016/j.icheatmasstransfer.2015.04.005
50. Ma, J., Sun, Y., Li, B., & Chen, H. (2016). Spectral collocation method for radiative–conductive porous fin with temperature dependent properties. Energy Conversion And Management, 111, 279–288. https://doi.org/10.1016/j.enconman.2015.12.054

## B References corresponding to the complete list of reviewed literature


51. Singh, K., Das, R., & Kundu, B. (2016). Approximate Analytical Method for Porous Stepped Fins with Temperature-Dependent Heat Transfer Parameters. Journal Of Thermophysics And Heat Transfer, 30(3), 661–672. https://doi.org/10.2514/1.t4831
52. Aly, S., Arif, A., Al-Athel, K., Mostaghimi, J., & Zubair, S. (2016). Performance of open pore metal foam heat sinks fabricated with thermally sprayed interface. Applied Thermal Engineering, 105, 411–424. https://doi.org/10.1016/j.applthermaleng.2016.03.012
53. Khani, F., Darvishi, M., Gorla, R., & Gireesha, B. (2016). Thermal analysis of a fully wet porous radial fin with natural convection and radiation using the spectral collocation method. International Journal Of Applied Mechanics And Engineering, 21(2), 377–392. https://doi.org/10.1515/ijame-2016-0023
54. Darvishi, M., Gorla, R. S. R., Khani, F., & Gireesha, B. (2016). Thermal analysis of natural convection and radiation in a fully wet porous fin. International Journal Of Numerical Methods For Heat & Fluid Flow, 26(8), 2419–2431. https://doi.org/10.1108/hff-06-2015-0230
55. Asadian, H., Zaretabar, M., Ganji, D. D., Gorji-Bandpy, M., & Sohrabi, S. (2016). Investigation of Heat Transfer in Rectangular Porous Fins $(Si3N_4)$ ( Si 3 N 4 ) with Temperature-Dependent Internal Heat Generation by Galerkin's Method (GM) and Akbari-Ganji's Method (AGM). International Journal Of Applied And Computational Mathematics, 3(4), 2987–3000. https://doi.org/10.1007/s40819-016-0279-z
56. Deshamukhya, T., Bhanja, D., Nath, S., Maji, A., & Choubey, G. (2017). Analytical study of temperature distribution in a rectangular porous fin considering both insulated and convective tip. AIP Conference Proceedings. https://doi.org/10.1063/1.4990184
57. Hoshyar, H. A., Rahimipetroudi, I., & Ganji, D. D. (2017). Heat Transfer Performance on Longitudinal Porous Fins with Temperature-Dependent Heat Generation, Heat Transfer Coefficient and Surface Emissivity. Mechanical & Materials Engineering/Iranian Journal Of Science And Technology. Transactions Of Mechanical Engineering, 43(2), 383–391. https://doi.org/10.1007/s40997-017-0126-9
58. Feng, S., Li, F., Zhang, F., & Lu, T. J. (2018b). Natural convection in metal foam heat sinks with open slots. Experimental Thermal And Fluid Science, 91, 354–362. https://doi.org/10.1016/j.expthermflusci.2017.07.010
59. Bilen, K., Gok, S., Olcay, A., & Solmus, I. (2017). Investigation of the effect of aluminum porous fins on heat transfer. Energy, 138, 1187–1198. https://doi.org/10.1016/j.energy.2017.08.015
60. Stark, J., Prasad, R., & Bergman, T. (2017). Experimentally validated analytical expressions for the thermal efficiencies and thermal resistances of porous metal foam-fins. International Journal Of Heat And Mass Transfer/International Journal Of Heat And Mass Transfer, 111, 1286–1295. https://doi.org/10.1016/j.ijheatmasstransfer.2017.03.041
61. Hazarika, S. A., Deshamukhya, T., Bhanja, D., & Nath, S. (2017). Thermal analysis of a constructal T-shaped porous fin with simultaneous heat and mass transfer. Chinese Journal Of Chemical Engineering/Chinese Journal Of Chemical Engineering, 25(9), 1121–1136. https://doi.org/10.1016/j.cjche.2017.03.034
62. Lu, G., Zhao, J., Lin, L., Wang, X., & Yan, W. (2017). A new scheme for reducing pressure drop and thermal resistance simultaneously in microchannel heat sinks with wavy porous fins. International Journal Of Heat And Mass Transfer/International Journal Of Heat And Mass Transfer, 111, 1071–1078. https://doi.org/10.1016/j.ijheatmasstransfer.2017.04.086
63. Ma, J., Sun, Y., & Li, B. (2017). Simulation of combined conductive, convective and radiative heat transfer in moving irregular porous fins by spectral element method. International Journal Of Thermal Sciences, 118, 475–487. https://doi.org/10.1016/j.ijthermalsci.2017.05.008
64. Sobamowo, M., Kamiyo, O., & Adeleye, O. (2017). Thermal performance analysis of a natural convection porous fin with temperature-dependent thermal conductivity and internal heat generation. Thermal Science And Engineering Progress, 1, 39–52. https://doi.org/10.1016/j.tsep.2017.02.007
65. Shateri, A., & Salahshour, B. (2018). Comprehensive thermal performance of convection–radiation longitudinal porous fins with various profiles and multiple nonlinearities. International Journal Of Mechanical Sciences, 136, 252–263. https://doi.org/10.1016/j.ijmecsci.2017.12.030
66. Abbasbandy, S., & Shivanian, E. (2019). The exact closed solution in the analysis of a natural convection porous fin with temperature-dependent thermal conductivity and internal heat generation. Canadian Journal Of Physics, 97(5), 566–575. https://doi.org/10.1139/cjp-2018-0242
67. Shamvedi, D., McCarthy, O. J., O'Donoghue, E., Danilenkoff, C., O'Leary, P., & Raghavendra, R. (2018). 3D Metal printed heat sinks with longitudinally varying lattice structure sizes using direct metal laser sintering. Virtual And Physical Prototyping, 13(4), 301–310. https://doi.org/10.1080/17452759.2018.1479528
68. Kiwan, S. (2018). On the Natural Convection Heat Transfer from an Inclined Surface with Porous Fins. Transport in Porous Media, 127(2), 295–307. https://doi.org/10.1007/s11242-018-1192-1
69. Hoseinzadeh, S., Moafi, A., Shirkhani, A., & Chamkha, A. J. (2019). Numerical Validation Heat Transfer of Rectangular Cross-Section Porous Fins. Journal Of Thermophysics And Heat Transfer, 33(3), 698–704. https://doi.org/10.2514/1.t5583
70. Oguntala, G. (2022). Investigation of Simultaneous Effects of Surface Roughness, Porosity and Magnetic Field of Rough Porous Micro-Fin under a Convective-Radiative Heat Transfer for Improved Electronic Cooling of Microprocessors. Bradford. https://ieeexplore.ieee.org/document/8515250
71. Sobamowo, G., Kamiyo, O., Salami, M., & Yinusa, A. (2019). Exploration of the effects of fin geometry and material properties on thermal performance of convective-radiative moving fins. https://www.semanticscholar.org/paper/Exploration-of-the-effects-of-fin-geometry-and-on-Sobamowo-Kamiyo/36f149cd81413bde08658b0881c9b7b6e10c4b6b
72. Zargar, O., Mollaghaee-Roozbahani, M., Bashirpour, M., & Baghani, M. (2019). The Application of Homotopy Analysis Method to Determine the Thermal Response of Convective-Radiative Porous Fins with Temperature-Dependent Properties. International Journal Of Applied Mechanics, 11(09), 1950089. https://doi.org/10.1142/s1758825119500893

## B References corresponding to the complete list of reviewed literature


73. Hoseinzadeh, S., Heyns, P. S., Chamkha, A. J., & Shirkhani, A. (2019). Thermal analysis of porous fins enclosure with the comparison of analytical and numerical methods. Journal Of Thermal Analysis And Calorimetry, 138(1), 727–735. https://doi.org/10.1007/s10973-019-08203-x
74. Gireesha, B., Sowmya, G., & Macha, M. (2019). Temperature distribution analysis in a fully wet moving radial porous fin by finite element method. International Journal Of Numerical Methods For Heat & Fluid Flow, 32(2), 453–468. https://doi.org/10.1108/hff-12-2018-0744
75. Shafiei, F., & Talaghat, M. R. (2019). Numerical and Galerkin's methods for thermal performance analysis of circular porous fins with various profiles when the surface temperature is higher/lower than the air temperature. Energy Sources. Part A, Recovery, Utilization, And Environmental Effects, 45(3), 8301–8319. https://doi.org/10.1080/15567036.2019.1677816
76. Sowmya, G., Gireesha, B., & Makinde, O. (2019). Thermal performance of fully wet longitudinal porous fin with temperature-dependent thermal conductivity, surface emissivity and heat transfer coefficient. Multidiscipline Modeling in Materials And Structures, 16(4), 749–764. https://doi.org/10.1108/mmms-08-2019-0147
77. Waseem, W., Sulaiman, M., Islam, S., Kumam, P., Nawaz, R., Raja, M. A. Z., Farooq, M., & Shoaib, M. (2020). A study of changes in temperature profile of porous fin model using cuckoo search algorithm. Alexandria Engineering Journal /Alexandria Engineering Journal, 59(1), 11–24. https://doi.org/10.1016/j.aej.2019.12.001
78. Gireesha, B., & Sowmya, G. (2020). Heat transfer analysis of an inclined porous fin using Differential Transform Method. International Journal Of Ambient Energy, 43(1), 3189–3195. https://doi.org/10.1080/01430750.2020.1818619
79. Deshamukhya, T., Bhanja, D., & Nath, S. (2020). Heat transfer enhancement through porous fins: A comprehensive review of recent developments and innovations. Proceedings Of The Institution Of Mechanical Engineers. Part C, Journal Of Mechanical Engineering Science, 235(5), 946–960. https://doi.org/10.1177/0954406220939600
80. Gupta, A., Gautam, N., Sahoo, S., & Mohanty, A. (2020). Performance evaluation of porous fin with prescribed tip temperature: An analytical and numerical approach. International Journal Of Heat And Mass Transfer/International Journal Of Heat And Mass Transfer, 156, 119736. https://doi.org/10.1016/j.ijheatmasstransfer.2020.119736
81. Kiwan, S., Alwan, H., & Abdelal, N. (2020b). An experimental investigation of the natural convection heat transfer from a vertical cylinder using porous fins. Applied Thermal Engineering, 179, 115673. https://doi.org/10.1016/j.applthermaleng.2020.115673
82. Deshamukhya, T., Bhanja, D., & Nath, S. (2020a). Optimization of constructal T-shaped porous fins under convective environment using Swarm Intelligence Algorithms. Proceedings Of The Institution Of Mechanical Engineers. Part G, Journal Of Aerospace Engineering, 234(14), 2100–2113. https://doi.org/10.1177/0954410020926660
83. Ndlovu, P. L., & Moitsheki, R. J. (2020). Steady state heat transfer analysis in a rectangular moving porous fin. Propulsion And Power Research, 9(2), 188–196. https://doi.org/10.1016/j.jppr.2020.03.002
84. Sowmya, G., BJ, G., Khan, M. I., Momani, S., & Hayat, T. (2020). Thermal investigation of fully wet longitudinal porous fin of functionally graded material. International Journal Of Numerical Methods For Heat & Fluid Flow, 30(12), 5087–5101. https://doi.org/10.1108/hff-12-2019-0908
85. Buonomo, B., Cascetta, F., Manca, O., & Sheremet, M. (2021). Heat transfer analysis of rectangular porous fins in local thermal non-equilibrium model. Applied Thermal Engineering, 195, 117237. https://doi.org/10.1016/j.applthermaleng.2021.117237
86. Deshamukhya, T., Bhanja, D., & Nath, S. (2021). A metaheuristic analysis of heat transfer rates through porous fins of tapered and step profiles: a comparative study. Neural Computing & Applications, 33(19), 12605–12619. https://doi.org/10.1007/s00521-021-05911-0
87. Oguntala, G. A., Sobamowo, G., Ahmed, Y., & Abd-Alhameed, R. (2019). Thermal Prediction of Convective-Radiative Porous Fin Heatsink of Functionally Graded Material Using Adomian Decomposition Method. Computation, 7(1), 19. https://doi.org/10.3390/computation7010019
88. Samudre, P., & Kailas, S. V. (2022b). Thermal performance enhancement in open-pore metal foam and foam-fin heat sinks for electronics cooling. Applied Thermal Engineering, 205, 117885. https://doi.org/10.1016/j.applthermaleng.2021.117885
89. Alhakami, H., Khan, N. A., Sulaiman, M., Alhakami, W., & Baz, A. (2022). On the Computational Study of a Fully Wetted Longitudinal Porous Heat Exchanger Using a Machine Learning Approach. Entropy, 24(9), 1280. https://doi.org/10.3390/e24091280
90. Ranjan, A., Das, R., Barik, D., Pal, S., Majumder, A., Deb, M., & Dennison, M. S. (2023). Heat Transfer and Performance Enhancement of Porous Split Elliptical Fins. International Journal Of Energy Research, 2023, 1–26. https://doi.org/10.1155/2023/9206017
91. Fathi, M., Heyhat, M. M., Targhi, M. Z., & Bigham, S. (2023). Porous-fin microchannel heat sinks for future micro-electronics cooling. International Journal Of Heat And Mass Transfer/International Journal Of Heat And Mass Transfer, 202, 123662. https://doi.org/10.1016/j.ijheatmasstransfer.2022.123662
92. Liu, X., Feng, H., Chen, L., & Ge, Y. (2023). Constructal design of a rectangular porous fin considering minimization of maximum temperature difference and pumping power consumption. Science China. Technological Sciences/Science China. Technological Sciences, 67(3), 919–929. https://doi.org/10.1007/s11431-023-2495-y
93. Goud, J. S., Srilatha, P., Kumar, R. V., Sowmya, G., Gamaoun, F., Nagaraja, K., Chohan, J. S., Khan, U., & Eldin, S. M. (2023). Heat transfer analysis in a longitudinal porous trapezoidal fin by non-Fourier heat conduction model: An application of artificial neural network with Levenberg–Marquardt approach. Case Studies in Thermal Engineering, 49, 103265. https://doi.org/10.1016/j.csite.2023.103265
94. Jalili, P., Alamdari, S. G., Jalili, B., Shater, A., & Ganji, D. D. (2024). Analytical and numerical investigation of heat transfer of porous fin in a local thermal non-equilibrium state. Heliyon, 10(4), e26424. https://doi.org/10.1016/j.heliyon.2024.e26424

# C Scripts

## C.1 Predicted temperature profiles for the experiment

```
# -*- coding: utf-8 -*-
"""
Created on Wed Apr 24 10:00:36 2024

@author: Wessel Schilders
"""
import numpy as np
import matplotlib.pyplot as plt

Type = 1            # 1 = adiabatic tip, 2 = fixed tip temperature
savefigure = True

Tb = np.array([48, 46, 43])         # Base temperatures
Tt = np.array([47, 27.5, 26.5])     # Tip temperatures (estimated from plot)
Te = 24                             # ambient temperature
hn = np.array([132, 210, 245])      # Effective convective heat transfer coefficients

k = np.array([218, 5.8, 5.8])       # Effective conductive heat transfer coefficients
L, H, t = 20e-3, 15e-3, 6.35e-3     # H depicts the lenght of the fin!!!
Ac = L*t                            # Fin cross-sectional area
P = 2*(t+L)                         # Fin periphery

colors = ['black', 'blue', 'red']
fin = ["Solid","Porous, glued",'Porous, thermal spray']
x = np.linspace(0,1,1000)

plt.figure(dpi = 500)
for i in range(len(Tt)):
    a = np.sqrt(hn[i]*P*H**2/k[i]/Ac)

    def T_fin(X):
        if Type == 1:
            # Adiabatic analytical prediction
            return -np.tanh(a)*np.sinh(a*X)+np.cosh(a*X)
        if Type == 2:
            # Fixed tip temperature analytical prediction
            return (((Tt[i]-Te)/(Tb[i]-Te)-np.cosh(a))/np.sinh(a))*np.sinh(a*X)+np.cosh(a*X)

    Temp = T_fin(x)*(Tb[i]-Te)+Te

    print(fin[i],"fin analytically predicted tip temperature:", round(Temp[-1],1))

    #plt.title('Predicted temperature profile from $T_b$ and $T_{tip}$')
    plt.plot(x, Temp, color = colors[i], label = fin[i])            # Adiabatic
    plt.plot(x[-1], Tt[i],"o", color = colors[i])
    plt.plot(x[0], Tb[i],"o", color = colors[i])
    #plt.plot(x, Tempt, '--', color = colors[i])                     # Fixed tip temperature
plt.xlabel('x/L [-]', size = 15)
plt.ylabel('T [$^\circ$C]', size = 15)
plt.legend()
plt.grid()
plt.xlim(-.025,1.025)
plt.ylim(min(Tt)-5,max(Tb)+5)
if  savefigure:
    plt.savefig("E:\Process, flow and energy\Thesis\Predicted temperature profile.jpg")
```

## C.2 Error estimation in measured average temperature

```
# -*- coding: utf-8 -*-
"""
Created on Tue Jun  4 15:12:43 2024

@author: Wessel Schilders
"""

import numpy as np
import matplotlib.pyplot as plt

n = 10
points = np.linspace(0,1,n)
D = 50e-3
Ac = np.pi*(D/2)**2
Tb = 50
Tt = np.array([45, 40, 35, 30,25,20,15])
x = np.linspace(0,1,100)
a = np.linspace(0.1,2,10)
Nu = a**2*Ac/D/D
error = np.zeros(len(a))
kelvin = 273

Te = 20
fig, (ax1, ax2) = plt.subplots(1, 2, figsize=(15, 5), dpi = 500)
fig.suptitle('Integration error in the case of four thermocouples', size = 20)
for k in range(len(Tt)):
    for j in range(len(a)):
        B = ((Tt[k]-Te)/(Tb-Te)-np.cosh(a[j]))/np.sinh(a[j])
        def T(X):
            return B*np.sinh(a[j]*X)+np.cosh(a[j]*X)

        Tavg_num_nd = 0
        for i in range(n-1):
            Tavg_num_nd = Tavg_num_nd + 0.5*(points[i+1]-points[i])*(T(points[i+1])+T(points[i]))
            Tavg_num = (Tavg_num_nd*(Tb-Te)+Te)

        Tavg = ((B*(np.cosh(a[j])-1)+np.sinh(a[j]))/a[j])*(Tb-Te)+Te
        #error[j] = ((Tavg_num-Tavg)/(Tavg+kelvin))*100
        error[j] = Tavg_num-Tavg
        if j == 2 and k==0:
            ax1.plot(points,(Tb-Te)*T(points)+Te, '--bo')
            ax1.plot(x,T(x)*(Tb-Te)+Te, color = 'r')
    if k%2==0:
        ax2.plot(Nu,error,'--', label = "$\Delta T$ = "+ str(Tb-Tt[k]) + '$^\circ$C')
        ax2.plot(Nu,error,'x',color = 'black')
        print(error)

ax1.grid()
ax1.set_xlabel('x/L [-]',size = 15)
ax1.set_ylabel('T $[^\circ C]$',size = 15)
ax2.grid()
ax2.legend()
ax2.set_xlabel('Nu [-]',size = 15)
ax2.set_ylabel('Error $^\circ C$',size = 15)
```

## C.3 Heat losses through the insulation material

```
close all
clear all

T = 235;
Te = 20;
w = 250e-3;
h = 60e-3;
r = 25e-3;
K = 0.09;
rho = 2.9e3;
c = 840;
dt = 10;
time = 0;
level = 16;
dT = 10;

imax = 100;
jmax = 100;
kmax = 31;

dx = w/(imax-1);
dy = w/(jmax-1);
dz = h/(kmax-1);

x = linspace(0,w,imax);
y = linspace(0,w,jmax);
z = linspace(0,h,kmax);

for k = 1:kmax
for j = 1:jmax
for i = 1:imax
    xplot(i,j,k) = x(i);
    yplot(i,j,k) = y(j);
    zplot(i,j,k) = z(k);
end
end
end

QW = zeros(imax, jmax,kmax);
QE = zeros(imax, jmax,kmax);
QS = zeros(imax, jmax,kmax);
QN = zeros(imax, jmax,kmax);
QD = zeros(imax, jmax,kmax);
QU = zeros(imax, jmax,kmax);

T_old = Te*ones(imax, jmax, kmax);
T_new = Te*ones(imax,jmax,kmax);

while dT > 0.001
for k = 2:kmax-1
for j = 2:jmax-1
for i = 2:imax-1
    if ((x(i)-w/2)^2+(y(j)-w/2)^2)^(1/2) < r && z(k) >= 0.0299999
        T_old(i,j,k) = T;
    end
    QW(i,j,k) = K*dy*dz*(T_old(i-1,j,k)-T_old(i,j,k))/dx;
    QE(i,j,k) = K*dy*dz*(T_old(i,j,k)-T_old(i+1,j,k))/dx;
    QS(i,j,k) = K*dx*dz*(T_old(i,j-1,k)-T_old(i,j,k))/dy;
    QN(i,j,k) = K*dx*dz*(T_old(i,j,k)-T_old(i,j+1,k))/dy;
    QD(i,j,k) = K*dx*dy*(T_old(i,j,k-1)-T_old(i,j,k))/dz;
    QU(i,j,k) = K*dx*dy*(T_old(i,j,k)-T_old(i,j,k+1))/dz;
    T_new(i,j,k) = T_old(i,j,k) + dt/rho/c/dx/dy/dz*(QW(i,j,k)+QS(i,j,k)+QD(i,j,k)-QE(i,j,k)-QN(i,j,k)-
QU(i,j,k));
```

```
end
end
end
T_new(1,:,:) = Te;
T_new(imax,:,:) = Te;
T_new(:,1,:) = Te;
T_new(:,jmax,:) = Te;
T_new(:,:,1) = T_new(:,:,2);
T_new(:,:,kmax) = T_new(:,:,kmax-1);
dT = max(max(max(T_new-T_old)));
T_old = T_new;
%surf(xplot(:,:,level),yplot(:,:,level),T_old(:,:,level))
%zlim([0 T+10]);
%pause(0.01)
time = time+dt;
minute = round(time/60);
end
minute
dT
```

## C.4 Visualization of experimental data

```
# -*- coding: utf-8 -*-
"""
Created on Thu Dec  5 13:50:43 2024

@author: Wessel Schilders
"""
import numpy as np
import matplotlib.pyplot as plt
from scipy import optimize

savefigure = False

# 0:solidV1, 1: SolidV2, 2: SolidH1, 3:9505V, 4:9505H, 5:9508V, 6:9508H, 7:9805V, 8:9805H
Title = np.array(["Solid fin, vertical orientation 1",
                  "Solid fin, vertical orientation",
                  "Solid fin, horizontal orientation",
                  "95 percent porosity, 0.5mm pore size, vertical orientation",
                  "95 percent porosity, 0.5mm pore size, Horizontal orientation",
                  "95 percent porosity, 0.8mm pore size, vertical orientation",
                  "95 percent porosity, 0.8mm pore size, horizontal orientation",
                  "98 percent porosity, 0.5mm pore size, vertical orientation",
                  "98 percent porosity, 0.5mm pore size, horizontal orientation"])
Type =     8

#Fin characteristics
D = 15e-3                       # m
L = 140e-3                      # m
P = np.pi*D                     # mm
Ac = np.pi*D**2/4               # mm^2

# Calculating effective conductivity
porosities = np.array([0, 0, 0, 0.95, 0.95, 0.95, 0.95, 0.98, 0.98])
epsilon = porosities[Type]
kf = 0.04                       # W/m/K
ks = 86                         # W/m/K
k = 0.35*(epsilon*kf+(1-epsilon)*ks) + (1-0.35)/(epsilon/kf+(1-epsilon)/ks)
#k = 25*k     #(Correction for k)

# Experimental data
if Type == 0:    # solidV1
    Q = 7.01
    Te = 18
    x_measured = np.array([0, 12.9, 28.6, 43.2, 59.3, 75.9, 91.8, 105.4, 122.5, 135.6])
    T_measured = np.array([80.2, 71.7, 63.8, 71.0, 65.8, 68.2, 67.8, 67.6, 57.7, 69.0])
if Type == 1:    # SolidV2
    Q = 4.6
    Te = 18.6
    x_measured = np.array([0, 14, 28, 42.5, 60.5, 76.8, 94.4, 108, 124, 136])
    T_measured = np.array([52.7, 52.2, 49.4, 48.6, 43.8, 42.2, 43.3, 41.5, 38.1, 37.3])
if Type == 2:    # SolidH1
    Q = 4.6
    Te = 18.3
    x_measured = np.array([0, 14, 28, 42.5, 60.5, 76.8, 94.4, 108, 124, 136])
    T_measured = np.array([50.9, 50.4, 46.7, 47.2, 46.6, 42.9, 46.8, 43.1, 45.0, 39.5])
if Type == 3:   # P9505V
    Q = 4.6
    Te = 17.1
    x_measured = np.array([0, 12.5, 28.4, 44.5, 59.5, 74.2, 88.0, 104.5, 122.1, 138.9])
    T_measured = np.array([47.2,31.2,26.1,21.3,18.9,17.7,16.5,16.5, 16.5, 16.3])
if Type == 4:   # P9505H
    Q = 4.61
    Te = 18.2
    x_measured = np.array([0, 12.5, 27.7, 44.5, 59.5, 74.2, 88.0, 104.5, 122.1, 138.9])
```

```
    T_measured = np.array([42.0, 25.1, 21.8, 19.6, 18.7, 18.4, 17.9, 18.0, 18.2, 18.5])
if Type == 5: # P9508V
    Q = 4.61
    Te = 17.0
    x_measured = np.array([0, 15.6, 31.1, 46.7, 62.2, 77.8, 93.3, 108.9, 124.4, 140.0])
    T_measured = np.array([47.1, 30.5, 20.9, 21.0, 18.5, 17.5 ,16.8, 17.2, 17.2, 17.5])
if Type == 6:   # P9508H
    Q = 4.71
    Te = 18.9
    x_measured = np.array([0, 15.6, 31.1, 46.7, 62.2, 77.8, 93.3, 108.9, 124.4, 140.0])
    T_measured = np.array([42.6, 24.5, 20.5, 19.5, 19.6, 18.6, 18.4, 18.7, 18.6, 18.8])
if Type == 7:   # P9805V
    Q = 4.67
    Te = 18.8
    x_measured = np.array([0, 20.1, 38, 52.7, 68.9, 84.8, 100.7, 112.5, 129.5, 142.3])
    T_measured = np.array([47.7, 29.1, 23.2, 22.0, 20.7, 19.7, 19.6, 19.4, 20.1, 19.1])
if Type == 8:   # P9805H
    Q = 4.71
    Te = 18.8
    x_measured = np.array([0, 20.1, 38, 52.7, 68.9, 84.8, 100.7, 112.5, 129.5, 142.3])
    T_measured = np.array([39.7, 23.7, 19.6, 20.0, 19.2, 18.9, 19.0, 18.7, 18.8, 18.7])
# T_sum = 0
# for i in range(len(T_measured)-1):
#     T_sum = T_sum + (T_measured[i+1])*(x_measured[i+1]-x_measured[i])+
#   0.5*(x_measured[i+1]-x_measured[i])*(T_measured[i]-T_measured[i+1])
# T_avg = T_sum/1000/x_measured[-1]

x_tilde = np.linspace(0,1,100)

def Temperature(x, A):
    T_tilde = -np.tanh(A)*np.sinh(A*x)+np.cosh(A*x)
    return T_tilde

alpha = optimize.curve_fit(Temperature, xdata = x_measured/x_measured[-1],
ydata = (T_measured-Te)/(T_measured[0]-Te))[0]
# Input above should be nondimensionalized!
# print(alpha)

T_regression = Temperature(x_tilde, alpha[0])*(T_measured[0]-Te)+Te
T_avg = 1/alpha[0]*(-np.tanh(alpha[0])*np.cosh(alpha[0])+np.sinh(alpha[0])+np.tanh(alpha[0]))
T_avg = T_avg*(T_measured[0]-Te)+Te
DT = T_avg-Te
A_exposed = Ac+x_measured[-1]/1000*P
hc = Q/A_exposed/(DT)
a = np.sqrt(hc*P*L*L/k/Ac)

# Possible correction for base temperature
T_analytical = Temperature(x_tilde,a)*(T_measured[0]-Te)+Te
if Type == 1:
    T_analytical = Temperature(x_tilde,a)*(T_measured[0]-Te)+Te
if Type == 2:
    T_analytical = Temperature(x_tilde,a)*(T_measured[0]-Te)+Te
# Scheffe band, confidence interval for the fit
Syx = np.sqrt(sum((T_measured-(Temperature(x_measured/x_measured[-1], alpha[0])*
(T_measured[0]-Te)+Te))**2)/(len(T_measured)-1))
Scheffe = np.sqrt(1/(len(T_measured))+(x_tilde*x_measured[-1]-np.mean(x_measured))**2/
(sum((x_measured-np.mean(x_measured))**2)))
ci = 2.571 * Syx * Scheffe

# Numerical error filter (remove temperature values below ambient or higher than previous value)
for i in range(len(T_analytical)-1):
    if T_analytical[i] < Te:
        T_analytical[i] = Te
    if T_analytical[i+1] > T_analytical[i]:
        T_analytical[i+1] = Te
```

```
plt.figure(1, dpi = 500)
plt.plot(x_measured,T_measured,".", color = 'black', label = "Measurement")
plt.plot(x_tilde*x_measured[-1],T_regression, '--', color = 'black', label = "Best fitting line")
plt.plot(x_tilde*x_measured[-1],T_analytical,color = 'green', label = "Analytical prediction,
with $k = 25k_e$",)
plt.fill_between(x_tilde*x_measured[-1], (T_regression-ci), (T_regression+ci), color='b',
                 alpha=.1, label = '95% regression interval')

plt.xlim(-5,140)
if Type > 0:
    plt.ylim(0,60)
plt.xlabel("Position along fin [mm]",fontsize=13)
plt.ylabel("Temperature [$^{\circ}C$]",fontsize=13)
if Type > 2:
    plt.legend(loc = 'upper right', fontsize = 11)
else:
    plt.legend(loc = 'lower left',fontsize=11)
plt.title(Title[Type],fontsize=13)

# Confidence intervals:
# linewidth = 3
# t = 2.57
# left = x_measured-linewidth/2
# right = x_measured+linewidth/2
# top = T_measured + t*CI
# bottom = T_measured - t*CI
# plt.plot([x_measured, x_measured], [top, bottom], color='black')
# plt.plot([left, right], [top, top], color="black")
# plt.plot([left, right], [bottom, bottom], color='black')

plt.grid()
if savefigure:
    plt.savefig('E:\Process, flow and energy\Thesis\\'  +str(Title[Type]) +" correction.jpg")

# Uncertainty hc:
varT = 0.003+0.01*0
varTavg = (0.013/np.sqrt(10))**2
#varTavg = (Syx/np.sqrt(10))**2
U_hc = np.sqrt((varT+varTavg)*(Q**2/P**2/L**2/(T_avg-Te)**4))
print(round(hc,1),"+/-",round(U_hc,1))
```

# D Raw experimental data

## D.1 Solid, vertical orientation, measurement 1

| Position | Difference | Channel | Thermocouple | ICE read 1 | ICE read 2 | ICE read 3 | ICE read 4 | ICE read 5 | Average |
|---|---|---|---|---|---|---|---|---|---|
| 0 | - | DAQ1 - A11 | S1 | 1.84 | 1.86 | 1.87 | 1.88 | 1.84 | **1.858** |
| 12.9 | 12.9 | DAQ1 - A22 | S2 | 0.76 | 0.74 | 0.73 | 0.77 | 0.72 | **0.744** |
| 28.6 | 15.7 | DAQ1 - A33 | S3 | 1.23 | 1.14 | 1.21 | 1.12 | 1.11 | **1.162** |
| 43.2 | 14.6 | DAQ1 - A44 | S4 | 0.94 | 0.96 | 1.05 | 0.94 | 1.03 | **0.984** |
| 59.3 | 16.1 | DAQ1 - A55 | S5 | 1.25 | 1.25 | 1.23 | 1.27 | 1.25 | **1.25** |
| 75.9 | 16.6 | DAQ1 - A66 | S6 | 0.67 | 0.64 | 0.66 | 0.64 | 0.66 | **0.654** |
| 91.8 | 15.9 | DAQ1 - A77 | S7 | 0.76 | 0.8 | 0.82 | 0.75 | 0.83 | **0.792** |
| 105.4 | 13.6 | DAQ1 - A88 | S8 | 0.54 | 0.56 | 0.52 | 0.56 | 0.46 | **0.528** |
| 122.5 | 17.1 | DAQ1 - A11 | S9 | 0.31 | 0.26 | 0.37 | 0.4 | 0.28 | **0.324** |
| 135.6 | 13.1 | DAQ1 - A22 | S10 | 0.68 | 0.7 | 0.69 | 0.7 | 0.71 | **0.696** |
| **Position** | **Difference** | **Channel** | **Thermocouple** | **BOIL read 1** | **BOIL read 2** | **BOIL read 3** | **BOIL read 4** | **BOIL read 5** | **Average** |
| 0 | - | DAQ1 - A11 | S1 | 106.52 | 106.55 | 106.63 | 106.66 | 106.6 | **106.592** |
| 12.9 | 12.9 | DAQ1 - A22 | S2 | 105.13 | 104.11 | 105.15 | 105.13 | 105.06 | **104.916** |
| 28.6 | 15.7 | DAQ1 - A33 | S3 | 105.25 | 105.34 | 105.28 | 105.33 | 105.45 | **105.33** |
| 43.2 | 14.6 | DAQ1 - A44 | S4 | 105.27 | 105.14 | 105.27 | 105.24 | 105.23 | **105.23** |
| 59.3 | 16.1 | DAQ1 - A55 | S5 | 104.2 | 103.97 | 104.11 | 104.15 | 103.9 | **104.066** |
| 75.9 | 16.6 | DAQ1 - A66 | S6 | 104.23 | 104.17 | 104.43 | 104.25 | 104.42 | **104.3** |
| 91.8 | 15.9 | DAQ1 - A77 | S7 | 104.62 | 104.67 | 104.71 | 104.6 | 104.59 | **104.638** |
| 105.4 | 13.6 | DAQ1 - A88 | S8 | 104.1 | 104.4 | 104.19 | 104.23 | 104.09 | **104.202** |
| 122.5 | 17.1 | DAQ1 - A11 | S9 | 105.11 | 105.13 | 105.03 | 105.25 | 105.1 | **105.124** |
| 135.6 | 13.1 | DAQ1 - A22 | S10 | 104.55 | 104.59 | 104.66 | 104.76 | 104.73 | **104.658** |

| T_0 | e_0 | T_100 | e_100 | a | b | Var(a) | Var(b) |
|---|---|---|---|---|---|---|---|
| 0 | 1.858 | 100 | 6.592 | 0.04734 | 1.858 | 2.87E-07 | 2.56E-04 |
| 0 | 0.744 | 100 | 4.916 | 0.04172 | 0.744 | 1.64E-05 | 3.44E-04 |
| 0 | 1.162 | 100 | 5.33 | 0.04168 | 1.162 | 7.06E-07 | 2.38E-03 |
| 0 | 0.984 | 100 | 5.23 | 0.04246 | 0.984 | 4.46E-07 | 2.18E-03 |
| 0 | 1.25 | 100 | 4.066 | 0.02816 | 1.25 | 1.29E-06 | 1.60E-04 |
| 0 | 0.654 | 100 | 4.3 | 0.03646 | 0.654 | 1.13E-06 | 1.44E-04 |
| 0 | 0.792 | 100 | 4.638 | 0.03846 | 0.792 | 3.07E-07 | 1.02E-03 |
| 0 | 0.528 | 100 | 4.202 | 0.03674 | 0.528 | 1.40E-06 | 1.38E-03 |
| 0 | 0.324 | 100 | 5.124 | 0.048 | 0.324 | 7.93E-07 | 2.82E-03 |
| 0 | 0.696 | 100 | 4.658 | 0.03962 | 0.696 | 6.48E-07 | 1.04E-04 |

| Measurements | | | | | Average | Corrected | var(error) | var(measurement) | var(Temp) |
|---|---|---|---|---|---|---|---|---|---|
| 86.23 | 85.99 | 86.21 | 86.22 | 86.06 | **86.1** | 80.2 | 0.002 | 0.010 | 0.012 |
| 75.4 | 75.8 | 76.1 | 75.8 | 75.1 | **75.6** | 71.7 | 0.085 | 0.122 | 0.207 |
| 67.44 | 68.18 | 67.52 | 67.61 | 68.08 | **67.8** | 63.8 | 0.005 | 0.092 | 0.097 |
| 75.61 | 75 | 74.97 | 75.01 | 75.2 | **75.2** | 71.0 | 0.004 | 0.058 | 0.062 |
| 68.44 | 68.55 | 68.92 | 68.83 | 70.1 | **69.0** | 65.8 | 0.006 | 0.351 | 0.357 |
| 71.55 | 71.61 | 71.49 | 71.17 | 71.48 | **71.5** | 68.2 | 0.005 | 0.023 | 0.029 |
| 71.46 | 71.55 | 70.8 | 71.2 | 71.6 | **71.3** | 67.8 | 0.002 | 0.087 | 0.090 |
| 70.7 | 70.8 | 70.8 | 70.4 | 71 | **70.7** | 67.6 | 0.008 | 0.038 | 0.046 |
| 62.1 | 61.6 | 60.3 | 60.8 | 60.2 | **61.0** | 57.7 | 0.005 | 0.548 | 0.553 |
| 73 | 72.9 | 72.4 | 72.4 | 72.4 | **72.6** | 69.0 | 0.003 | 0.074 | 0.077 |

| Constantane | H | Tamb | U | I | P |
|---|---|---|---|---|---|
| Copper | L | 17.979472 | 11.99 | 0.585 | 7.01415 |
| Pressure ice | 1011 | hPa | T | 0 | C |
| Pressure boil | 1011 | hPa | T | 100 | C |

## D.2 Solid, vertical orientation, measurement 2

| Position | Difference | Channel | Thermocouple | ICE read 1 | ICE read 2 | ICE read 3 | ICE read 4 | ICE read 5 | Average |
|---|---|---|---|---|---|---|---|---|---|
| 0 | - | DAQ1 - A11 | S1 | 1.84 | 1.86 | 1.87 | 1.88 | 1.84 | **1.858** |
| 14 | 14 | DAQ1 - A22 | S2 | 0.76 | 0.74 | 0.73 | 0.77 | 0.72 | **0.744** |
| 28 | 14 | DAQ1 - A33 | S3 | 1.23 | 1.14 | 1.21 | 1.12 | 1.11 | **1.162** |
| 42.5 | 14.5 | DAQ1 - A44 | S4 | 0.94 | 0.96 | 1.05 | 0.94 | 1.03 | **0.984** |
| 60.5 | 18 | DAQ1 - A55 | S5 | 1.25 | 1.25 | 1.23 | 1.27 | 1.25 | **1.25** |
| 76.8 | 16.3 | DAQ1 - A66 | S6 | 0.67 | 0.64 | 0.66 | 0.64 | 0.66 | **0.654** |
| 94.4 | 17.6 | DAQ1 - A77 | S7 | 0.76 | 0.8 | 0.82 | 0.75 | 0.83 | **0.792** |
| 108 | 13.6 | DAQ1 - A88 | S8 | 0.54 | 0.56 | 0.52 | 0.56 | 0.46 | **0.528** |
| 124 | 16 | DAQ1 - A11 | S9 | 0.31 | 0.26 | 0.37 | 0.4 | 0.28 | **0.324** |
| 136 | 12 | DAQ1 - A22 | S10 | 0.68 | 0.7 | 0.69 | 0.7 | 0.71 | **0.696** |
| **Position** | **Difference** | **Channel** | **Thermocouple** | **BOIL read 1** | **BOIL read 2** | **BOIL read 3** | **BOIL read 4** | **BOIL read 5** | **Average** |
| 0 | - | DAQ1 - A11 | S1 | 106.52 | 106.55 | 106.63 | 106.66 | 106.6 | **106.592** |
| 14 | 14 | DAQ1 - A22 | S2 | 105.13 | 104.11 | 105.15 | 105.13 | 105.06 | **104.916** |
| 28 | 14 | DAQ1 - A33 | S3 | 105.25 | 105.34 | 105.28 | 105.33 | 105.45 | **105.33** |
| 42.5 | 14.5 | DAQ1 - A44 | S4 | 105.27 | 105.14 | 105.27 | 105.24 | 105.23 | **105.23** |
| 60.5 | 18 | DAQ1 - A55 | S5 | 104.2 | 103.97 | 104.11 | 104.15 | 103.9 | **104.066** |
| 76.8 | 16.3 | DAQ1 - A66 | S6 | 104.23 | 104.17 | 104.43 | 104.25 | 104.42 | **104.3** |
| 94.4 | 17.6 | DAQ1 - A77 | S7 | 104.62 | 104.67 | 104.71 | 104.6 | 104.59 | **104.638** |
| 108 | 13.6 | DAQ1 - A88 | S8 | 104.1 | 104.4 | 104.19 | 104.23 | 104.09 | **104.202** |
| 124 | 16 | DAQ1 - A11 | S9 | 105.11 | 105.13 | 105.03 | 105.25 | 105.1 | **105.124** |
| 136 | 12 | DAQ1 - A22 | S10 | 104.55 | 104.59 | 104.66 | 104.76 | 104.73 | **104.658** |

| T_0 | e_0 | T_100 | e_100 | a | b | Var(a) | Var(b) |
|---|---|---|---|---|---|---|---|
| 0 | 1.858 | 100 | 6.592 | 0.04734 | 1.858 | 2.87E-07 | 2.56E-04 |
| 0 | 0.744 | 100 | 4.916 | 0.04172 | 0.744 | 1.64E-05 | 3.44E-04 |
| 0 | 1.162 | 100 | 5.33 | 0.04168 | 1.162 | 7.06E-07 | 2.38E-03 |
| 0 | 0.984 | 100 | 5.23 | 0.04246 | 0.984 | 4.46E-07 | 2.18E-03 |
| 0 | 1.25 | 100 | 4.066 | 0.02816 | 1.25 | 1.29E-06 | 1.60E-04 |
| 0 | 0.654 | 100 | 4.3 | 0.03646 | 0.654 | 1.13E-06 | 1.44E-04 |
| 0 | 0.792 | 100 | 4.638 | 0.03846 | 0.792 | 3.07E-07 | 1.02E-03 |
| 0 | 0.528 | 100 | 4.202 | 0.03674 | 0.528 | 1.40E-06 | 1.38E-03 |
| 0 | 0.324 | 100 | 5.124 | 0.048 | 0.324 | 7.93E-07 | 2.82E-03 |
| 0 | 0.696 | 100 | 4.658 | 0.03962 | 0.696 | 6.48E-07 | 1.04E-04 |

| Measurements | | | | | Average | Corrected | var(error) | var(measurement) | var(Temp) |
|---|---|---|---|---|---|---|---|---|---|
| 56.8 | 56.6 | 56.8 | 57 | 57.3 | **56.9** | 57.2 | 0.001 | 0.056 | 0.057 |
| 56.2 | 56.4 | 56.2 | 56.3 | 56 | **56.2** | 52.2 | 0.045 | 0.018 | 0.063 |
| 54 | 54.1 | 54.1 | 53.7 | 53.9 | **54.0** | 49.4 | 0.004 | 0.022 | 0.026 |
| 52 | 52 | 51.8 | 51.9 | 52.1 | **52.0** | 48.6 | 0.003 | 0.010 | 0.014 |
| 46.8 | 46.6 | 46.7 | 47.1 | 47.1 | **46.9** | 43.8 | 0.003 | 0.042 | 0.045 |
| 45.3 | 45.2 | 44.4 | 44 | 44.1 | **44.6** | 42.2 | 0.002 | 0.300 | 0.302 |
| 45.8 | 45.4 | 45.3 | 45.1 | 45.8 | **45.5** | 43.3 | 0.002 | 0.078 | 0.079 |
| 44 | 43.7 | 43.8 | 43.5 | 43.2 | **43.6** | 41.5 | 0.004 | 0.074 | 0.078 |
| 41 | 41.7 | 41.2 | 41.9 | 41.6 | **41.5** | 38.1 | 0.004 | 0.110 | 0.114 |
| 40.9 | 40.6 | 40.7 | 40.4 | 40.6 | **40.6** | 37.3 | 0.001 | 0.026 | 0.027 |

| Constantane | H | Tamb | U | I | P |
|---|---|---|---|---|---|
| Copper | L | 18.607638 | 9.8 | 0.48 | 4.704 |
| Pressure ice | 1011 | hPa | T | 0 | C |
| Pressure boil | 1011 | hPa | T | 100 | C |

## D.3 Solid, horizontal orientation

| Position | Difference | Channel | Thermocouple | ICE read 1 | ICE read 2 | ICE read 3 | ICE read 4 | ICE read 5 | Average |
|---|---|---|---|---|---|---|---|---|---|
| 0 | - | DAQ1 - A11 | S1 | 1.84 | 1.86 | 1.87 | 1.88 | 1.84 | **1.858** |
| 14 | 14 | DAQ1 - A22 | S2 | 0.76 | 0.74 | 0.73 | 0.77 | 0.72 | **0.744** |
| 28 | 14 | DAQ1 - A33 | S3 | 1.23 | 1.14 | 1.21 | 1.12 | 1.11 | **1.162** |
| 42.5 | 14.5 | DAQ1 - A44 | S4 | 0.94 | 0.96 | 1.05 | 0.94 | 1.03 | **0.984** |
| 60.5 | 18 | DAQ1 - A55 | S5 | 1.25 | 1.25 | 1.23 | 1.27 | 1.25 | **1.25** |
| 76.8 | 16.3 | DAQ1 - A66 | S6 | 0.67 | 0.64 | 0.66 | 0.64 | 0.66 | **0.654** |
| 94.4 | 17.6 | DAQ1 - A77 | S7 | 0.76 | 0.8 | 0.82 | 0.75 | 0.83 | **0.792** |
| 108 | 13.6 | DAQ1 - A88 | S8 | 0.54 | 0.56 | 0.52 | 0.56 | 0.46 | **0.528** |
| 124 | 16 | DAQ1 - A11 | S9 | 0.31 | 0.26 | 0.37 | 0.4 | 0.28 | **0.324** |
| 136 | 12 | DAQ1 - A22 | S10 | 0.68 | 0.7 | 0.69 | 0.7 | 0.71 | **0.696** |
| **Position** | **Difference** | **Channel** | **Thermocouple** | **BOIL read 1** | **BOIL read 2** | **BOIL read 3** | **BOIL read 4** | **BOIL read 5** | **Average** |
| 0 | - | DAQ1 - A11 | S1 | 106.52 | 106.55 | 106.63 | 106.66 | 106.6 | **106.592** |
| 14 | 14 | DAQ1 - A22 | S2 | 105.13 | 104.11 | 105.15 | 105.13 | 105.06 | **104.916** |
| 28 | 14 | DAQ1 - A33 | S3 | 105.25 | 105.34 | 105.28 | 105.33 | 105.45 | **105.33** |
| 42.5 | 14.5 | DAQ1 - A44 | S4 | 105.27 | 105.14 | 105.27 | 105.24 | 105.23 | **105.23** |
| 60.5 | 18 | DAQ1 - A55 | S5 | 104.2 | 103.97 | 104.11 | 104.15 | 103.9 | **104.066** |
| 76.8 | 16.3 | DAQ1 - A66 | S6 | 104.23 | 104.17 | 104.43 | 104.25 | 104.42 | **104.3** |
| 94.4 | 17.6 | DAQ1 - A77 | S7 | 104.62 | 104.67 | 104.71 | 104.6 | 104.59 | **104.638** |
| 108 | 13.6 | DAQ1 - A88 | S8 | 104.1 | 104.4 | 104.19 | 104.23 | 104.09 | **104.202** |
| 124 | 16 | DAQ1 - A11 | S9 | 105.11 | 105.13 | 105.03 | 105.25 | 105.1 | **105.124** |
| 136 | 12 | DAQ1 - A22 | S10 | 104.55 | 104.59 | 104.66 | 104.76 | 104.73 | **104.658** |

| T_0 | e_0 | T_100 | e_100 | a | b | Var(a) | Var(b) |
|---|---|---|---|---|---|---|---|
| 0 | 1.858 | 100 | 6.592 | 0.04734 | 1.858 | 2.87E-07 | 2.56E-04 |
| 0 | 0.744 | 100 | 4.916 | 0.04172 | 0.744 | 1.64E-05 | 3.44E-04 |
| 0 | 1.162 | 100 | 5.33 | 0.04168 | 1.162 | 7.06E-07 | 2.38E-03 |
| 0 | 0.984 | 100 | 5.23 | 0.04246 | 0.984 | 4.46E-07 | 2.18E-03 |
| 0 | 1.25 | 100 | 4.066 | 0.02816 | 1.25 | 1.29E-06 | 1.60E-04 |
| 0 | 0.654 | 100 | 4.3 | 0.03646 | 0.654 | 1.13E-06 | 1.44E-04 |
| 0 | 0.792 | 100 | 4.638 | 0.03846 | 0.792 | 3.07E-07 | 1.02E-03 |
| 0 | 0.528 | 100 | 4.202 | 0.03674 | 0.528 | 1.40E-06 | 1.38E-03 |
| 0 | 0.324 | 100 | 5.124 | 0.048 | 0.324 | 7.93E-07 | 2.82E-03 |
| 0 | 0.696 | 100 | 4.658 | 0.03962 | 0.696 | 6.48E-07 | 1.04E-04 |

| Measurements | | | | | Average | Corrected | var(error) | var(measurement) | var(Temp) |
|---|---|---|---|---|---|---|---|---|---|
| 55.2 | 55.1 | 54.8 | 55.2 | 55 | **55.1** | 50.9 | 0.001 | 0.022 | 0.023 |
| 54.3 | 54.5 | 54.4 | 54.3 | 54.2 | **54.3** | 50.4 | 0.042 | 0.010 | 0.052 |
| 49.5 | 49.6 | 49.6 | 49.8 | 49.7 | **49.6** | 46.7 | 0.004 | 0.010 | 0.014 |
| 50 | 50 | 50.2 | 50.1 | 50.2 | **50.1** | 47.2 | 0.003 | 0.008 | 0.011 |
| 49.8 | 49.9 | 49.9 | 49.8 | 49.5 | **49.8** | 46.6 | 0.003 | 0.022 | 0.025 |
| 45.2 | 45.3 | 45.4 | 45.4 | 45.2 | **45.3** | 42.9 | 0.002 | 0.008 | 0.010 |
| 49 | 49.3 | 49.1 | 49.1 | 49.2 | **49.1** | 46.8 | 0.002 | 0.010 | 0.012 |
| 45.1 | 45.4 | 45.5 | 45.4 | 45.5 | **45.4** | 43.1 | 0.004 | 0.022 | 0.026 |
| 48.6 | 48.7 | 48.6 | 48.8 | 48.9 | **48.7** | 45.0 | 0.004 | 0.014 | 0.018 |
| 43.4 | 43.2 | 42.8 | 42.5 | 42.8 | **42.9** | 39.5 | 0.001 | 0.102 | 0.104 |

| Constantane | H | Tamb | U | I | P |
|---|---|---|---|---|---|
| Copper | L | 18.319524 | 9.8 | 0.48 | 4.704 |
| Pressure ice | 1011 | hPa | T | 0 | C |
| Pressure boil | 1011 | hPa | T | 100 | C |

## D.4 Porous 9505, vertical orientation

| Position | Difference | Channel | Thermocouple | ICE read 1 | ICE read 2 | ICE read 3 | ICE read 4 | ICE read 5 | Average |
|---|---|---|---|---|---|---|---|---|---|
| 0 | - | DAQ1 - A11 | P9505 1 | 0.21 | 0.2 | 0.24 | 0.14 | 0.24 | **0.206** |
| 12.5 | 12.5 | DAQ1 - A22 | P9505 2 | 3.19 | 3.17 | 3.24 | 3.21 | 3.22 | **3.206** |
| 27.7 | 15.2 | DAQ1 - A33 | P9505 3 | 0.93 | 1.05 | 0.94 | 0.95 | 1.03 | **0.98** |
| 44.5 | 16.8 | DAQ1 - A44 | P9505 4 | 0.94 | 1.02 | 0.96 | 0.93 | 1.01 | **0.972** |
| 59.5 | 15 | DAQ1 - A55 | P9505 5 | 1.23 | 1.15 | 1.21 | 1.23 | 1.24 | **1.212** |
| 74.2 | 14.7 | DAQ1 - A66 | P9505 6 | 1.01 | 0.93 | 1.01 | 1.03 | 0.95 | **0.986** |
| 88 | 13.8 | DAQ1 - A77 | P9505 7 | 1.27 | 1.35 | 1.26 | 1.29 | 1.27 | **1.288** |
| 104.5 | 16.5 | DAQ1 - A88 | P9505 8 | 0.58 | 0.57 | 0.58 | 0.63 | 0.61 | **0.594** |
| 122.1 | 17.6 | DAQ1 - A11 | P9505 9 | 0.85 | 0.84 | 0.84 | 0.86 | 0.8 | **0.838** |
| 138.9 | 16.8 | DAQ1 - A22 | P9505 10 | 0.46 | 0.46 | 0.47 | 0.48 | 0.57 | **0.488** |
| **Position** | **Difference** | **Channel** | **Thermocouple** | **BOIL read 1** | **BOIL read 2** | **BOIL read 3** | **BOIL read 4** | **BOIL read 5** | **Average** |
| 0 | - | DAQ1 - A11 | P9505 1 | 105.53 | 105.52 | 105.46 | 105.44 | 105.5 | **105.49** |
| 12.5 | 12.5 | DAQ1 - A22 | P9505 2 | 107.48 | 107.37 | 107.43 | 107.42 | 107.4 | **107.42** |
| 27.7 | 15.2 | DAQ1 - A33 | P9505 3 | 105.87 | 105.54 | 105.78 | 105.95 | 105.91 | **105.81** |
| 44.5 | 16.8 | DAQ1 - A44 | P9505 4 | 105.52 | 105.6 | 105.49 | 105.76 | 105.52 | **105.578** |
| 59.5 | 15 | DAQ1 - A55 | P9505 5 | 104.66 | 104.73 | 104.68 | 104.67 | 104.82 | **104.712** |
| 74.2 | 14.7 | DAQ1 - A66 | P9505 6 | 103.86 | 104.07 | 103.92 | 104.14 | 103.9 | **103.978** |
| 88 | 13.8 | DAQ1 - A77 | P9505 7 | 104.61 | 104.65 | 104.62 | 104.46 | 104.71 | **104.61** |
| 104.5 | 16.5 | DAQ1 - A88 | P9505 8 | 104.63 | 104.54 | 104.47 | 104.68 | 104 | **104.464** |
| 122.1 | 17.6 | DAQ1 - A11 | P9505 9 | 105.75 | 105.63 | 105.8 | 105.66 | 105.62 | **105.692** |
| 138.9 | 16.8 | DAQ1 - A22 | P9505 10 | 104.68 | 104.41 | 104.65 | 104.54 | 104.33 | **104.522** |

| T_0 | e_0 | T_100 | e_100 | a | b | Var(a) | Var(b) |
|---|---|---|---|---|---|---|---|
| 0 | 0.206 | 100 | 5.49 | 0.05284 | 0.206 | 2.54E-07 | 1.34E-03 |
| 0 | 3.206 | 100 | 7.42 | 0.04214 | 3.206 | 1.90E-07 | 5.84E-04 |
| 0 | 0.98 | 100 | 5.81 | 0.0483 | 0.98 | 2.39E-06 | 2.48E-03 |
| 0 | 0.972 | 100 | 5.578 | 0.04606 | 0.972 | 1.10E-06 | 1.34E-03 |
| 0 | 1.212 | 100 | 4.712 | 0.035 | 1.212 | 4.55E-07 | 1.06E-03 |
| 0 | 0.986 | 100 | 3.978 | 0.02992 | 0.986 | 1.31E-06 | 1.50E-03 |
| 0 | 1.288 | 100 | 4.61 | 0.03322 | 1.288 | 7.90E-07 | 1.06E-03 |
| 0 | 0.594 | 100 | 4.464 | 0.0387 | 0.594 | 5.96E-06 | 5.04E-04 |
| 0 | 0.838 | 100 | 5.692 | 0.04854 | 0.838 | 5.43E-07 | 4.16E-04 |
| 0 | 0.488 | 100 | 4.522 | 0.04034 | 0.488 | 2.00E-06 | 1.74E-03 |

| Measurements | | | | | Average | Corrected | var(error) | var(measurement) | var(Temp) |
|---|---|---|---|---|---|---|---|---|---|
| 50.78 | 50.55 | 50.41 | 50.23 | 50.21 | **50.4** | 47.2 | 0.002 | 0.045 | 0.047 |
| 35.9 | 35.84 | 36.02 | 36 | 35.82 | **35.9** | 31.2 | 0.001 | 0.007 | 0.007 |
| 28.3 | 28.35 | 28.52 | 28.37 | 28.5 | **28.4** | 26.1 | 0.004 | 0.007 | 0.012 |
| 23.6 | 23.99 | 23.3 | 23 | 22.9 | **23.4** | 21.3 | 0.002 | 0.160 | 0.162 |
| 20.8 | 20.3 | 20.4 | 20.4 | 20.5 | **20.5** | 18.6 | 0.001 | 0.030 | 0.031 |
| 19.3 | 19.4 | 19.3 | 19.2 | 19.3 | **19.3** | 17.7 | 0.002 | 0.004 | 0.006 |
| 18.4 | 18.5 | 18.6 | 18.6 | 18.5 | **18.5** | 16.6 | 0.001 | 0.006 | 0.007 |
| 17.8 | 17.9 | 17.8 | 17.9 | 17.9 | **17.9** | 16.6 | 0.002 | 0.002 | 0.005 |
| 18.7 | 18.6 | 18.7 | 18.6 | 18.6 | **18.6** | 16.9 | 0.001 | 0.002 | 0.003 |
| 18 | 18.2 | 18.3 | 18.2 | 18.3 | **18.2** | 17.0 | 0.002 | 0.012 | 0.014 |

| Constantane | H | Tamb | U | I | P |
|---|---|---|---|---|---|
| Copper | L | 17.10977 | 9.8 | 0.48 | 4.704 |
| Pressure ice | 1011 | hPa | T | 0 | C |
| Pressure boil | 1019 | hPa | T | 100 | C |

## D.5 Porous 9505, horizontal orientation

| Position | Difference | Channel | Thermocouple | ICE read 1 | ICE read 2 | ICE read 3 | ICE read 4 | ICE read 5 | Average |
|---|---|---|---|---|---|---|---|---|---|
| 0 | - | DAQ1 - A11 | P9505 1 | 0.21 | 0.2 | 0.24 | 0.14 | 0.24 | **0.206** |
| 12.5 | 12.5 | DAQ1 - A22 | P9505 2 | 3.19 | 3.17 | 3.24 | 3.21 | 3.22 | **3.206** |
| 27.7 | 15.2 | DAQ1 - A33 | P9505 3 | 0.93 | 1.05 | 0.94 | 0.95 | 1.03 | **0.98** |
| 44.5 | 16.8 | DAQ1 - A44 | P9505 4 | 0.94 | 1.02 | 0.96 | 0.93 | 1.01 | **0.972** |
| 59.5 | 15 | DAQ1 - A55 | P9505 5 | 1.23 | 1.15 | 1.21 | 1.23 | 1.24 | **1.212** |
| 74.2 | 14.7 | DAQ1 - A66 | P9505 6 | 1.01 | 0.93 | 1.01 | 1.03 | 0.95 | **0.986** |
| 88 | 13.8 | DAQ1 - A77 | P9505 7 | 1.27 | 1.35 | 1.26 | 1.29 | 1.27 | **1.288** |
| 104.5 | 16.5 | DAQ1 - A88 | P9505 8 | 0.58 | 0.57 | 0.58 | 0.63 | 0.61 | **0.594** |
| 122.1 | 17.6 | DAQ1 - A11 | P9505 9 | 0.85 | 0.84 | 0.84 | 0.86 | 0.8 | **0.838** |
| 138.9 | 16.8 | DAQ1 - A22 | P9505 10 | 0.46 | 0.46 | 0.47 | 0.48 | 0.57 | **0.488** |
| **Position** | **Difference** | **Channel** | **Thermocouple** | **BOIL read 1** | **BOIL read 2** | **BOIL read 3** | **BOIL read 4** | **BOIL read 5** | **Average** |
| 0 | - | DAQ1 - A11 | P9505 1 | 105.53 | 105.52 | 105.46 | 105.44 | 105.5 | **105.49** |
| 12.5 | 12.5 | DAQ1 - A22 | P9505 2 | 107.48 | 107.37 | 107.43 | 107.42 | 107.4 | **107.42** |
| 27.7 | 15.2 | DAQ1 - A33 | P9505 3 | 105.87 | 105.54 | 105.78 | 105.95 | 105.91 | **105.81** |
| 44.5 | 16.8 | DAQ1 - A44 | P9505 4 | 105.52 | 105.6 | 105.49 | 105.76 | 105.52 | **105.578** |
| 59.5 | 15 | DAQ1 - A55 | P9505 5 | 104.66 | 104.73 | 104.68 | 104.67 | 104.82 | **104.712** |
| 74.2 | 14.7 | DAQ1 - A66 | P9505 6 | 103.86 | 104.07 | 103.92 | 104.14 | 103.9 | **103.978** |
| 88 | 13.8 | DAQ1 - A77 | P9505 7 | 104.61 | 104.65 | 104.62 | 104.46 | 104.71 | **104.61** |
| 104.5 | 16.5 | DAQ1 - A88 | P9505 8 | 104.63 | 104.54 | 104.47 | 104.68 | 104 | **104.464** |
| 122.1 | 17.6 | DAQ1 - A11 | P9505 9 | 105.75 | 105.63 | 105.8 | 105.66 | 105.62 | **105.692** |
| 138.9 | 16.8 | DAQ1 - A22 | P9505 10 | 104.68 | 104.41 | 104.65 | 104.54 | 104.33 | **104.522** |

| T_0 | e_0 | T_100 | e_100 | a | b | Var(a) | Var(b) |
|---|---|---|---|---|---|---|---|
| 0 | 0.206 | 100 | 5.49 | 0.05284 | 0.206 | 2.54E-07 | 1.34E-03 |
| 0 | 3.206 | 100 | 7.42 | 0.04214 | 3.206 | 1.90E-07 | 5.84E-04 |
| 0 | 0.98 | 100 | 5.81 | 0.0483 | 0.98 | 2.39E-06 | 2.48E-03 |
| 0 | 0.972 | 100 | 5.578 | 0.04606 | 0.972 | 1.10E-06 | 1.34E-03 |
| 0 | 1.212 | 100 | 4.712 | 0.035 | 1.212 | 4.55E-07 | 1.06E-03 |
| 0 | 0.986 | 100 | 3.978 | 0.02992 | 0.986 | 1.31E-06 | 1.50E-03 |
| 0 | 1.288 | 100 | 4.61 | 0.03322 | 1.288 | 7.90E-07 | 1.06E-03 |
| 0 | 0.594 | 100 | 4.464 | 0.0387 | 0.594 | 5.96E-06 | 5.04E-04 |
| 0 | 0.838 | 100 | 5.692 | 0.04854 | 0.838 | 5.43E-07 | 4.16E-04 |
| 0 | 0.488 | 100 | 4.522 | 0.04034 | 0.488 | 2.00E-06 | 1.74E-03 |

| Measurements | | | | | Average | Corrected | var(error) | var(measurement) | var(Temp) |
|---|---|---|---|---|---|---|---|---|---|
| 44.8 | 44.6 | 44.7 | 44.5 | 44.3 | **44.6** | 42.0 | 0.002 | 0.030 | 0.031 |
| 29.8 | 29.5 | 29.4 | 29.5 | 29.6 | **29.6** | 25.1 | 0.001 | 0.018 | 0.019 |
| 23.8 | 24 | 24 | 24.1 | 23.8 | **23.9** | 21.8 | 0.004 | 0.014 | 0.018 |
| 21.5 | 21.4 | 21.7 | 21.6 | 21.4 | **21.5** | 19.6 | 0.002 | 0.014 | 0.015 |
| 20.5 | 20.4 | 20.6 | 20.4 | 20.6 | **20.5** | 18.7 | 0.001 | 0.008 | 0.009 |
| 20 | 20 | 19.9 | 19.9 | 20 | **20.0** | 18.4 | 0.002 | 0.002 | 0.004 |
| 20 | 19.8 | 19.7 | 19.9 | 19.8 | **19.8** | 17.9 | 0.001 | 0.010 | 0.012 |
| 19.4 | 19.4 | 19.3 | 19.1 | 19.3 | **19.3** | 18.0 | 0.002 | 0.012 | 0.014 |
| 20 | 19.8 | 20.1 | 20 | 20.1 | **20.0** | 18.2 | 0.001 | 0.012 | 0.013 |
| 19.7 | 19.6 | 19.8 | 20.1 | 19.9 | **19.8** | 18.5 | 0.002 | 0.030 | 0.032 |

| Constantane | H | Tamb | U | I | P |
|---|---|---|---|---|---|
| Copper | L | 18.1868 | 9.8 | 0.47 | 4.61 |
| Pressure ice | 1011 | hPa | T | 0 | C |
| Pressure boil | 1019 | hPa | T | 100 | C |

## D.6 Porous 9508, vertical orientation

| Position | Difference | Channel | Thermocouple | ICE read 1 | ICE read 2 | ICE read 3 | ICE read 4 | ICE read 5 | Average |
|---|---|---|---|---|---|---|---|---|---|
| 0 | - | DAQ1 - A11 | P9508 1 | -0.28 | -0.32 | -0.23 | -0.28 | -0.18 | **-0.258** |
| 14.9 | 14.9 | DAQ1 - A22 | P9508 2 | 0.14 | 0.06 | 0.08 | 0.06 | 0.13 | **0.094** |
| 31 | 16.1 | DAQ1 - A33 | P9508 3 | 0.45 | 0.39 | 0.39 | 0.4 | 0.41 | **0.408** |
| 46 | 15 | DAQ1 - A44 | P9508 4 | 0.5 | 0.58 | 0.57 | 0.6 | 0.57 | **0.564** |
| 61 | 15 | DAQ1 - A55 | P9508 5 | 0.59 | 0.71 | 0.75 | 0.66 | 0.68 | **0.678** |
| 78 | 17 | DAQ1 - A66 | P9508 6 | 0.44 | 0.47 | 0.38 | 0.58 | 0.43 | **0.46** |
| 95.8 | 17.8 | DAQ1 - A77 | P9508 7 | 0.7 | 0.63 | 0.64 | 0.64 | 0.65 | **0.652** |
| 109.2 | 13.4 | DAQ1 - A88 | P9508 8 | -0.11 | -0.05 | -0.08 | -0.14 | -0.06 | **-0.088** |
| 126.7 | 17.5 | DAQ1 - A11 | P9508 9 | 0.52 | 0.53 | 0.64 | 0.53 | 0.56 | **0.556** |
| 140 | 13.3 | DAQ1 - A22 | P9508 10 | 0.06 | 0.09 | 0.11 | 0.13 | 0.06 | **0.09** |
| **Position** | **Difference** | **Channel** | **Thermocouple** | **BOIL read 1** | **BOIL read 2** | **BOIL read 3** | **BOIL read 4** | **BOIL read 5** | **Average** |
| 0 | - | DAQ1 - A11 | P9508 1 | 106.73 | 106.85 | 106.91 | 106.62 | 106.83 | **106.788** |
| 14.9 | 14.9 | DAQ1 - A22 | P9508 2 | 105.01 | 104.73 | 105.088 | 105.05 | 105.11 | **104.9976** |
| 31 | 16.1 | DAQ1 - A33 | P9508 3 | 106.02 | 105.92 | 106.07 | 106.18 | 106.01 | **106.04** |
| 46 | 15 | DAQ1 - A44 | P9508 4 | 106.35 | 106.35 | 106.48 | 106.42 | 106.5 | **106.42** |
| 61 | 15 | DAQ1 - A55 | P9508 5 | 104.25 | 104.34 | 104.3 | 104.36 | 104.52 | **104.354** |
| 78 | 17 | DAQ1 - A66 | P9508 6 | 104.17 | 104.27 | 104.15 | 104.21 | 104.26 | **104.212** |
| 95.8 | 17.8 | DAQ1 - A77 | P9508 7 | 104.28 | 104.38 | 104.34 | 104.27 | 104.36 | **104.326** |
| 109.2 | 13.4 | DAQ1 - A88 | P9508 8 | 103.98 | 104.1 | 104.09 | 104.05 | 104.12 | **104.068** |
| 126.7 | 17.5 | DAQ1 - A11 | P9508 9 | 105.92 | 106.07 | 105.97 | 106.03 | 106 | **105.998** |
| 140 | 13.3 | DAQ1 - A22 | P9508 10 | 105.44 | 105.52 | 105.41 | 105.51 | 105.44 | **105.464** |

| T_0 | e_0 | T_100 | e_100 | a | b | Var(a) | Var(b) |
|---|---|---|---|---|---|---|---|
| 0 | -0.258 | 100 | 6.788 | 0.07046 | -0.258 | 1.28E-06 | 2.34E-03 |
| 0 | 0.094 | 100 | 4.9976 | 0.049036 | 0.094 | 2.02E-06 | 1.18E-03 |
| 0 | 0.408 | 100 | 6.04 | 0.05632 | 0.408 | 7.74E-07 | 4.96E-04 |
| 0 | 0.564 | 100 | 6.42 | 0.05856 | 0.564 | 5.10E-07 | 1.14E-03 |
| 0 | 0.678 | 100 | 4.354 | 0.03676 | 0.678 | 1.12E-06 | 2.86E-03 |
| 0 | 0.46 | 100 | 4.212 | 0.03752 | 0.46 | 6.70E-07 | 4.44E-03 |
| 0 | 0.652 | 100 | 4.326 | 0.03674 | 0.652 | 2.52E-07 | 6.16E-04 |
| 0 | -0.088 | 100 | 4.068 | 0.04156 | -0.088 | 3.55E-07 | 1.10E-03 |
| 0 | 0.556 | 100 | 5.998 | 0.05442 | 0.556 | 4.56E-07 | 1.94E-03 |
| 0 | 0.09 | 100 | 5.464 | 0.05374 | 0.09 | 2.62E-07 | 7.60E-04 |

| Measurements | | | | | Average | Corrected | var(error) | var(measurement) | var(Temp) |
|---|---|---|---|---|---|---|---|---|---|
| 50.5 | 50.3 | 50.4 | 50.4 | 50.5 | **50.4** | 47.1 | 0.005 | 0.006 | 0.011 |
| 32.4 | 32.8 | 32.4 | 32.2 | 32 | **32.4** | 30.5 | 0.003 | 0.070 | 0.073 |
| 22.6 | 22.5 | 22.5 | 22.5 | 22.6 | **22.5** | 20.9 | 0.001 | 0.002 | 0.003 |
| 23 | 22.8 | 22.8 | 22.8 | 22.9 | **22.9** | 21.0 | 0.001 | 0.006 | 0.008 |
| 20 | 19.9 | 19.9 | 19.8 | 19.8 | **19.9** | 18.5 | 0.003 | 0.006 | 0.009 |
| 18.6 | 18.7 | 18.6 | 18.7 | 18.6 | **18.6** | 17.5 | 0.005 | 0.002 | 0.007 |
| 18 | 18 | 18 | 18.2 | 18.3 | **18.1** | 16.8 | 0.001 | 0.016 | 0.017 |
| 17.7 | 17.9 | 17.9 | 18 | 18 | **17.9** | 17.2 | 0.001 | 0.012 | 0.013 |
| 18.8 | 18.8 | 18.8 | 18.7 | 18.8 | **18.8** | 17.2 | 0.002 | 0.002 | 0.004 |
| 18.6 | 18.5 | 18.5 | 18.6 | 18.5 | **18.5** | 17.5 | 0.001 | 0.002 | 0.003 |

| Constantane | H | Tamb | U | I | P |
|---|---|---|---|---|---|
| Copper | L | 17.01458 | 9.8 | 0.47 | 4.61 |
| Pressure ice | 1011 | hPa | T | 0 | C |
| Pressure boil | 1019 | hPa | T | 100 | C |

## D.7 Porous 9508, horizontal orientation

| Position | Difference | Channel | Thermocouple | ICE read 1 | ICE read 2 | ICE read 3 | ICE read 4 | ICE read 5 | Average |
|---|---|---|---|---|---|---|---|---|---|
| 0 | - | DAQ1 - A11 | P9508 1 | -0.28 | -0.32 | -0.23 | -0.28 | -0.18 | **-0.258** |
| 14.9 | 14.9 | DAQ1 - A22 | P9508 2 | 0.14 | 0.06 | 0.08 | 0.06 | 0.13 | **0.094** |
| 31 | 16.1 | DAQ1 - A33 | P9508 3 | 0.45 | 0.39 | 0.39 | 0.4 | 0.41 | **0.408** |
| 46 | 15 | DAQ1 - A44 | P9508 4 | 0.5 | 0.58 | 0.57 | 0.6 | 0.57 | **0.564** |
| 61 | 15 | DAQ1 - A55 | P9508 5 | 0.59 | 0.71 | 0.75 | 0.66 | 0.68 | **0.678** |
| 78 | 17 | DAQ1 - A66 | P9508 6 | 0.44 | 0.47 | 0.38 | 0.58 | 0.43 | **0.46** |
| 95.8 | 17.8 | DAQ1 - A77 | P9508 7 | 0.7 | 0.63 | 0.64 | 0.64 | 0.65 | **0.652** |
| 109.2 | 13.4 | DAQ1 - A88 | P9508 8 | -0.11 | -0.05 | -0.08 | -0.14 | -0.06 | **-0.088** |
| 126.7 | 17.5 | DAQ1 - A11 | P9508 9 | 0.52 | 0.53 | 0.64 | 0.53 | 0.56 | **0.556** |
| 140 | 13.3 | DAQ1 - A22 | P9508 10 | 0.06 | 0.09 | 0.11 | 0.13 | 0.06 | **0.09** |
| **Position** | **Difference** | **Channel** | **Thermocouple** | **BOIL read 1** | **BOIL read 2** | **BOIL read 3** | **BOIL read 4** | **BOIL read 5** | **Average** |
| 0 | - | DAQ1 - A11 | P9508 1 | 106.73 | 106.85 | 106.91 | 106.62 | 106.83 | **106.788** |
| 14.9 | 14.9 | DAQ1 - A22 | P9508 2 | 105.01 | 104.73 | 105.088 | 105.05 | 105.11 | **104.9976** |
| 31 | 16.1 | DAQ1 - A33 | P9508 3 | 106.02 | 105.92 | 106.07 | 106.18 | 106.01 | **106.04** |
| 46 | 15 | DAQ1 - A44 | P9508 4 | 106.35 | 106.35 | 106.48 | 106.42 | 106.5 | **106.42** |
| 61 | 15 | DAQ1 - A55 | P9508 5 | 104.25 | 104.34 | 104.3 | 104.36 | 104.52 | **104.354** |
| 78 | 17 | DAQ1 - A66 | P9508 6 | 104.17 | 104.27 | 104.15 | 104.21 | 104.26 | **104.212** |
| 95.8 | 17.8 | DAQ1 - A77 | P9508 7 | 104.28 | 104.38 | 104.34 | 104.27 | 104.36 | **104.326** |
| 109.2 | 13.4 | DAQ1 - A88 | P9508 8 | 103.98 | 104.1 | 104.09 | 104.05 | 104.12 | **104.068** |
| 126.7 | 17.5 | DAQ1 - A11 | P9508 9 | 105.92 | 106.07 | 105.97 | 106.03 | 106 | **105.998** |
| 140 | 13.3 | DAQ1 - A22 | P9508 10 | 105.44 | 105.52 | 105.41 | 105.51 | 105.44 | **105.464** |

| T_0 | e_0 | T_100 | e_100 | a | b | Var(a) | Var(b) |
|---|---|---|---|---|---|---|---|
| 0 | -0.258 | 100 | 6.788 | 0.07046 | -0.258 | 1.28E-06 | 2.34E-03 |
| 0 | 0.094 | 100 | 4.9976 | 0.049036 | 0.094 | 2.02E-06 | 1.18E-03 |
| 0 | 0.408 | 100 | 6.04 | 0.05632 | 0.408 | 7.74E-07 | 4.96E-04 |
| 0 | 0.564 | 100 | 6.42 | 0.05856 | 0.564 | 5.10E-07 | 1.14E-03 |
| 0 | 0.678 | 100 | 4.354 | 0.03676 | 0.678 | 1.12E-06 | 2.86E-03 |
| 0 | 0.46 | 100 | 4.212 | 0.03752 | 0.46 | 6.70E-07 | 4.44E-03 |
| 0 | 0.652 | 100 | 4.326 | 0.03674 | 0.652 | 2.52E-07 | 6.16E-04 |
| 0 | -0.088 | 100 | 4.068 | 0.04156 | -0.088 | 3.55E-07 | 1.10E-03 |
| 0 | 0.556 | 100 | 5.998 | 0.05442 | 0.556 | 4.56E-07 | 1.94E-03 |
| 0 | 0.09 | 100 | 5.464 | 0.05374 | 0.09 | 2.62E-07 | 7.60E-04 |

| Measurements | | | | | Average | Corrected | var(error) | var(measurement) | var(Temp) |
|---|---|---|---|---|---|---|---|---|---|
| 45.5 | 45.6 | 45.6 | 45.7 | 45.6 | **45.6** | 42.6 | 0.005 | 0.004 | 0.009 |
| 26.2 | 25.8 | 26.3 | 26 | 26.2 | **26.1** | 24.5 | 0.002 | 0.032 | 0.034 |
| 21.9 | 22 | 22.1 | 22.4 | 22.3 | **22.1** | 20.5 | 0.001 | 0.034 | 0.035 |
| 21.3 | 21.5 | 21.3 | 21.4 | 21.3 | **21.4** | 19.5 | 0.001 | 0.006 | 0.008 |
| 21 | 21.2 | 21.1 | 21 | 20.9 | **21.0** | 19.6 | 0.003 | 0.010 | 0.014 |
| 19.7 | 19.8 | 19.8 | 19.9 | 19.9 | **19.8** | 18.6 | 0.005 | 0.006 | 0.010 |
| 19.9 | 19.8 | 19.7 | 19.8 | 19.8 | **19.8** | 18.4 | 0.001 | 0.004 | 0.005 |
| 19.6 | 19.4 | 19.4 | 19.5 | 19.4 | **19.5** | 18.7 | 0.001 | 0.006 | 0.008 |
| 20.2 | 20.2 | 20.5 | 20.1 | 20.4 | **20.3** | 18.6 | 0.002 | 0.022 | 0.024 |
| 19.9 | 20.1 | 19.8 | 19.9 | 20.1 | **20.0** | 18.8 | 0.001 | 0.014 | 0.015 |

| Constantane | H | Tamb | U | I | P |
|---|---|---|---|---|---|
| Copper | L | 18.91838 | 9.81 | 0.48 | 4.71 |
| Pressure ice | 1011 | hPa | T | 0 | C |
| Pressure boil | 1019 | hPa | T | 100 | C |

## D.8 Porous 9805, vertical orientation

| Position | Difference | Channel | Thermocouple | ICE read 1 | ICE read 2 | ICE read 3 | ICE read 4 | ICE read 5 | Average |
|---|---|---|---|---|---|---|---|---|---|
| 0 | - | DAQ1 - A11 | P9805 1 | 1.98 | 1.99 | 2.15 | 2.09 | 2.2 | **2.082** |
| 20.1 | 20.1 | DAQ1 - A22 | P9805 2 | 0.31 | 0.29 | 0.3 | 0.32 | 0.33 | **0.31** |
| 38 | 17.9 | DAQ1 - A33 | P9805 3 | 1.81 | 1.85 | 1.9 | 2.02 | 1.87 | **1.89** |
| 52.7 | 14.7 | DAQ1 - A44 | P9805 4 | 0.62 | 0.61 | 0.64 | 0.66 | 0.62 | **0.63** |
| 68.9 | 16.2 | DAQ1 - A55 | P9805 5 | 0.8 | 0.74 | 0.76 | 0.84 | 0.86 | **0.8** |
| 84.8 | 15.9 | DAQ1 - A66 | P9805 6 | 0.53 | 0.6 | 0.59 | 0.61 | 0.62 | **0.59** |
| 100.7 | 15.9 | DAQ1 - A77 | P9805 7 | -0.09 | 0.16 | 0.24 | 0.28 | -0.12 | **0.094** |
| 112.5 | 11.8 | DAQ1 - A88 | P9805 8 | -0.23 | -0.11 | -0.19 | -0.13 | -0.11 | **-0.154** |
| 129.5 | 17 | DAQ1 - A11 | P9805 9 | 0.24 | 0.14 | 0.15 | 0.26 | 0.16 | **0.19** |
| 142.3 | 12.8 | DAQ1 - A22 | P9805 10 | 0 | 0.02 | 0.01 | 0.08 | 0.06 | **0.034** |
| **Position** | **Difference** | **Channel** | **Thermocouple** | **BOIL read 1** | **BOIL read 2** | **BOIL read 3** | **BOIL read 4** | **BOIL read 5** | **Average** |
| 0 | - | DAQ1 - A11 | P9805 1 | 106.73 | 106.79 | 107 | 106.46 | 106.53 | **106.702** |
| 20.1 | 20.1 | DAQ1 - A22 | P9805 2 | 105.12 | 105.11 | 105.15 | 105.09 | 105.13 | **105.12** |
| 38 | 17.9 | DAQ1 - A33 | P9805 3 | 106.73 | 107.1 | 106.83 | 106.51 | 106.88 | **106.81** |
| 52.7 | 14.7 | DAQ1 - A44 | P9805 4 | 105.07 | 105.15 | 105.06 | 105.21 | 105.19 | **105.136** |
| 68.9 | 16.2 | DAQ1 - A55 | P9805 5 | 104.4 | 104.36 | 104.42 | 104.5 | 104.41 | **104.418** |
| 84.8 | 15.9 | DAQ1 - A66 | P9805 6 | 103.23 | 103.25 | 103.3 | 103.56 | 103.22 | **103.312** |
| 100.7 | 15.9 | DAQ1 - A77 | P9805 7 | 104.81 | 104.79 | 104.82 | 104.77 | 105.08 | **104.854** |
| 112.5 | 11.8 | DAQ1 - A88 | P9805 8 | 103.77 | 103.63 | 103.9 | 103.92 | 104.11 | **103.866** |
| 129.5 | 17 | DAQ1 - A11 | P9805 9 | 104.14 | 104.35 | 103.71 | 104.43 | 104.69 | **104.264** |
| 142.3 | 12.8 | DAQ1 - A22 | P9805 10 | 104.58 | 104.67 | 104.48 | 104.67 | 104.58 | **104.596** |

| x1 | g1 | x2 | g2 | a | b | var(a) | var(b) |
|---|---|---|---|---|---|---|---|
| 0 | 2.082 | 100 | 6.702 | 0.0462 | 2.082 | 4.46E-06 | 7.52E-03 |
| 0 | 0.31 | 100 | 5.12 | 0.0481 | 0.31 | 6.00E-08 | 2.00E-04 |
| 0 | 1.89 | 100 | 6.81 | 0.0492 | 1.89 | 4.22E-06 | 5.10E-03 |
| 0 | 0.63 | 100 | 5.136 | 0.04506 | 0.63 | 4.06E-07 | 3.20E-04 |
| 0 | 0.8 | 100 | 4.418 | 0.03618 | 0.8 | 4.18E-07 | 2.08E-03 |
| 0 | 0.59 | 100 | 3.312 | 0.02722 | 0.59 | 1.71E-06 | 1.00E-03 |
| 0 | 0.094 | 100 | 4.854 | 0.0476 | 0.094 | 4.10E-06 | 2.80E-02 |
| 0 | -0.154 | 100 | 3.866 | 0.0402 | -0.154 | 2.80E-06 | 2.30E-03 |
| 0 | 0.19 | 100 | 4.264 | 0.04074 | 0.19 | 1.10E-05 | 2.48E-03 |
| 0 | 0.034 | 100 | 4.596 | 0.04562 | 0.034 | 5.93E-07 | 9.44E-04 |

| Measurements | | | | | Average | Corrected | var(error) | var(measurement) | var(Temp) |
|---|---|---|---|---|---|---|---|---|---|
| 52.3 | 52.1 | 52.1 | 52.3 | 52.1 | **52.2** | 47.7 | 0.018 | 0.010 | 0.027 |
| 31.2 | 31 | 31.1 | 31.1 | 31.3 | **31.1** | 29.1 | 0.000 | 0.010 | 0.011 |
| 26.6 | 26.1 | 26.3 | 26.4 | 26.3 | **26.3** | 23.2 | 0.007 | 0.026 | 0.034 |
| 23.7 | 23.6 | 23.5 | 23.9 | 24 | **23.7** | 22.0 | 0.001 | 0.034 | 0.035 |
| 22.2 | 22.5 | 22.3 | 22.3 | 22.4 | **22.3** | 20.7 | 0.002 | 0.010 | 0.013 |
| 21.1 | 20.7 | 20.9 | 20.8 | 20.9 | **20.9** | 19.7 | 0.002 | 0.018 | 0.019 |
| 20.7 | 20.6 | 20.6 | 20.7 | 20.8 | **20.7** | 19.6 | 0.030 | 0.006 | 0.035 |
| 19.8 | 20.1 | 19.9 | 20.1 | 20.2 | **20.0** | 19.4 | 0.003 | 0.022 | 0.025 |
| 21.1 | 21.2 | 21.4 | 20.9 | 20.9 | **21.1** | 20.1 | 0.007 | 0.036 | 0.043 |
| 20.3 | 20.2 | 19.9 | 20.2 | 19.8 | **20.1** | 19.1 | 0.001 | 0.038 | 0.039 |

| Constantane | H | Tamb | U | I | P |
|---|---|---|---|---|---|
| Copper | L | 18.804912 | 9.81 | 0.476 | 4.67 |
| Pressure ice | 1011 | hPa | T | 0 | C |
| Pressure boil | 1011 | hPa | T | 100 | C |

## D.9 Porous 9805, horizontal orientation

| Position | Difference | Channel | Thermocouple | ICE read 1 | ICE read 2 | ICE read 3 | ICE read 4 | ICE read 5 | Average |
|---|---|---|---|---|---|---|---|---|---|
| 0 | - | DAQ1 - A11 | P9805 1 | 1.98 | 1.99 | 2.15 | 2.09 | 2.2 | **2.082** |
| 20.1 | 20.1 | DAQ1 - A22 | P9805 2 | 0.31 | 0.29 | 0.3 | 0.32 | 0.33 | **0.31** |
| 38 | 17.9 | DAQ1 - A33 | P9805 3 | 1.81 | 1.85 | 1.9 | 2.02 | 1.87 | **1.89** |
| 52.7 | 14.7 | DAQ1 - A44 | P9805 4 | 0.62 | 0.61 | 0.64 | 0.66 | 0.62 | **0.63** |
| 68.9 | 16.2 | DAQ1 - A55 | P9805 5 | 0.8 | 0.74 | 0.76 | 0.84 | 0.86 | **0.8** |
| 84.8 | 15.9 | DAQ1 - A66 | P9805 6 | 0.53 | 0.6 | 0.59 | 0.61 | 0.62 | **0.59** |
| 100.7 | 15.9 | DAQ1 - A77 | P9805 7 | -0.09 | 0.16 | 0.24 | 0.28 | -0.12 | **0.094** |
| 112.5 | 11.8 | DAQ1 - A88 | P9805 8 | -0.23 | -0.11 | -0.19 | -0.13 | -0.11 | **-0.154** |
| 129.5 | 17 | DAQ1 - A11 | P9805 9 | 0.24 | 0.14 | 0.15 | 0.26 | 0.16 | **0.19** |
| 142.3 | 12.8 | DAQ1 - A22 | P9805 10 | 0 | 0.02 | 0.01 | 0.08 | 0.06 | **0.034** |
| **Position** | **Difference** | **Channel** | **Thermocouple** | **BOIL read 1** | **BOIL read 2** | **BOIL read 3** | **BOIL read 4** | **BOIL read 5** | **Average** |
| 0 | - | DAQ1 - A11 | P9805 1 | 106.73 | 106.79 | 107 | 106.46 | 106.53 | **106.702** |
| 20.1 | 20.1 | DAQ1 - A22 | P9805 2 | 105.12 | 105.11 | 105.15 | 105.09 | 105.13 | **105.12** |
| 38 | 17.9 | DAQ1 - A33 | P9805 3 | 106.73 | 107.1 | 106.83 | 106.51 | 106.88 | **106.81** |
| 52.7 | 14.7 | DAQ1 - A44 | P9805 4 | 105.07 | 105.15 | 105.06 | 105.21 | 105.19 | **105.136** |
| 68.9 | 16.2 | DAQ1 - A55 | P9805 5 | 104.4 | 104.36 | 104.42 | 104.5 | 104.41 | **104.418** |
| 84.8 | 15.9 | DAQ1 - A66 | P9805 6 | 103.23 | 103.25 | 103.3 | 103.56 | 103.22 | **103.312** |
| 100.7 | 15.9 | DAQ1 - A77 | P9805 7 | 104.81 | 104.79 | 104.82 | 104.77 | 105.08 | **104.854** |
| 112.5 | 11.8 | DAQ1 - A88 | P9805 8 | 103.77 | 103.63 | 103.9 | 103.92 | 104.11 | **103.866** |
| 129.5 | 17 | DAQ1 - A11 | P9805 9 | 104.14 | 104.35 | 103.71 | 104.43 | 104.69 | **104.264** |
| 142.3 | 12.8 | DAQ1 - A22 | P9805 10 | 104.58 | 104.67 | 104.48 | 104.67 | 104.58 | **104.596** |

| x1 | y1 | x2 | y2 | a | b | var(a) | var(b) |
|---|---|---|---|---|---|---|---|
| 0 | 2.082 | 100 | 6.702 | 0.0462 | 2.082 | 4.46E-06 | 7.52E-03 |
| 0 | 0.31 | 100 | 5.12 | 0.0481 | 0.31 | 6.00E-08 | 2.00E-04 |
| 0 | 1.89 | 100 | 6.81 | 0.0492 | 1.89 | 4.22E-06 | 5.10E-03 |
| 0 | 0.63 | 100 | 5.136 | 0.04506 | 0.63 | 4.06E-07 | 3.20E-04 |
| 0 | 0.8 | 100 | 4.418 | 0.03618 | 0.8 | 4.18E-07 | 2.08E-03 |
| 0 | 0.59 | 100 | 3.312 | 0.02722 | 0.59 | 1.71E-06 | 1.00E-03 |
| 0 | 0.094 | 100 | 4.854 | 0.0476 | 0.094 | 4.10E-06 | 2.80E-02 |
| 0 | -0.154 | 100 | 3.866 | 0.0402 | -0.154 | 2.80E-06 | 2.30E-03 |
| 0 | 0.19 | 100 | 4.264 | 0.04074 | 0.19 | 1.10E-05 | 2.48E-03 |
| 0 | 0.034 | 100 | 4.596 | 0.04562 | 0.034 | 5.93E-07 | 9.44E-04 |

| Measurements | | | | | Average | Corrected | var(error) | var(measurement) | var(Temp) |
|---|---|---|---|---|---|---|---|---|---|
| 43.7 | 43.8 | 43.8 | 43.7 | 43.9 | **43.8** | 39.7 | 0.015 | 0.006 | 0.020 |
| 25.3 | 25.1 | 25.2 | 25.3 | 25.3 | **25.2** | 23.7 | 0.000 | 0.006 | 0.007 |
| 22.7 | 22.5 | 22.7 | 22.7 | 22.6 | **22.6** | 19.6 | 0.007 | 0.006 | 0.013 |
| 21.6 | 21.7 | 21.6 | 21.4 | 21.6 | **21.6** | 20.0 | 0.000 | 0.010 | 0.010 |
| 20.8 | 20.6 | 20.8 | 20.8 | 20.8 | **20.8** | 19.2 | 0.002 | 0.006 | 0.009 |
| 20.2 | 20.1 | 19.9 | 20 | 20.1 | **20.1** | 18.9 | 0.002 | 0.010 | 0.012 |
| 20.1 | 20 | 20.1 | 20 | 20 | **20.0** | 19.0 | 0.029 | 0.002 | 0.032 |
| 19.3 | 19.1 | 19.3 | 19.4 | 19.7 | **19.4** | 18.7 | 0.003 | 0.038 | 0.042 |
| 19.9 | 19.8 | 19.7 | 19.7 | 19.9 | **19.8** | 18.8 | 0.006 | 0.008 | 0.014 |
| 19.7 | 19.4 | 19.6 | 19.8 | 19.7 | **19.6** | 18.7 | 0.001 | 0.018 | 0.020 |

| Constantane | H | Tamb | U | I | P |
|---|---|---|---|---|---|
| Copper | L | 18.8 | 9.9 | 0.476 | 4.71 |
| Pressure ice | 1011 | hPa | T | 0 | C |
| Pressure boil | 1011 | hPa | T | 100 | C |